Ultrafast Spectral Dynamics of a Rhenium Photocatalyst

by

Laura M. Kiefer

A dissertation submitted in partial fulfillment
of the requirements for the degree of
Doctor of Philosophy
(Chemistry)
in the University of Michigan
2017

Doctoral Committee:

Professor Kevin J. Kubarych, Chair
Professor Eitan Geva
Professor Roseanne Sension
Professor Vanessa Sih

To my Dad, Mom and Husband

Acknowledgements

I would like to first thank my advisor, Kevin Kubarych, for giving me the freedom and opportunity to decide which direction I wanted to go with each project throughout my PhD. His insight was invaluable and he truly helped me mature as a scientist. I even think programming is okay now.

I would also like to thank all of the professors who believed in me, saw my potential and helped me realize it, from my instructors at both Macomb Community College and Wayne State University to my mentors here at the University of Michigan, including Roseanne Sension, Eitan Geva and Vanessa Sih.

I would like to thank my former and current lab members: Dr. John King, who helped me develop skills on the laser table as well as understand the observables of 2DIR; Dr. Aaron White, who helped me program more elegantly and provided mental stimulation with his daily quick-witted puns; Kim Daley, Peter Eckert, Ved Roy and Lindsay Michocki for allowing me to become a mentor that used more positive reinforcement over time.

Lastly, I would like to thank my husband, Nikolas Kiefer and my family, Joan Visger, Brian Visger and Bub Visger, for their love and support.

Table of Contents

List of Figures

List of Tables

List of Abbreviations

1,10-phen: 1,10-phenanthroline
^{1}MLCT: singlet metal-to-ligand charge transfer
2DIR: two-dimensional infrared (spectroscopy)
2D: two-dimensional
3D: three-dimensional
^{3}MLCT: triplet metal-to-ligand charge transfer
AN: acceptor number
BBO: beta-barium borate
bpy: bipyridine
CCD: charged coupled device
COOH: carboxylic acid
CT: charge transfer
DFG: difference frequency generation
DFT: density functional theory
DMB: 4,4'-dimethylbypyridine
DMF: dimethyl formamide
DN: donor number
DSSC: dye-sensitized solar cell
ET: electron transfer
FFCF: frequency-fluctuation correlation function
FpP: cyclopentadienylcarbonyl-diphenylphosphinobutanoyliron
FTIR: Fourier transform infrared (spectroscopy)
fwhm: full width half max
FRET: Förster resonance energy transfer
fs: femtosecond
LLCT: ligand-to-ligand charge transfer
IVR: intramolecular vibrational redistribution
ISC: intersystem-crossing
MIP: migration insertion polymerization
MLCT: metal-to-ligand charge transfer
mM: milliMolar
N3: (cis-bis(isothiocyanato)bis(2,2'-bipyridyl-4,4'-dicarb-oxylato)ruthenium(II)
N719: (cis-bis(isothiocyanato)bis(2,2'-bipyridyl-4,4'-dicarb-oxylato)ruthenium(II) bis-tetrabutylammonium ($Ru(dcbpy)_2(NCS)_2$ 2TBA)
nJ: nanoJoule
nm: nanometer
NOE: nuclear Overhauser effect
NOESY: nuclear Overhauser effect spectroscopy
PFpP: polycyclopentadienylcarbonyl-diphenylphosphinobutanoyliron
ps: picosecond
QM/MM: quantum mechanics/molecular mechanics
t-2DIR: transient two dimensional
t-Butyl: *tert*-butyl
TEOA: triethanolamine
THF: tetrahydrofuran
UV: ultraviolet
Vis: visible

Abstract

This thesis encompasses the spectroscopic investigations of the photo-initiated CO_2 reduction catalyst, $Re(bpy)(CO)_3Cl$, in multiple states along the photocatalytic cycle. The objective of these experiments was to better understand how involved things such as the electrostatics and the solvent(s) are at each step in the reaction mechanism. The spectroscopic techniques used include two-dimensional infrared (2DIR), transient-2DIR, UV-pump/IR-probe, FTIR and UV-Vis. 2DIR was used to characterize the electronic ground state dynamics of the Re photocatalyst in multiple solvent environments. These served as a reference for comparison the next experiments, which implemented the use of transient-2DIR to mimic the initiation step of the photocatalysis reaction. This experiment was the first to characterize a quasi-equilibrated electronic excited state, by electronically exciting the molecule, then waiting until it is equilibrated in a triplet metal-to-ligand transfer (^{3}MLCT) state to probe with the equilibrium 2DIR pulses. We observe a two-fold slowdown in ground state spectral dynamics around the in-phase symmetric vibrational mode and a decrease in the vibrational lifetime by a factor of five. This technique offers the ability to study somewhat long-lived electronic states independent of the ground state.

Because the 4,4'-tert-butyl bipyridine substituted Re compound is the most efficient catalyst, 2DIR experiments were conducted on Re compound with either electron withdrawing or electron donating groups on the bipyridine to observe possible changes in the dynamics from the resulting changes in electrostatics. No changes due to the substituents were observed. A solvent study was also conducted on this series of compounds to understand the role the solvent plays in the reaction, since the efficiency of the CO_2 reduction reaction is solvent dependent, and the spectral diffusion decay time increased as the nucleophilicity of the solvent increased.

A key step of the reaction mechanism involves a sacrificial electron donor, often triethanolamine (TEOA); a step believed to be diffusion controlled. The next set of experiments focused on changing the concentration of TEOA in the solvent tetrahydrofuran (THF), to observe a possible concentration effect on the dynamics. This was important to characterize because the optimal catalytic activity occurs at a 1:5 ratio of TEOA:solvent. UV-Vis experiments on betaine-30, a molecule with similar dipole moment as the $Re(bpy)(CO)_3Cl$, in the different mixtures confirmed occurrence of preferential solvation. A spectral diffusion slowdown occurs at the optimal ratio of TEOA:solvent for the solvents that the TEOA exhibits preferential solvation in (THF, CH_3CN) , but does not for the one that doesn't (DMSO). The preferential solvation was confirmed after UV-Vis pump/IR probe experiments revealed a presence of the singly reduced species peak, indicative that electron transfer has occurred, on a timescale faster than diffusion (<70 ps). This result offers insight to a previously never mentioned mechanistic detail of this electron transfer.

The next experiments focused on the effect of preferential solvation monitored from the perspective of both the solute and preferential solvator by selecting two molecules with vibrational bands in close proximity to each other. The combination involved a solution of Na^+SCN^- , a molecule known to preferentially solvate betaine-30, with the Re complex in THF. No changes occur in the spectral dynamics as the concentration of each species is altered. Surprisingly, an energy transfer occurs from the totally symmetric band of the Re to both of the bands of the Na^+SCN^- (one from the contact ion pair and one from a dimer of two contact ion pairs) on a timescale independent of the two bands involved, indicating the occurrence of non-Gaussian dynamics.

The next work focused on ultrafast structural fluctuations of a small polymer (PfPp) that incorporates site-specific vibrational probes within the polymer studied with two-dimensional infrared spectroscopy. The chain ends were found to spectrally diffuse slower than do the inner chain sites. As the conditions are altered from dilute solution to a solvent-free film, the heterogeneity in site dynamics becomes reduced due to the crowding influence of neighboring

molecules. A computational model based on a coarse grained force field and Langevin dynamics simulations yields site-specific motional fluctuations consistent with the experimental observations, providing clear evidence that the ultrafast spectral diffusion measurements report polymer motional dynamics.

The final work in this thesis incorporates using 2DIR to determine the spectral diffusion and vibrational lifetimes on the CN stretching modes of the DSSC dye N719 in DMF both free and bound to Mg-doped TiO_2 nanoparticles. We were able to resolve the previously unresolved two CN stretches from the SCN ligands using nonrephasing spectra. Whether the N719 is bound to the TiO_2 or not, the spectral diffusion times are same for both modes, while their inhomogeneities are different. The spectral diffusion times are the same for all modes, whether bound to TiO_2 or not, but the TiO_2-bound molecules have shorter lifetimes (bound: 41 ± 2 ps, free: 52 ± 2 ps). This decrease is attributed to the N719 having more relaxation pathways that arise from the TiO_2.

Chapter 1

Introduction

1.1 INTRODUCTION

Despite centuries of experimental chemistry, even today many chemists employ largely or even entirely empirical methods to determine ideal reaction conditions. The simplest, prototypical chemical reaction: A + B $\rightarrow$ products, involves *at a minimum* three distinct species given the presence of the solvent. Though imagined to be distributed homogeneously throughout the solution, it is clear that differences in electrostatic interactions and structural flexibility should often, if not always, lead to preferred arrangements of the interacting molecules. This property was unintentionally discovered when a color change occurred after mixing different solvents with iodine[1]. When combined, the interactions become altered depending on the solvent, leading to a deviation from the results based on a homogeneous solution hypothesis. In all likelihood, most mixtures behave like this, with one species having a preferential attraction toward another—it is the basis of our understanding of nonideal solutions. The heterogeneous interactions can be weak or strong, and due to the vast combinatorial complexity, practical chemists typically screen reaction conditions empirically. For multi-step processes, such as those encountered in photocatalysis, various intermediates likely have different interactions with the solvent or other reactants as the course of the photocycle proceeds. Being able to study chemical reactions at multiple stages in a reaction mechanism would offer insight into the roles that these preferential interactions have in influencing overall reaction outcomes. The work in this dissertation highlights several key stages of a photocatalysis reaction, where previously unidentified preferential

interactions emerge as playing important roles, often decisively so, in electron transfer and solvent exchange.

The solvent, through these preferential interactions, can influence the outcomes of solution phase reactions. Individual solvent properties, or even more complicated aspects of the mixture may govern structural dynamics as well as reaction energetics, for example modulating transition state energies or fluctuations underlying charge transfer. Most solvent properties are described macroscopically and often without rigorous physical definitions. For example, viscosity, polarity, nucleophilicity, electrophilicity can all be found to impart control over reaction outcomes, despite the fact that not one of these properties can be determined without recourse to an empirical scale or trend. The polarity of the solvent takes into account the overall intermolecular interactions between the solvent and solute that are governed by electrostatics (i.e. dielectric constants, polarizabilities, permanent molecular dipole moments, etc.)[2], though without regard to microscopic solvent packing or other specific interactions. The size solvent, which may be characterized by the free volume, allows or prevents specific interactions of the solvent and the reactants due to the solvent packing around the solute. Viscosity can only be linked to physically well-defined friction within certain models. The donicity, or nucleophilicity, of the solvent characterizes the tendencies for a solvent molecule to donate its electron density towards the reactants[3], but relies entirely on an empirical scale. Finally, the acceptor number of the solvent is another empirical parameter describing the electrophilic properties of the solvent[4]. All of these properties work together to help the reaction proceed, and if the role that each of these properties plays in the outcome of the reaction is understood, optimization of the reaction can be achieved by choosing specific properties wisely. This is the approach we take for the catalysis reactions: understanding the role and influence of the solvent in each step of the reaction mechanism. This goal can be achieved by isolating the intermediates and performing 2DIR experiments in multiple solvent environments. The ultrafast resolution of 2DIR experiments are able to report on solvent induced effects that occur on a sub-picosecond to tens of picoseconds timescale.

1.2 $Re(bpy)(CO)_3Cl$ AS A CO_2 REDUCTION PHOTOCATALYST

The members of the rhenium(I)-bipyridine family are energy harvesting complexes that are activated by visible light, a first step in a series of photoinduced catalysis reactions, such as the reduction of CO_2 to form CO and formate [5]. Such catalysis could provide an avenue to reduce greenhouse gases while producing a source of clean renewable energy. These complexes are also of fundamental interest due to their complex excited state dynamics making them paradigms of photoinduced charge transfer (CT) and intersystem crossing (ISC) processes [6-9]. The photocatalytic cycle is depicted in **Figure 1.1 A**, with all known key intermediate steps labeled. The initiation step involves a near-UV pulse that excites the molecule into a singlet metal-to-ligand charge transfer (^{1}MLCT) electronic excited state, and after intersystem crossing through multiple pathways, the complex relaxes into a thermally equilibrated triplet MLCT state (^{3}MLCT) (**Fig 1.1 A,B**). This long-lived redox-active excited state can initiate a wide range of reactions, from charge transfer to catalysis. Although the photophysics immediately following optical excitation has received extensive experimental and theoretical attention[10-17], what makes the excited species functional as a catalyst is the relatively long lifetime of the excited state. Hence, the dynamical processes relevant to subsequent chemical reactivity, such as reduction by a sacrificial electron donor, occur on timescales that are completely decoupled from the initial photoexcitation.

This class of rhenium polypyridyl complexes has been widely investigated using the techniques of resonance Raman, time-resolved infrared, femtosecond fluorescence, fluorescence upconversion and UV-vis transient absorption in order to map the identity of excited states as well as to determine the timescales of the excitation and relaxation processes[13, 15, 18]. After the initial excitation and intersystem-crossing (ISC) on a sub-200 fs timescale, the relaxation can follow multiple pathways, proceeding via a combination of triplet ligand-to-ligand charge transfer and triplet metal-to-ligand charge transfer states, all of which have intra-ligand contributions (i.e. mixed states) (**Fig 1.1 B**). The LLCT state can either emit (phosphoresce) or relax to the energetically lower MLCT state (~10 ps) [8]. The ISC rate is both solvent and ligand dependent, but it does not scale with the spin-orbit coupling constant of the halide ligand [13-15]. The charge transfer was more recently reported to be a two-center type by x-ray absorption spectroscopy, originating from both the metal and the halide and transferring to the bipyridine ligand[19]. Although there are certainly important intermediate dynamical events immediately following optical excitation, these

are primarily responsible for the overall quantum yield. The species of principal interest to photocatalysis is the long-lived ^{3}MLCT state, which is at equilibrium, at least with respect to the non-electronic degrees of freedom. Unlike electronic-based spectroscopy approaches, 2DIR offers the opportunity to study independently the ground state and excited state dynamics, enabling direct comparison.

Thus far, many of the photocatalytic events have been optimized by brute force, including which solvent to use and how much sacrificial electron donor is needed, etc.. Using the technique of 2DIR, we are able to shed light on the role of each reagent at each known step in the photocatalytic mechanism. 2DIR offers understanding of solvation dynamics, changes in dynamics resulting from electron density rearrangements within the Re complex, concentration-dependent dynamics in solvent mixtures and the effect of preferential solvation on the dynamics. 2DIR helps to answer the question, "why are these conditions optimal?". The knowledge gained from this photocycle can then be used in a broader manner for other complex reactions.

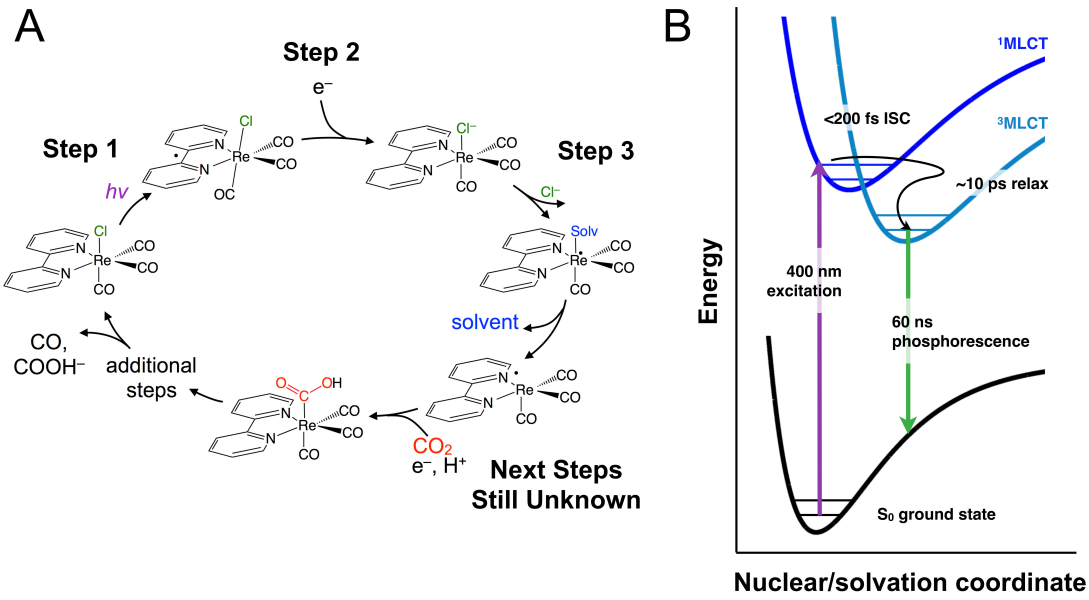

Figure 1.1: A) The CO_2 reduction photocatalytic mechanism of $Re(bpy)(CO)_3Cl$ highlighting key intermediate steps; B) potential diagram featuring visible excitation, inter-system crossing, vibrational relaxation, phosphorescence with their respective timescales.

1.3 TWO-DIMENSIONAL INFRARED SPECTROSCOPY

Molecular vibrations occur in the near- to mid-infrared region (0.8 – 25 μm; 14,000 – 400 cm^{-1}). Their location reveals the identity of the stretching, bending, rocking and wagging motions of the bonds between specific atom types, with the wavenumbers < 4000, cm^{-1} assigned to fundamental vibrations and the higher wavenumbers designated to overtones. For organic molecules, the frequencies of these motions are located primarily in the 500 – 1,800 cm^{-1} and 2,800 – 4000 cm^{-1} regions, with a few less common chemical signatures in the 2100 – 2400 cm^{-1} range. In between these lies a clutter free spectral region where organic-metal vibrational stretches show up, making them ideal probes of molecules. Because this bare region is not convoluted with other stretching modes, this leaves little ambiguity towards identification of the vibrational bands being studied. A common technique of measuring the vibrational spectrum of a molecule is Fourier transform infrared (FTIR) spectroscopy. While this technique is informative about identifying features of a given molecule and relative dephasing timescales due to the observed bandwidths and the uncertainty principle, it does not reveal dynamic information and couplings that may occur between the vibrational modes. To do this, another dimension must be incorporated to correlate a frequency that is excited with a frequency that is detected, a method referred to as two-dimensional infrared spectroscopy (2DIR). By changing the time delay between the laser pulses that result in the excitation and detection frequencies, dynamic, or time-dependent, information can be obtained on the system being studied. The experimental technique is described in detail below.

The basic concept of a 2DIR experiment involves three ultrafast infrared pulses (2000 cm^{-1} center frequency, 125 cm^{-1} bandwidth, 500 nJ, 120 fs) that interact with the sample, generating a signal that can be detected. The duration of the pulses allows for measuring ultrafast dynamics, on the sub-picosecond timescale. The three pulses are arranged in a background-free geometry, referred to as a box-car geometry. The first two pulses are used to excite the molecule into vibrational populations or coherences, which relax or dephase over time. A third pulse interacts with the sample, causing it to emit a signal. Each pulse, or field (E_1, E_2, and E_3), that interacts with the sample has an associated wave vector ($\mathbf{k_1}$, $\mathbf{k_2}$, and $\mathbf{k_3}$, respectively). These pulses are separated by time delays t_1 and t_2, which produce the signal that emits during t_3. The two phase-matched

signals required for extracting the observables in a 2DIR experiment are rephasing ($\mathbf{k_r} = -\mathbf{k_1} + \mathbf{k_2} + \mathbf{k_3}$) and nonrephasing ($\mathbf{k_n} = +\mathbf{k_1} - \mathbf{k_2} + \mathbf{k_3}$). We directly obtain the detection frequency information by using a spectrometer, and the excitation frequency axis is determined by Fourier transforming the signal with respect to the time delay between the first two pulses (t_1). The experimental excitation frequency spectral resolution is roughly 3 cm^{-1}.

Observables For each time delay between excitation pulse pair and the probe pulse (t_2), a rephasing (photon echo) and nonrephasing 2D spectrum is obtained. Subtracting the signal amplitudes of a diagonal peak from both of these experiments at each value of t_2 gives us the inhomogeneity index (**Eq. 1**), which is proportional to the normalized frequency-fluctuation correlation function (FFCF), an observable unique to 2DIR that is described in detail in the next section.

In our 2DIR experiments, we do not directly measure the FFCF, but instead measure the inhomogeneity index, *I(t)* (**Eq. 1.1**), which is proportional to the normalized FFCF and we will refer to it in the text as an FFCF, and in the figures as *C(t)*.

$$I(t_2) = \frac{A_r(t_2) - A_n(t_2)}{A_r(t_2) + A_n(t_2)} \qquad (1.1)$$

We obtain $I(t)$ by inserting the rephasing and nonrephasing amplitudes (A_r and A_n, respectively) of a given peak into equation (1.1) at each waiting time delay.

Either of the individual 2D experiments (rephasing/nonrephasing) can also be used to obtain intramolecular vibrational redistribution (IVR) times and vibrational lifetimes through exponential fits to the waiting time dependent peak amplitudes. For the case of IVR, the time constants are obtained through a bi-exponential fit of the waiting time (t_2) trace of the rephasing signal cross-peak between the two transitions. The rise of the cross peak amplitude is attributed to IVR, and the longer timescale decay arises from vibrational energy relaxation.

Spectral Diffusion The most significant observable in 2DIR spectroscopy is the FFCF, which characterizes equilibrium fluctuations and the loss of frequency correlation induced by fluctuations of the solvent or of the probed solute itself[20]. The FFCF is defined as $C(t) = \langle \delta\omega(0)\delta\omega(t) \rangle$

, where $\delta\omega(t) = \omega(t) - \langle\omega\rangle$ is the instantaneous fluctuation of the frequency ω from the average <ω>. Both the external forces due to the solvent and the internal environment, such as electron density, contribute to slight frequency shifts that, in principle, reveal energetic and dynamical information. Organic probes, such as carbonyls, bound to a transition metal center are not only sensors of the external environment, they also reflect changes in the internal structure, which due to coupling can be extended throughout the entire molecule.

Transient-2DIR A modification of the equilibrium 2DIR experiment, referred to as transient-2DIR, involves incorporating a UV-Vis pulse prior to the 2DIR sequence to electronically excite the molecule of interest or to dissociate a bond[21-27]. The remainder of this brief discussion only focuses only on a photoexcitation using the UV-Vis pulse. The time delay between the UV-Vis pulse and the remaining pulses determines what type of information can be extracted from the experiment. With short time delays, the electronic excited state undergoes rapid relaxation processes, possibly interconverting between charge-transfer states, and these processes modulate the vibrational frequency making it impossible to interpret *C(t)*[22-23]. When longer time delays are incorporated, molecules with long-lived excited states such as triplets, a quasi-equilibrium can be established on the electronically excited state: the first pulse electronically excites the molecule, it undergoes all of its relaxation processes, and a fraction settles to an equilibrated distribution with respect to all of the non-electronic degrees of freedom. It is referred to as a quasi-equilibrated state because, in the context of the Re Lehn catalyst studied in this work, it takes tens of picoseconds to relax and it remains in this state for tens of nanoseconds, so in terms of our measurement timescales, it is equilibrated and therefore, we can view a 2D-IR measurement of this state to be a probe of the equilibrium fluctuations. With this method, the dynamics of an electronic ground state species and a quasi-equilibrated electronic excited state can be studied independently, instead of the conventional method of fluorescence, which reports the difference in energy between the states[28].

1.4 THESIS OUTLINE

The remainder of this thesis discusses the use of 2DIR and transient-2DIR spectroscopy to

characterize the spectral dynamics of multiple intermediates in the photocatalytic reduction of CO_2 via $Re(bpy)(CO)_3Cl$ (a photosensitizer/homogeneous catalyst) in multiple solvents as well as to study the effects of preferential solvation, explore the site-specific dynamics in the short polymer PfPp and finally, to discuss the changes in spectral dynamics resulting from binding a dye-sensitized solar cell (DSSC) molecule, N719, to TiO_2 nanoparticles[29-30]. Chapter 2 describes a new approach to studying electronic excited states using the technique of transient-2DIR. This work described is the first instance of reporting spectral dynamics from a quasi-equilibrated electronic excited state. This state is the result of the initiation of the photo-catalysis CO_2 reduction reaction using $Re(bpy)(CO)_3Cl$. The quasi-equilibrium was reached by adjusting the time delay between the UV excitation (initiation) pulse and the 2DIR pulse sequence to be long enough for the triplet metal-to-ligand charge transfer (^{3}MLCT) state to relax to its vibrational ground state[18, 31-32]. 2DIR experiments were also conducted on the electronic ground state as a reference of comparison for the electronic excited state results.

Chapter 3 focuses on what changes, if any, pertain to a change in the electrostatics on the molecule or the solvent the molecule is in. The idea was to alter the electrostatics, similar to the effect of the ^{3}MLCT reported in chapter 2, but not as drastic. A comparison of the dynamics of the synthesized catalysts $Re(4,4'R_2\text{-}bpy)(CO)_3Cl$, where the R group is either electron withdrawing or electron donating group, showed no change in dynamics between the different species. For each of these compounds, 2DIR experiments were conducted in each of the three solvents, acetonitrile (CH_3CN), tetrahydrofuran (THF) and dimethyl sulfoxide (DMSO), all aprotic polar solvents relative to the catalysis reaction.

Chapter 4 describes the effect that the sacrificial electron donor, triethanolamine (TEOA), has on the spectral dynamics. A UV-Vis study of betaine-30, a compound with an uncomplicated electronic excited state and having a similar molecular dipole moment as $Re(bpy)(CO)_3Cl$, in varying ratios of solvent:TEOA (solvets: CH_3CN , THF, DMSO) showed that the TEOA preferentially solvates the betaine-30 in solvents who possesses a permanent molecular dipole moment less than the TEOA. The next experiments focused on the photocatalytic reaction mixture of $Re(bpy)(CO)_3Cl$ in varying ratios of solvent:TEOA. Equilibrium 2DIR experiments were conducted on each of these mixtures to observe how the results may relate to the actual catalysis reaction.

The UV-Vis experiments could not be performed on the Re catalyst due to the complicated nature of its electronic excited states, so to confirm preferential solvation, we instead performed UV-pump (440 nm)-IR probe experiments on $Re(bpy)(CO)_3Cl$ in the most catalytically relevant mixture of 20% TEOA to 80% THF and compared these results to those without in pure THF. We hoped to and did observe the singly-reduced species at a time faster than that which would be observed via diffusion of the TEOA, confirming that preferential solvation does occur. This observation has not been reported in the community that studies this photocatalytic system, and so this sheds light on a new way to think about the contributing mechanisms of these reactions.

Chapter 5 explores preferential solvation through the perspective of both the solute and preferred solvent. Again, the Re compound was used for this study and the molecule that was selected to preferentially solvate around the photocatalyst, was Na^+SCN^-, because it was previously shown to preferentially solvate betaine-30. Equilibrium 2DIR experiments were performed on multiple concentrations of the Na^+SCN^- in THF. A surprising energy transfer from the Re complex to the multiple Na^+SCN^- configurations in the solution was observed.

Chapter 6 ventures away from the well-studied photo-catalytic system and describes the results of experiments on a short polymer, with monomeric units that contain iron-carbonyl probes. The special detail about this polymer is the end unit contains a different probe (iron-dicarbonyl) than the middle units (iron-monocarbonyl), both observable in 2DIR spectra. This allows for site-specific monitoring of the spectral dynamics. 2DIR experiments were conducted on three different polymer environments: dilute, concentrated and film. These experiments were complemented by Langevin simulations using a coarse grained model.

Chapter 7 discusses the first instance that the two close-lying bands of the CN stretches in the DSSC, N719, have been spectroscopically resolved. We were able to do this by taking advantage of the phase properties of a nonrephasing spectrum, which elongate along the anti-diagonal, so two bands close in energy appear as separate peaks on the diagonal[33]. Since the peaks could be resolved, information unique to each of the bands could be monitored. The dye molecules were studied both free in solution and bound to TiO_2 nanoparticles in solution in the solvent DMF. The solvent choice seemed to affect the anharmonicity of the higher frequency mode, but more experiments are needed to confirm such an affect.

The concluding chapter of this thesis reiterates the key concepts learned in the experiments and offers suggestions of how these learned concepts can be applied to more applicable systems.

REFERENCES

1. Hildebrand, J. H.; Glascock, B. L., The Color of Iodine Solutions. *Journal of the American Chemical Society* 1909, *31*, 26-31.
2. Reichardt, C., Solvatochromic Dyes as Solvent Polarity Indicators. *Chemical Reviews* 1994, *94* (8), 2319-2358.
3. Marcus, Y., The Properties of Organic Liquids that are Relevant to Their Use as Solvating Solvents. *Chemical Society Reviews* 1993, *22* (6), 409-416.
4. Mayer, U.; Gutmann, V.; Gerger, W., Acceptor Number - Quantitative Empirical Parameter for Electrophilic Properties of Solvents. *Monatshefte Fur Chemie* 1975, *106* (6), 1235-1257.
5. Morris, A. J.; Meyer, G. J.; Fujita, E., Molecular Approaches to the Photocatalytic Reduction of Carbon Dioxide for Solar Fuels. *Acc. Chem. Res.* 2009, *42* (12), 1983-1994.
6. Vlček, A.; Zalis, S., Modeling of charge-transfer transitions and excited states in d(6) transition metal complexes by DFT techniques. *Coord. Chem. Rev.* 2007, *251* (3-4), 258-287.
7. Takeda, H.; Koike, K.; Morimoto, T.; Inumaru, H.; Ishitani, O., Photochemistry and Photocatalysis of Rhenium(I) Diimine Complexes. In *Advances in Inorganic Chemistry, Vol 63: Inorganic Photochemistry*, VanEldik, R.; Stochel, G., Eds. 2011; Vol. 63, pp 137-186.
8. Vlček, A., Jr., Ultrafast Excited-State Processes in Re(I) Carbonyl-Diimine Complexes: From Excitation to Photochemistry. In *Top. Organomet. Chem.*, 2010; Vol. 29, pp 73-114.
9. Kumar, A.; Sun, S.-S.; Lees, A. J., Photophysics and Photochemistry of Organometallic Rhenium Diimine Complexes. In *Top. Organomet. Chem.*, 2010; Vol. 29, pp 1-35.
10. Asbury, J. B.; Wang, Y. Q.; Lian, T. Q., Time-dependent vibration Stokes shift during solvation: Experiment and theory. *Bull. Chem. Soc. Jpn.* 2002, *75* (5), 973-983.
11. Stufkens, D. J.; Vlček, A., Ligand-Dependent Excited State Behaviour of Re(I) and Ru(II) Carbonyl-Diimine Complexes. *Coordination Chemistry Reviews* 1998, *177*, 127-179.

12. Dattelbaum, D. M.; Omberg, K. M.; Schoonover, J. R.; Martin, R. L.; Meyer, T. J., Application of Time-Resolved Infrared Spectroscopy to Electronic Structure in Metal-to-Ligand Charge-Transfer Excited States. *Inorganic Chemistry* **2002,** *41* (23), 6071-6079.

13. Cannizzo, A.; Blanco-Rodriguez, A. M.; El Nahhas, A.; Sebera, J.; Zalis, S.; Vlček, A.; Chergui, M., Femtosecond fluorescence and intersystem crossing in rhenium(I) carbonyl-bipyridine complexes. *J. Am. Chem. Soc.* **2008,** *130* (28), 8967-8974.

14. El Nahhas, A.; Cannizzo, A.; van Mourik, F.; Blanco-Rodriguez, A. M.; Zalis, S.; Vlček, A.; Chergui, M., Ultrafast Excited-State Dynamics ef Re(L)(CO)(3)(bpy) (n) Complexes: Involvement of the Solvent. *J. Phys. Chem. A* **2010,** *114* (22), 6361-6369.

15. El Nahhas, A.; Consani, C.; Blanco-Rodriguez, A. M.; Lancaster, K. M.; Braem, O.; Cannizzo, A.; Towrie, M.; Clark, I. P.; Zalis, S.; Chergui, M.; Vlček, A., Ultrafast Excited-State Dynamics of Rhenium(I) Photosensitizers Re(Cl)(CO)(3)(N,N) and Re(imidazole)(CO)(3)(N,N) (+): Diimine Effects. *Inorg. Chem.* **2011,** *50* (7), 2932-2943.

16. Heydova, R.; Gindensperger, E.; Romano, R.; Sykora, J.; Vlček, A., Jr.; Zalis, S.; Daniel, C., Spin-Orbit Treatment of UV-vis Absorption Spectra and Photophysics of Rhenium(I) Carbonyl-Bipyridine Complexes: MS-CASPT2 and TD-DFT Analysis. *Journal of Physical Chemistry A* **2012,** *116* (46), 11319-11329.

17. Sato, S.; Matubara, Y.; Koike, K.; Falkenstrom, M.; Katayama, T.; Ishibashi, Y.; Miyasaka, H.; Taniguchi, S.; Chosrowjan, H.; Mataga, N.; Fukazawa, N.; Koshihara, S.; Onda, K.; Ishitani, O., Photochemistry of fac- Re(bpy)(CO)3Cl. *Chem. Eur. J.* **2012,** *18* (49), 15722-15734.

18. Liard, D. J.; Busby, M.; Matousek, P.; Towrie, M.; Vlček, A., Picosecond Relaxation of ^{3}MLCT Excited States of $[Re(Etpy)(CO)_3(dmb)]^+$ and $Re(Cl)(CO)_3(bpy)$ as Revealed by Time-Resolved Resonance Raman, UV-vis, and IR Absorption Spectroscopy. *Journal of Physical Chemistry A* **2004,** *108* (13), 2363-2369.

19. El Nahhas, A.; van der Veen, R. M.; Penfold, T. J.; Pham, V. T.; Lima, F. A.; Abela, R.; Blanco-Rodriguez, A. M.; Zalis, S.; Vlček, A.; Tavernelli, I.; Rothlisberger, U.; Milne, C. J.; Chergui, M., X-ray Absorption Spectroscopy of Ground and Excited Rhenium-Carbonyl Diimine-Complexes: Evidence for a Two-Center Electron Transfer. *Journal of Physical Chemistry A* **2013,** *117* (2), 361-369.

20. Demirdoven, N.; Khalil, M.; Tokmakoff, A., Correlated Vibrational Dynamics Revealed by Two-Dimensional Infrared Spectroscopy. *Physical Review Letters* 2002, *89* (23).

21. Bredenbeck, J.; Helbing, J.; Behrendt, R.; Renner, C.; Moroder, L.; Wachtveitl, J.; Hamm, P., Transient 2D-IR Spectroscopy: Snapshots of the Nonequilibrium Ensemble During the Picosecond Conformational Transition of a Small Peptide. *Journal of Physical Chemistry B* 2003, *107* (33), 8654-8660.

22. Bredenbeck, J.; Helbing, J.; Hamm, P., Solvation Beyond the Linear Response Regime. *Physical Review Letters* 2005, *95* (8).

23. Hamm, P., Three-Dimensional-IR Spectroscopy: Beyond the Two-Point Frequency Fluctuation Correlation Function. *Journal of Chemical Physics* 2006, *124* (12), 124506.

24. Chung, H. S.; Ganim, Z.; Jones, K. C.; Tokmakoff, A., Transient 2D IR Spectroscopy of Ubiquitin Unfolding Dynamics. *Proceedings of the National Academy of Sciences of the United States of America* 2007, *104* (36), 14237-14242.

25. Chung, H. S.; Khalil, M.; Smith, A. W.; Tokmakoff, A., Transient Two-Dimensional IR Spectrometer for Probing Nanosecond Temperature-Jump Kinetics. *Review of Scientific Instruments* 2007, *78* (6).

26. Cervetto, V.; Hamm, P.; Helbing, J., Transient 2D-IR Spectroscopy of Thiopeptide Isomerization. *Journal of Physical Chemistry B* 2008, *112* (28), 8398-8405.

27. Baiz, C. R.; McCanne, R.; Kubarych, K. J., Structurally Selective Geminate Rebinding Dynamics of Solvent-Caged Radicals Studied with Nonequilibrium Infrared Echo Spectroscopy. *Journal of the American Chemical Society* 2009, *131* (38), 13590.

28. Vanderzwan, G.; Hynes, J. T., Time-Dependent Fluorescence Solvent Shifts, Dielectric Friction, and Nonequilibrium Solvation in Polar-Solvents. *Journal of Physical Chemistry* 1985, *89* (20), 4181-4188.

29. Hawecker, J.; Lehn, J. M.; Ziessel, R., Efficient Photochemical Reduction of CO_2 to CO by Visible Light Irradiation of Systems Containing $Re(bipy)(CO)_3X$ or $[Ru(bipy)_3]^{2+}$-Co^{2+} Combinations as Homogeneous Catalysts. *Journal of the Chemical Society-Chemical Communications* 1983, (9), 536-538.

30. Desilvestro, J.; Gratzel, M.; Kavan, L.; Moser, J.; Augustynski, J., Highly Efficient Sensitization of Titanium-Dioxide. *Journal of the American Chemical Society* 1985, *107* (10), 2988-2990.

31. Cannizzo, A.; Blanco-Rodriguez, A. M.; El Nahhas, A.; Sebera, J.; Zalis, S.; Vlček, A.; Chergui, M., Femtosecond Fuorescence and Intersystem Crossing in Rhenium(I) Carbonyl-Bipyridine Complexes. *Journal of the American Chemical Society* 2008, *130* (28), 8967-8974.

32. El Nahhas, A.; Cannizzo, A.; van Mourik, F.; Blanco-Rodriguez, A. M.; Zalis, S.; Vlček, A.; Chergui, M., Ultrafast Excited-State Dynamics of $[Re(L)(CO)_3(bpy)]^n$ Complexes: Involvement of the Solvent. *Journal of Physical Chemistry A* 2010, *114* (22), 6361-6369.

33. Khalil, M.; Demirdoven, N.; Tokmakoff, A., Coherent 2D IR Spectroscopy: Molecular Structure and Dynamics in Solution. *Journal of Physical Chemistry A* 2003, *107* (27), 5258-5279.

Chapter 2

Spectral Dynamics of a Rhenium Photo-Catalyst in the Electronic Ground and Excited States

The work presented in this chapter has been published in the following papers:

1. L. M. Kiefer, J. T. King, K. J. Kubarych, "*Equilibrium Excited State Dynamics of a Photoactivated Catalyst Measured with Ultrafast Transient 2DIR*", J. Phys. Chem. A, **118**, 9853 (2014)
2. L. M. Kiefer, J. T. King, K. J. Kubarych, "*Dynamics of Rhenium Photocatalysts Revealed Through Ultrafast Multidimensional Spectroscopy*", Acc. Chem. Res., **48**, 1123 (2015)

2.1 INTRODUCTION

As discussed in chapter 1, members of the rhenium(I)-bipyridine family are important energy harvesting complexes whose catalysis in initiated by visible light, a first step in a series of photo-induced catalysis reactions, primarily the reduction of CO_2 to form CO and formate [1]. The initiation begins with a near-UV pulse that excites the molecule into a singlet metal-to-ligand charge transfer (^{1}MLCT) electronic excited state, and after intersystem crossing through multiple pathways, the complex relaxes into a thermally equilibrated triplet MLCT state (^{3}MLCT) (**Fig 2.1a,b**). This long-lived redox-active excited state can initiate a wide range of reactions, from charge transfer to catalysis. Although the photophysics immediately following optical excitation has received extensive experimental and theoretical attention [2-10], what makes the excited species functional as a catalyst is the relatively long lifetime of the excited state. Two-dimensional infrared (2DIR) spectroscopy has proven to be exceptionally powerful in revealing dynamics of ground electronic state systems, including catalysts, but so far it has only been applied sparingly to

transient excited state species [11-17]. Here we directly, and separately, investigate the dynamics of both the ground and excited states of *fac*-$Re(CO)_3(bpy)Cl$ (bpy= 2,2'-bipyridine), finding marked differences in both the timescales of the decay of vibrational frequency correlation and of the vibrational energy relaxation. These findings will enable detailed characterizations of solvent effects and molecular flexibility, aiding the design and control of photocatalysts from a dynamical perspective. This work indicates that transient 2D-IR (t-2DIR) is a powerful tool to study the quasi-equilibrium dynamics of excited electronic states by referencing the observations to the fully characterized ground state species. This work is the first example of such a comparison.

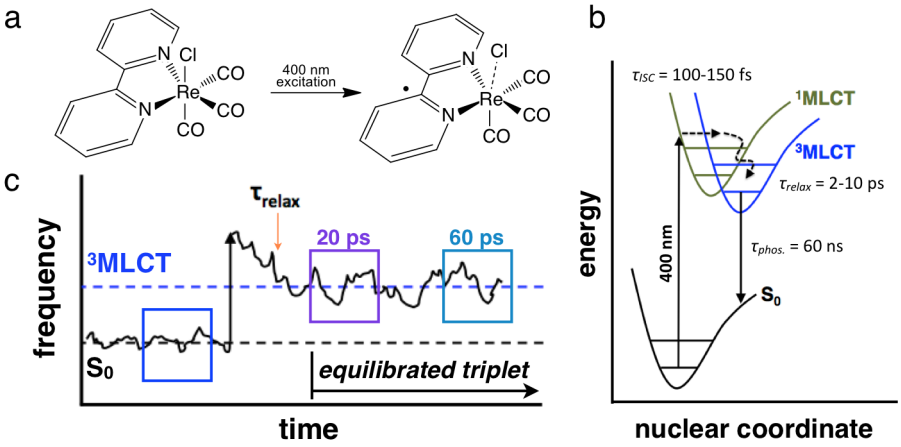

Figure 2.1: a) MLCT from rhenium to bipyridine ligand via 400 nm light, b) potential diagram featuring visible excitation, inter-system crossing, vibrational relaxation, phosphorescence with their respective timescales, c) cartoon representing a frequency trajectory of an initially equilibrated ground state molecule that, following optical excition (vertical black arrow) and subesequent nonequilibrium relaxation, ultimately yields a "quasi-equilibrium" triplet state after a relaxation period τ_{relax}.

The LLCT state can either emit (phosphoresce) or relax to the energetically lower MLCT state (~10 ps) [18]. The ISC rate is both solvent and ligand dependent, but it does not scale with the spin-orbit coupling constant of the halide ligand [3-4, 8]. The charge transfer was more recently reported to be a two-center type by x-ray absorption spectroscopy, originating from both the metal and the halide and transferring to the bipyridine ligand[19]. Although there are certainly important intermediate dynamical events immediately following optical excitation, these are primarily responsible for the overall quantum yield. The species of principal interest to photocatalysis is the long-lived ^{3}MLCT state, which is at equilibrium, at least with respect to the non-electronic degrees of freedom. Unlike electronic-based spectroscopy approaches, 2DIR offers

the opportunity to study independently the ground state and excited state dynamics, enabling direct comparison. The key challenge is to time resolve and obtain reliable time constants for the frequency-frequency correlation function (FFCF), an observable unique to 2D spectroscopy, on the excited state using transient 2DIR.

2.2 EXPERIMENTAL METHODS

Our 2DIR experiments are conducted using three mid-IR pulses (2000 cm^{-1} center frequency, 125 cm^{-1} bandwidth) that interact with the sample in a background-free box geometry. Two of these pulses are used to excite the molecule, preparing vibrational populations of the carbonyl modes, and the signal is emitted following the interaction with the third pulse. The IR pulses are generated from an 800 nm pulse (~1 mJ, 100 fs) from a Ti:Sapphire regenerative amplifier that is split and sent into two separate β-barium borate optical parametric amplifiers (OPAs), the outputs of which are difference frequency mixed in separate GaSe crystals producing independently tunable mid-IR pulses. The emitted signal is heterodyne detected with a local oscillator reference following chirped-pulse upconversion to the visible by mixing the two mid-IR fields in a 5% MgO doped $LiNbO_3$ crystal as described previously. The signal is obtained, more specifically, by three fields, E_1, E_2, and E_3, that interact with the sample, with wave vectors $\mathbf{k_1}$, $\mathbf{k_2}$, and $\mathbf{k_3}$, respectively, that are separated by delays t_1 and t_2, which produce the signal that emits during t_3. The two phase-matched signals required to measure spectral diffusion dynamics are the rephasing ($\mathbf{k_r} = -\mathbf{k_1} + \mathbf{k_2} + \mathbf{k_3}$) and nonrephasing ($\mathbf{k_n} = +\mathbf{k_1} - \mathbf{k_2} + \mathbf{k_3}$). In the 2DIR experiments, we directly obtain the detection frequency information by using a spectrometer, and we obtain the excitation frequency axis by Fourier transforming the signal with respect to the time delay between the first two pulses (t_1). The experimental excitation frequency spectral resolution is roughly 3 cm^{-1}.[20] For each time delay between excitation pulse pair and the probe pulse (t_2), a rephasing (photon echo) and nonrephasing 2D spectrum is obtained. Subtracting the signal amplitudes of a diagonal peak from both of these experiments at each value of t_2 gives us the inhomogeneity index, which is proportional to the normalized FFCF (**Eq. 1**) [21]. We also use either of the individual 2D experiments (rephasing/nonrephasing) to obtain intramolecular vibrational redistribution (IVR) times and vibrational lifetimes through exponential fits to waiting time

dependent peak amplitudes. For the case of IVR, the time constants are obtained through a bi-exponential fit of the waiting time (t_2) trace of the rephasing signal cross-peak between the two transitions. The rise of the cross peak amplitude is attributed to IVR, and the longer timescale decay arises from vibrational energy relaxation.

2DIR. A significant capability of 2DIR spectroscopy is the characterization of equilibrium fluctuations through the FFCF, which allows one to monitor the loss of frequency correlation induced by fluctuations of the solvent or of the probed solute itself. The FFCF is defined as $C(t) = \langle \delta\omega(0)\delta\omega(t) \rangle$, where $\delta\omega(t) = \omega(t) - \langle \omega \rangle$ is the instantaneous fluctuation of the frequency ω from the average $<\omega>$. Both the external forces due to the solvent and the internal environment, such as electron density, contribute to slight frequency shifts that in principal reveal energetic and dynamical information. Carbonyl ligands bound to a transition metal center are not only sensors of the external environment, they also reflect changes in the internal structure, which due to coupling can be extended throughout the entire molecule. Recent work by Massari *et al.* has shown that the carbonyl on the metal center of Vaska's complex, for example, senses solvent differently depending on whether or not the complex has a bound dioxygen ligand [22-23].

While the FFCF measurement provides powerful insight into solute and solvent fluctuations within electronic ground state species, there are fundamental limitations in applying such measurements to an electronic excited state. Namely, correlation functions are typically most meaningful when the system is at equilibrium, or when the observable being measured is ergodic. It is not straightforward to interpret *C(t)* when an electronic excited state is undergoing rapid relaxation processes that modulate the vibrational frequency [24]. For molecules with long-lived excited states such as triplets, however, it is possible to establish an equilibrium on the electronically excited state, at least in terms of our measurements on timescales of tens of picoseconds. **Figure 2.1c** shows a schematic cartoon depicting vibrational probe frequency fluctuations before during and after excitation to the excited electronic state.

Transient 2DIR techniques have been applied to study photoinduced reactions, such as charge transfer, ligand dissociation, geminate rebinding and conformational transitions [13, 15, 25-27]. In current practice, t-2DIR mainly focuses on non-equilibrium processes by observing time-

dependent transition frequencies and amplitudes [11-12, 25, 28-29]. Several t-2DIR experiments have been performed on $Re(CO)_3(dmb)Cl$ (dmb=4,4'-dimethyl-2,2'-bipyridine) where the vibrational probes monitored the excited electronic state during intersystem crossing and other relaxation processes [12, 24, 28]. The study presented here uses t-2DIR to investigate the ^{3}MLCT state of $Re(CO)_3(bpy)Cl$ after these intramolecular relaxation processes have occurred, and the excited state species is prepared to serve as a catalyst.

2.3 RESULTS

Ground State Analysis. A full characterization of the ground state species is required in order to serve as an internal reference against which to compare the excited state. The ground state equilibrium 2DIR spectrum probes the CO modes, which have exceptionally strong oscillator strength in a background-free (1900-2200 cm^{-1}) region of the IR spectrum. $Re(CO)_3(bpy)Cl$ has three normal modes: an out-of-phase symmetric stretch, an asymmetric stretch and an in-phase symmetric stretch, referred to as A'(2), A'', and A'(1) respectively. The former two peaks are often referred to as the "asymmetric stretches," even though A'(2) is an out-of-phase symmetric stretch. The linear IR absorption spectrum in THF (**Fig 2.2a**) shows two broader peaks for A'(2) and A'' at 1894 cm^{-1} (12.8 cm^{-1}, fwhm) and 1917 cm^{-1} (12.6 cm^{-1}, fwhm), respectively, and a very narrow A'(1) peak at 2019 cm^{-1} (6.3 cm^{-1}, fwhm). The narrow linewidth in the A'(1) suggests that this totally symmetric mode is likely mostly homogeneously broadened and possesses different sensitivity to the solvent than do the lower frequency modes. In our 2DIR experiments, we do not directly measure the FFCF, but instead measure the inhomogeneity index, *I(t)* (**Eq. 2.1**), which is proportional to the normalized FFCF and we will refer to it in the text as an FFCF, and in the figures as *C(t)*.

$$I(t_2) = \frac{A_r(t_2) - A_n(t_2)}{A_r(t_2) + A_n(t_2)} \qquad (2.1)$$

We obtain $I(t)$ by inserting the rephasing and nonrephasing amplitudes (A_r and A_n, respectively) of a given peak into equation (2.1) at each waiting time delay. A representative 2DIR absolute rephasing spectrum at an early waiting time (1.2 ps) is shown in **Figure 2.2b**. Only the A'' and A'(1) modes, as well as their cross-peaks and the cross-peaks between A'(2) and A'', are in this spectra

due to our IR bandwidth limitations. 2DIR experiments in the electronic ground state reveal that both of the lower frequency modes show similar spectral diffusion decay times while the totally symmetric mode shows a decay that is twice as slow as the other modes (**Fig 2.2c**). The low frequency oscillations in the first portion of the FFCF are due to the fact that multiple vibrational modes are excited coherently, leading to quantum beats, which are common in metal carbonyl complexes with few-cm^{-1} linewidths [30]. All three of the bands do indeed display spectral dynamics, indicating both inhomogeneous broadening and spectral diffusion within each band, with the narrower high frequency band exhibiting less inhomogeneous broadening than the two lower

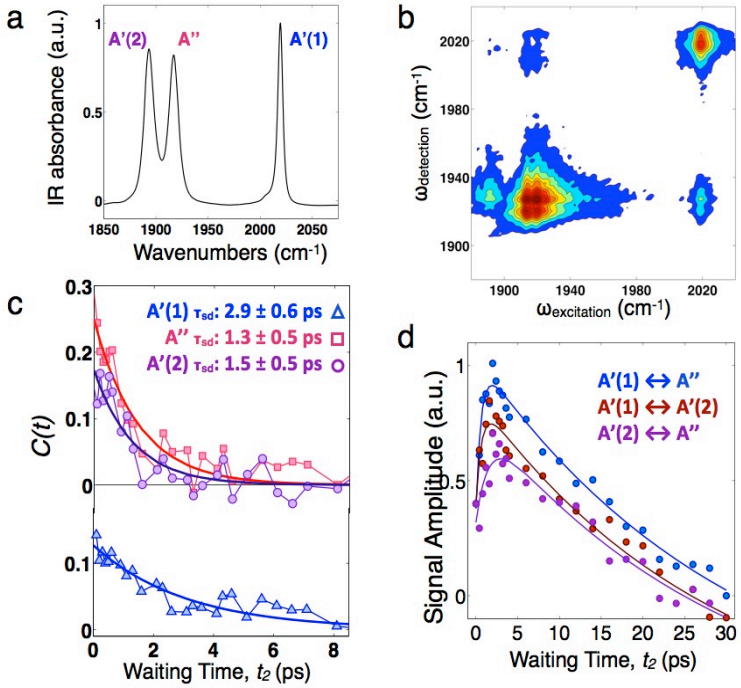

Figure 2.2: (a) FTIR spectrum of $Re(CO)_3(bpy)Cl$ in THF showing the CO stretching modes. The completely symmetric mode (A'(1)) shows little spectral broadening (2019 cm^{-1},fwhm 6.3 cm^{-1}) in the polar solvent, while the asymmetric modes (A'' and A'(2) modes) are significantly broadened (1894 and 1917 cm^{-1},fwhm 12.7 and 12.8 cm^{-1}, respectively). (b) A absolute rephasing 2DIR spectra of the A" and A'(1) modes at t_2 =1.2 ps in THF. (c) FFCFs of the three vibrational modes. The FFCFs of the A'' and A'(2) mode decay on similar timescales, while the A'(1) mode shows a two-fold slowdown in spectral diffusion. Note, the A'(1) FFCF is offset for clarity. (d) Rephasing amplitudes from the cross-peaks of all three CO stretching modes. The rise is due to IVR and the decay is due to vibrational relaxation.

frequency modes. The two lower frequency asymmetric modes exhibit similar spectral diffusion times of 1.3 ± 0.5 ps (A'(2)) and 1.5 ± 0.3 ps (A''). The same broadening and spectral diffusion trends can be seen in multiple polar solvents (**Fig 2.3**). The A" and A'(2) modes have roughly the same spectral dynamics within the same solvent, but are solvent dependent (**Table 2.1**). The three

Table 2.1. Frequency-frequency correlation function decay times (τ_{SD}) for all three of the carbonyl stretching modes of $Re(CO)_3(bpy)Cl$ in polar solvents

	A'(1) (ps)	A" (ps)	A'(2) (ps)
DMSO	4.5 ± 0.9	3.2 ± 0.5	4.2 ± 0.4
THF	2.9 ± 0.8	1.5 ± 0.3	1.3 ± 0.5
CH_3CN	1.7 ± 0.7	1.7 ± 0.7	1.6 ± 0.4

modes should not have a drastically different response to solvent dynamics, but a fully symmetric mode may be an anomaly. In an earlier study on $Mn_2(CO)_{10}$, a similar anomalous behavior of a highly symmetric mode was observed, suggesting there may be a symmetry dependent susceptibility to frequency fluctuations in metal carbonyl complexes.[30] Pshenichnikov *et al* also reported observations of different dynamics between the symmetric and asymmetric modes of water molecules in acetonitrile solution,[31] so the fact that symmetric and asymmetric modes can undergo different dynamics may be a somewhat general phenomenon. We are currently exploring the detailed quantum chemical nature of symmetry-specific broadening.

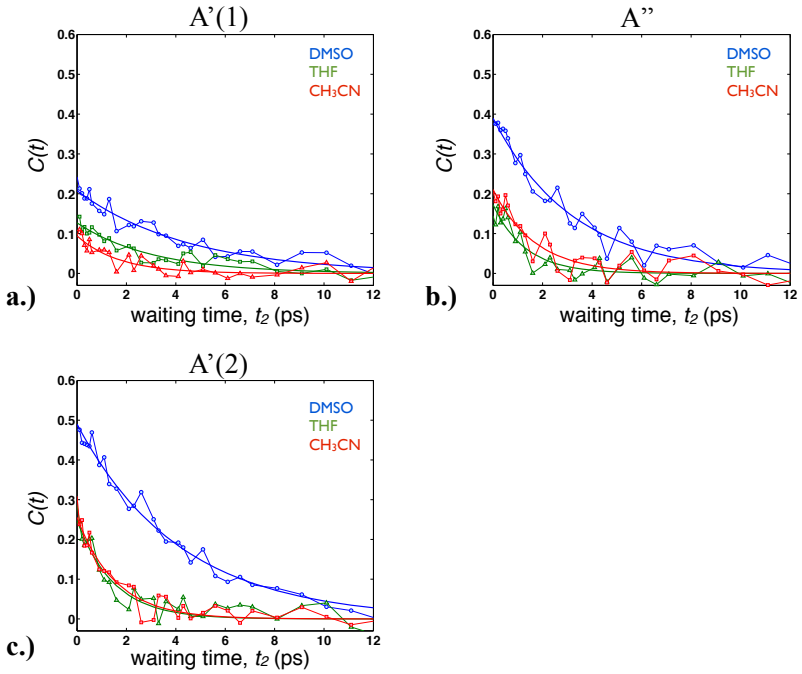

Figure 2.3: Frequency-fluctuation correlation function decays of the $[Re(bpy)(CO)_3Cl]$ a.) A'(1) mode, b.) A" mode and c.) A'(2) mode in the solvents DMSO, THF and CH_3CN.

The cross-peaks of the equilibrium 2DIR spectra were analyzed to reveal vibrational lifetimes and the time constants for intramolecular vibrational redistribution (IVR). The rephasing

amplitudes from the crosspeaks over the different time delays (**Fig 2.2d**) were fit with a bi-exponential function, where the fast growth is due to IVR and the much slower decay arises from vibrational relaxation. We found that all three modes have vibrational lifetimes of ~ 25 ps (THF). The intramolecular vibrational redistribution between the two lower frequency modes is slower (1.5 ± 0.4 ps) than it is between either of the low frequency modes and the high frequency mode (0.7 ± 0.3 ps). This result is counterintuitive, since the two lower frequency modes are more closely spaced in energy, and hence, might be expected to randomize vibrational energy more rapidly. However, the energy gap is only one contribution to IVR, and although we have not performed a detailed anharmonic analysis, the faster IVR must be due either to enhanced anharmonic coupling between the low and high frequency modes, or to a preponderance of the bath's density of states at the higher (102 and 125 cm^{-1}) difference frequencies than at the lower (23 cm^{-1}) difference frequency. The spectral density of THF in the relevant frequency range (0-200 cm^{-1}) has been obtained using optical Kerr effect spectroscopy, and shows a roughly four-fold greater amplitude near 25 cm^{-1} than at 100 cm^{-1}, suggesting that the unexpectedly slower IVR between the low frequency modes is due to the reduced anharmonic coupling between them [32].

Excited State Analysis. The transient 2DIR technique introduces a UV or visible pump preceding the conventional 2DIR pulse sequence (**Fig 2.4b**). Absorption of the 400 nm actinic pump pulse excites $Re(CO)_3(bpy)Cl$ into a singlet metal-to-ligand charge transfer state (Re --> bpy) forming $[Re(II)(CO)_3(bpy^-)Cl]^+$. Following intersystem crossing, the complex relaxes into a ^{3}MLCT state where it remains for ~60 nanoseconds. Because the detection in this fifth-order nonlinear technique is not background-free, we implement a chopper and report difference t-2DIR spectra (**Figs 2.4a; 2.5c,d; 2.6a**), as described in detail previously [15]. In the excited state, all three modes shift to higher frequencies due to the weakening of Re—>CO π back-bonding, which enhances the carbonyl triple bond character. Our Gaussian calculations using the functional PBEO (PBE1PBE), the basis 6-31+G(d) (LanL2DZ pseudopotential for Re) and CPCM (polarizable conductor calculation model) method for the solvent[33], agree with previous work by Hamm *et al*. showing that the A'(2) mode frequency shifts more than twice as much as the frequency of the A" mode, from 1894 cm^{-1} to 1981 cm^{-1}, while the A'' shifts from 1917 cm^{-1} to 1950 cm^{-1} [28]. The A'(1) mode

shifts from 2019 cm^{-1} in the electronic ground state to 2059 cm^{-1} in the ^{3}MLCT state. The blue shifts of the excited state frequencies are seen in t-2DIR difference spectra (**Figs 2.4a; 2.5c,d; 2.6a**). The FFCF of the A'(1) mode in this state clearly shows spectral diffusion that decays in 4.7 ± 0.5 ps, indicating that the excited state vibration is inhomogeneously broadened to some degree (**Fig 2.4c**). For the t-2DIR measurements of the A'(1) mode, we compared the spectral dynamics at delays of 20 and 60 ps between the actinic pulse and the 2DIR probe to assess whether or not the

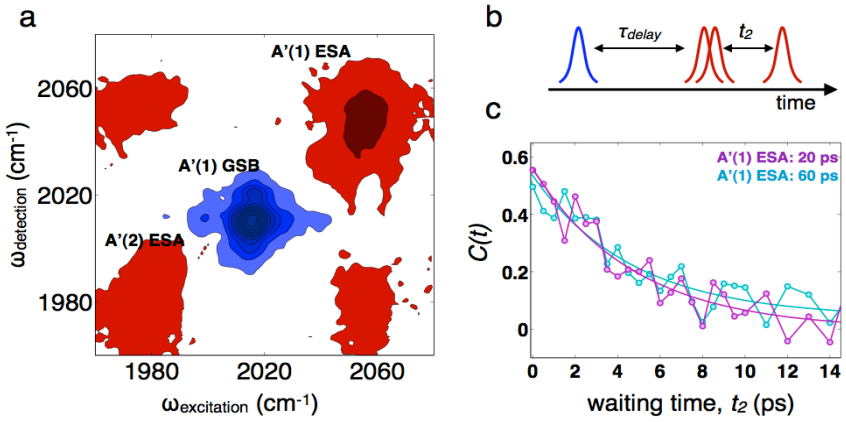

Figure 2.4: (a) t-2DIR spectrum of the A'(1) vibrational mode, where the ground state bleach (GSB, blue) of the A'(1) mode and the excited state absorptions (ESA, red) of the A'(2) mode and A'(1) mode are clearly seen, complete with crosspeaks between the ESA peaks. The spectrum was collected with a 60 ps time delay between the 400 nm excitation pulse and the 2DIR detection sequence (b). (c) FFCFs of the A'(1) mode in the excited state. The spectral dynamics at two time delays, 60 ps and 20 ps, show identical decay times, indicating that the system has reached equilibrium on the ^{3}MLCT state by 20 ps.

excited state has reached equilibrium. Both FFCF decay functions were fit with single exponentials, $f(t)=a*exp(-x/b)+c$, where a is the amplitude, b is the decay time, and c is the offset. For the 20 ps time delay, a=0.51, b=4.71 ± 0.50 ps, and c=0 and for the 60 ps time delay, a= 0.49, b= 4.71 ± 0.49 ps and c= 0.04. Indeed, the FFCF decays are indistinguishable, indicating that by 20 ps, the ^{3}MLCT state is equilibrated with respect to the non-electronic degrees of freedom.

We also performed the t-2DIR experiment on the A'(1) mode of $Re(CO)_3$(4,4'-tert-butyl-2,2'-bpy)Cl in THF to compare the spectral diffusion times of the unsubstituted and tert-butyl substituted compounds. The spectral diffusion in the electronic ground state (~3.3 ps), which will be discussed in more detail in a later chapter, is slower than the ^{3}MLCT state (~4 ps), but not to the same extent as with the unsubstituted high frequency mode (S_0: ~3 ps, ^{3}MLCT: 4.7 ps). The

more pronounced difference is in the inhomogeneity of the electronic excited state. The contribution of inhomogeneous broadening to an absorption lineshape is determined by the value of the FFCF at t=0, $C(0)$. The initial value of the correlation function reflects the degree to which dephasing during t_1 cannot be reversed by an echo pulse sequence. Generally speaking, the closer

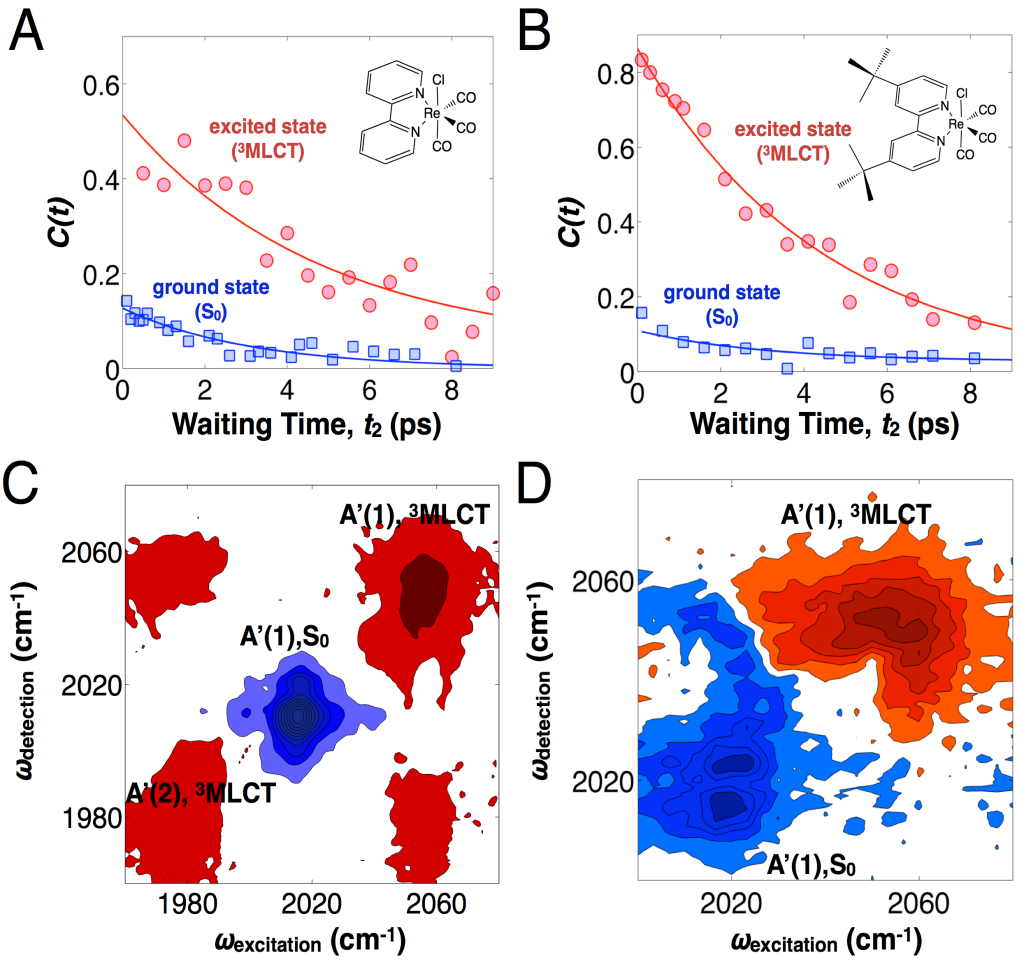

Figure 2.5: (A) the FFCF of $Re(CO)_3(bpy)Cl$ in THF in the S_0 state (blue squares) and the ^{3}MLCT state (red circles); (B) the FFCF of $Re(CO)_3$(4,4'-*tert*-butyl-bpy)Cl in THF in the S_0 state (blue squares) and the ^{3}MLCT state (red circles); (C) difference spectrum of $Re(CO)_3(bpy)Cl$ in THF; (D) difference spectrum of $Re(CO)_3$(4,4'-*tert*-butyl-bpy)Cl in THF.

to 1 the initial value of the correlation function is, the more the lineshape is dominated by inhomogeneous, and, hence, reversible, broadening. The inhomogeneity for both the unsubstituted and substituted compounds was found to be the same at ~0.1. Upon electronic excitation, however, the inhomogeneity of the high frequency mode of $Re(CO)_3(bpy)Cl$ increases as evidenced by an intercept of 0.56, while the intercept of the same mode of $Re(CO)_3$(4,4'-tert-butyl-2,2'-bpy)Cl becomes 0.86 (**Figure 2.5A,B**). It remains to be determined what the origin of this

pronounced increase in inhomogeneity is, and how it depends on solvent. Future studies using molecular dynamics simulations performed using alternatively the geometry, force field, and charges for the ground and excited state species may help to pinpoint the structural and dynamical changes associated with the charge redistribution.

In addition to the high-frequency symmetric mode, we also recorded the t-2DIR spectra

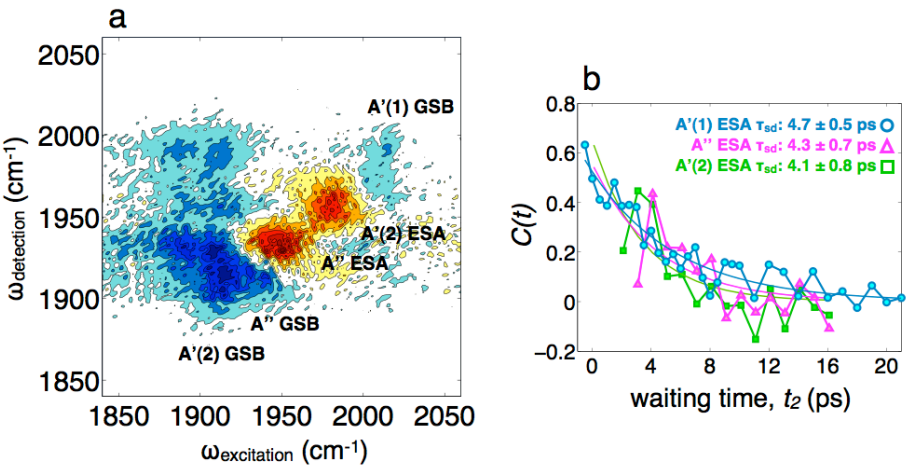

Figure 2.6: (a) t-2DIR spectrum of the A'' and A'(2) vibrational modes showing clear ESAs for the A'(2) and A'' modes, as well as GSBs with cross peaks. The ESA modes are labeled according to work done by Hamm and coworkers. (b) Excited state FFCFs for the three vibrational modes, showing nearly identical decay times. Compared to the ground state spectral dynamics, the modes in the excited state experience slower spectral diffusion, indicating slower solvent fluctuations around the excited state structure.

and FFCFs of the two low-frequency modes of $Re(CO)_3(bpy)Cl$, which are far weaker and more challenging to measure (**Fig 2.6a**). In the ^{3}MLCT state, two asymmetric modes exhibit spectral diffusion on the same time scale as the symmetric mode (**Fig 2.6b**). The lack of pronounced spectral broadening in the excited state is likely due to the fact that the energy separation of the singlet and triplet excited states is not large enough to produce a noticeable temperature increase (**Fig 2.6a**).

2.4 DISCUSSION

Based on the 2DIR measurements of carbonyl spectral diffusion and vibrational relaxation, the ground and excited triplet states of $Re(CO)_3(bpy)Cl$ exhibit markedly distinct dynamics. The FFCF decay, often taken to be a measure of solvation dynamics, is threefold slower in the ^{3}MLCT excited state relative to the ground singlet state S_0. In contrast, vibrational energy relaxation is 8

times *faster* in the ^{3}MLCT state (S_0: ~25 ps; ^{3}MLCT: ~3.2 ps). Besides differences in timescales, the A'(1) vibrational mode, which appears mostly homogeneously broadened in the ground state, becomes more inhomogeneously broadened in the excited state, exhibiting spectral diffusion on the same time scale as the other carbonyl modes. Due to the *trans*-influence, changes in electron density of the bipyridine ligand likely influence the equatorial carbonyls more than the axial carbonyl upon MLCT, leading to an unequal redistribution of electron density. In this new electronic environment, several structural and dynamical changes can combine to produce new spectral and energy relaxation dynamics, as discussed below.

In general, changes in spectral dynamics as sensed by the FFCF can be attributed to three largely separate origins. First, changes in solvent friction can alter the microscopic collisions and solvation shell dynamics, as we have detailed in studies of rigid metal carbonyl complexes used specifically to probe solvation [34]. Second, differences in the solute's electrostatic profile (eg. dipole moment, polarizability, etc.) can modify the solute-solvent coupling, solvation dynamics, and solvent packing. Third, subtle changes in the solute's electronic structure—changes that may be insufficient to substantially alter the solvation dynamics directly—could modify how the probed vibrational frequencies vary due to environmental or structural fluctuations. It is a major challenge for future work to accurately model the mapping of vibrational frequencies to both internal structural deformations and to electrostatic fluctuations of the solvation environment. It is a major challenge for future work to accurately model the mapping of vibrational frequencies to both internal structural deformations and to electrostatic fluctuations of the solvation environment.

Solvent Dynamics. The dramatic threefold slowdown in the FFCF on the excited state is unlikely to be due entirely to changes in solvent dynamics. In previous work using rigid complexes, we found straightforward linear dependencies of spectral diffusion on solvent viscosity using the linear alcohol series [30]. Remarkably, the calibration obtained earlier with cyclopentadienyl manganese tricarbonyl predicts a spectral diffusion time of 1.7 ps in THF (viscosity = 0.46 cP), which agrees quantitatively with our measured value for $Re(CO)_3(bpy)Cl$. To achieve the measured slowdown

would require a viscosity of 3.8 cP, an 8-fold increase. Hence, it is unlikely that the ^{3}MLCT state rigidifies the local solvent shell to this degree.

Change in Dielectric Friction. Upon charge transfer, the electron density rearranges, causing the molecular dipole moment to change in both magnitude and direction. Hence, dipolar and polarizability interactions with the solvent likely occur with different magnitudes in the electronic ground and excited states. A key advantage of using equilibrium and transient 2D-IR to probe different electronic states is that those states can be interrogated separately. Electronic spectroscopy methods, such as time-resolved fluorescence monitor the changes in the electronic energy gap, thus mixing ground and excited state dynamics. Nevertheless, our results are consistent with numerous time-resolved fluorescence measurements of polar solvation interpretation within the framework of continuum solvent models. The decreased magnitude of the ^{3}MLCT dipole moment (5.8 D) relative to that of the ground state (14.1 D) leads to reduced solvent dielectric friction due to weaker interactions with the solvent[35]. Since the dielectric friction scales as the square of the permanent dipole moment, we would predict a ~6-fold slowdown.

Our calculations of one measure of the electrostatic profile, the permanent dipole moment, of $Re(CO)_3(bpy)Cl$ in its ground singlet (S_0) and lowest excited triplet (^{3}MLCT) states show a pronounced ~8.3 Debye (D) decrease upon electronic excitation. The basic physics of polar solvation is relatively well understood, and many measurements of dynamic Stokes shifts have been used to characterize the nonequilibrium solvation dynamics accompanying and following the charge redistribution caused by optical excitation[35]. In many careful studies, the validity of linear response theory has been tested and found to hold, particularly by supporting the experiments with molecular simulation[36]. In developing a molecular interpretation of polar solvation, it has been fruitful to partition the solvent response into two categories distinguished by their range of interactions. That is, the response is separated into short-range dispersive forces (i.e. close collisions), and long-range electrostatics.[35] In adopting a reduced description of the system, where one focuses only on a small spectroscopically addressable subset of the degrees of freedom, it is customary to invoke dissipative dynamics via some sort of friction. Hence, the friction may be likewise partitioned into that arising from short-range collisions, and long-range electrostatics.

This latter contribution, which is denoted "dielectric friction," is most influenced by the change in the charge density within a solute molecule. The concept of dielectric friction was originally due to Nee and Zwanzig,[37] and was updated to help analyze dynamic Stokes shift measurements by van der Zwan and Hynes[38]. Careful work by Maroncelli put the concept of continuum dielectric friction on solid footing in the context of his extensive systematic studies of coumarin 153 in a wide range of solvents[35].

Assuming that there are no significant changes to any solvent parameters, and only the solute's dipole moment is modified by electronic excitation, we can compare the relative dielectric friction ζ_{NZ} for two electronic states with dipole moment magnitudes μ_{ground} and μ_{excite}, respectively as:

$$\frac{\zeta_{NZ,ground}}{\zeta_{NZ,excite}} = \frac{\mu_{ground}^2}{\mu_{excite}^2} \qquad (2.2)$$

Thus, changes in the dielectric friction can be straightforwardly mapped to the changes in the solute's permanent dipole moment. In the present case, where the computed dipole moments are 14.1 D (S_0) and 5.8 D (^{3}MLCT), we would estimate a relative friction of $14.1^2/5.8^2 = 6$, which is within a factor of two of the observed three-fold slowdown of excited state spectral diffusion relative to that on the ground state. Since greater dielectric friction induces faster solvation dynamics due to stronger coupling to the continuum dielectric, we would likewise expect faster spectral diffusion on the ground state, which is predicted to have a 6-fold increase in dielectric friction. Maroncelli's study found that solvation times estimated from calculated dielectric friction typically overestimate the effect of dielectric friction by roughly 40%. While we would not necessarily expect quantitative agreement with dynamic fluorescence Stokes shift measurements, it is encouraging to see similar trends using the substantially different observable of equilibrium and transient 2D-IR spectroscopy. Although the magnitude of the friction change is roughly twice the observed dynamical slowdown, the quantitative link between dielectric friction and vibrational spectral diffusion remains an open question. Indeed, this work is the first report of spectral

diffusion on different electronic states, and clearly future studies will investigate continuum dielectric friction further.

Change in Molecular Flexibility. The final factor that may contribute to the spectral diffusion slowdown from ground to electronic excited state involves the flexibility of the molecule. When the MLCT occurs, -back bonding weakens and the C O bonds strengthen causing the carbonyl stretching bands to blue shift. On the other hand, DFT calculations also show a collective red-shift of low frequency skeletal modes in the excited state relative to the ground state. Increased flexibility has both energetic and dynamical consequences. Red-shifted low-frequency modes increase the vibrational entropy in the excited state. Our DFT results indicate a small 2.5 cal mol^{-1} K^{-1} change in vibrational entropy between the ground and excited ^{3}MLCT states, corresponding to a negligible ~0.3% change in the number of accessible microstates. Given this small entropic difference, the enhanced flexibility of the excited state likely contributes only dynamically to the slowdown in spectral diffusion. In analogy with isolated molecule studies of intramolecular vibrational redistribution, where lowered torsional barriers were found to facilitate faster vibrational energy transfer by increasing anharmonic couplings, it is possible that the much faster vibrational relaxation within the ^{3}MLCT state is due to the softening of the skeletal modes [39]. Thus, both observed trends of faster vibrational relaxation and slower spectral diffusion are understandable using appropriate applications of isolated molecule dynamics and of continuum solvation dynamics. Hence, we are optimistic that the role of "solvent effects" in determining energetic and dynamical aspects of excited state photocatalysis will be systematically understood and controlled.

2.5 CONCLUSION

Equilibrium two-dimensional infrared spectroscopy and transient two-dimensional infrared spectroscopy were used to completely characterize the spectral dynamics in the ground S_0 electronic state and ^{3}MLCT excited state species, respectively, of the photocatalyst $Re(CO)_3(bpy)Cl$. In THF, the ^{3}MLCT excited state undergoes spectral diffusion that is three times slower than its ground state counterpart (S_0: ~1.4 ps; ^{3}MLCT: ~ 4.5 ps), and vibrational relaxation that nearly an order of magnitude faster (S_0: ~25 ps; ^{3}MLCT: ~3.2 ps). We attribute the difference

in spectral dynamics to multiple sources including changes in solvent friction and the solute's electronic structure, which modifies the catalyst's electrostatic profile.

The electronic ground state spectral dynamics are found to be solvent dependent. A similar solvent dependence on the electronic excited state dynamics could alter the photocatalyst's selectivity and efficiency for one or more steps in the complex photocycle. It is known that solvent fluctuations underlie the microscopic dynamics of charge transfer processes through changes in solvation structure, coupling, and dynamics[36-37]. Such changes throughout the photocatalytic cycle may influence selectivity, turnover number, and overall catalytic efficiency. Many investigators have studied the effects of solvent in the overall catalytic cycle of rhenium-bipyridyl complexes, finding that the solvent plays a large role in product selectivity as well as during key steps where the solvent itself coordinates to the Re center. Despite the appreciation that the solvent plays such an important role in the overall photocatalytic cycle, few comparative solvent studies have been performed on the initiation step of the catalysis. Our work shows that it is indeed possible to extract the full array of spectral dynamics (spectral diffusion, vibrational relaxation, and vibrational energy transfer) of the ^{3}MLCT excited state from demanding transient 2D IR experiments. Moreover, we show that it is possible to reference the observed changes to a completely characterized ground electronic state species, where very high level structural and quantum chemical data are available or straightforwardly obtained. Such experiments offer an opportunity to elucidate the role of each solvent in a particular outcome, such as the generation of a desired product or high catalytic efficiency. The first step will be to characterize the dynamical solvent effects at multiple stages within the catalytic cycle, including the initiation step, where we have now successfully characterized THF. In future work, we will apply this powerful spectroscopic method to species visited along the complex photocycle, including chemical modifications to the pseudohalide and bipyridyl ligands. This study highlights the power of transient 2DIR spectroscopy to provide novel perspectives into the fundamental dynamics of photocatalysts just as they are poised to carry out their function.

REFERENCES

1. Morris, A. J.; Meyer, G. J.; Fujita, E., Molecular Approaches to the Photocatalytic Reduction of Carbon Dioxide for Solar Fuels. *Acc. Chem. Res.* 2009, *42* (12), 1983-1994.

2. Liard, D. J.; Busby, M.; Matousek, P.; Towrie, M.; Vlček, A., Picosecond Relaxation of ^{3}MLCT Excited States of $[Re(Etpy)(CO)_3(dmb)]^+$ and $Re(Cl)(CO)_3(bpy)$ as Revealed by Time-Resolved Resonance Raman, UV-vis, and IR Absorption Spectroscopy. *Journal of Physical Chemistry A* 2004, *108* (13), 2363-2369.

3. Cannizzo, A.; Blanco-Rodriguez, A. M.; El Nahhas, A.; Sebera, J.; Zalis, S.; Vlček, A.; Chergui, M., Femtosecond Fluorescence and Intersystem Crossing in Rhenium(I) Carbonyl-Bipyridine Complexes. *J. Am. Chem. Soc.* 2008, *130* (28), 8967-8974.

4. El Nahhas, A.; Consani, C.; Blanco-Rodriguez, A. M.; Lancaster, K. M.; Braem, O.; Cannizzo, A.; Towrie, M.; Clark, I. P.; Zalis, S.; Chergui, M.; Vlček, A., Ultrafast Excited-State Dynamics of Rhenium(I) Photosensitizers $Re(Cl)(CO)_3(N,N)$ and $[Re(imidazole)(CO)_3(N,N)]^+$: Diimine Effects. *Inorg. Chem.* 2011, *50* (7), 2932-2943.

5. Asbury, J. B.; Wang, Y. Q.; Lian, T. Q., Time-Dependent Vibration Stokes Shift During Solvation: Experiment and Theory. *Bull. Chem. Soc. Jpn.* 2002, *75* (5), 973-983.

6. Stufkens, D. J.; Vlček, A., Ligand-Dependent Excited State Behaviour of Re(I) and Ru(II) Carbonyl-Diimine Complexes. *Coordination Chemistry Reviews* 1998, *177*, 127-179.

7. Dattelbaum, D. M.; Omberg, K. M.; Schoonover, J. R.; Martin, R. L.; Meyer, T. J., Application of Time-Resolved Infrared Spectroscopy to Electronic Structure in Metal-to-Ligand Charge-Transfer Excited States. *Inorganic Chemistry* 2002, *41* (23), 6071-6079.

8. El Nahhas, A.; Cannizzo, A.; van Mourik, F.; Blanco-Rodriguez, A. M.; Zalis, S.; Vlček, A.; Chergui, M., Ultrafast Excited-State Dynamics of $[Re(L)(CO)_3(bpy)]^n$ Complexes: Involvement of the Solvent. *J. Phys. Chem. A* 2010, *114* (22), 6361-6369.

9. Heydova, R.; Gindensperger, E.; Romano, R.; Sykora, J.; Vlček, A., Jr.; Zalis, S.; Daniel, C., Spin-Orbit Treatment of UV-vis Absorption Spectra and Photophysics of Rhenium(I) Carbonyl-Bipyridine Complexes: MS-CASPT2 and TD-DFT Analysis. *Journal of Physical Chemistry A* 2012, *116* (46), 11319-11329.

10. Sato, S.; Matubara, Y.; Koike, K.; Falkenstrom, M.; Katayama, T.; Ishibashi, Y.; Miyasaka, H.; Taniguchi, S.; Chosrowjan, H.; Mataga, N.; Fukazawa, N.; Koshihara, S.; Onda, K.; Ishitani, O., Photochemistry of *fac*-Re(bpy)$(CO)_3$Cl. *Chem. Eur. J.* 2012, *18* (49), 15722-15734.

11. Bredenbeck, J.; Hamm, P., Transient 2D-IR Spectroscopy: Towards a Molecular Movie. *Chimia* 2007, *61* (1-2), 45-46.

12. Bredenbeck, J.; Helbing, J.; Kolano, C.; Hamm, P., Ultrafast 2D-IR Spectroscopy of Transient Species. *Chemphyschem* 2007, *8* (12), 1747-1756.

13. Chung, H. S.; Ganim, Z.; Jones, K. C.; Tokmakoff, A., Transient 2D IR Spectroscopy of Ubiquitin Unfolding Dynamics. *Proceedings of the National Academy of Sciences of the United States of America* 2007, *104* (36), 14237-14242.

14. Chung, H. S.; Khalil, M.; Smith, A. W.; Tokmakoff, A., Transient Two-Dimensional IR Spectrometer for Probing Nanosecond Temperature-Jump Kinetics. *Review of Scientific Instruments* 2007, *78* (6).

15. Baiz, C. R.; McCanne, R.; Nee, M. J.; Kubarych, K. J., Orientational Dynamics of Transient Molecules Measured by Nonequilibrium Two-Dimensional Infrared Spectroscopy. *Journal of Physical Chemistry A* 2009, *113* (31), 8907-8916.

16. King, J. T.; Ross, M. R.; Kubarych, K. J., Water-Assisted Vibrational Relaxation of a Metal Carbonyl Complex Studied with Ultrafast 2D-IR. *Journal of Physical Chemistry B* 2012, *116* (12), 3754-3759.

17. Rosenfeld, D. E.; Gengeliczki, Z.; Smith, B. J.; Stack, T. D. P.; Fayer, M. D., Structural Dynamics of a Catalytic Monolayer Probed by Ultrafast 2D IR Vibrational Echoes. *Science* 2011, *334* (6056), 634-639.

18. Vlček, A., Ultrafast Excited-State Processes in Re(I) Carbonyl-Diimine Complexes: From Excitation to Photochemistry. In *Photophysics of Organometallics*, Lees, A. J., Ed. 2010; Vol. 29, pp 73-114.

19. El Nahhas, A.; van der Veen, R. M.; Penfold, T. J.; Pham, V. T.; Lima, F. A.; Abela, R.; Blanco-Rodriguez, A. M.; Zalis, S.; Vlček, A.; Tavernelli, I.; Rothlisberger, U.; Milne, C. J.; Chergui, M., X-ray Absorption Spectroscopy of Ground and Excited Rhenium-Carbonyl Diimine-Complexes: Evidence for a Two-Center Electron Transfer. *Journal of Physical Chemistry A* 2013, *117* (2), 361-369.

20. Ogilvie, J. P.; Kubarych, K. J., Multidimensional Electronic and Vibrational Spectroscopy: An Ultrafast Probe of Molecular Relaxation and Reaction Dynamics. In *Advances in Atomic, Molecular, and Optical Physics, Vol 57*, Arimondo, E.; Berman, P. R.; Lin, C. C., Eds. 2009; Vol. 57, pp 249-321.

21. Roberts, S. T.; Loparo, J. J.; Tokmakoff, A., Characterization of spectral diffusion from two-dimensional line shapes. *J. Chem. Phys.* 2006, *125* (8).

22. Huber, C. J.; Anglin, T. C.; Jones, B. H.; Muthu, N.; Cramer, C. J.; Massari, A. M., Vibrational Solvatochromism in Vaska's Complex Adducts. *Journal of Physical Chemistry A* 2012, *116* (37), 9279-9286.

23. Jones, B. H.; Huber, C. J.; Massari, A. M., Solvation Dynamics of Vaska's Complex by 2D-IR Spectroscopy. *Journal of Physical Chemistry C* 2011, *115* (50), 24813-24822.

24. Bredenbeck, J.; Helbing, J.; Hamm, P., Solvation Beyond the Linear Response Regime. *Physical Review Letters* 2005, *95* (8).

25. Bredenbeck, J.; Helbing, J.; Behrendt, R.; Renner, C.; Moroder, L.; Wachtveitl, J.; Hamm, P., Transient 2D-IR Spectroscopy: Snapshots of the Nonequilibrium Ensemble During the Picosecond Conformational Transition of a Small Peptide. *Journal of Physical Chemistry B* 2003, *107* (33), 8654-8660.

26. Baiz, C. R.; McCanne, R.; Kubarych, K. J., Structurally Selective Geminate Rebinding Dynamics of Solvent-Caged Radicals Studied with Nonequilibrium Infrared Echo Spectroscopy. *Journal of the American Chemical Society* 2009, *131* (38), 13590.

27. Cervetto, V.; Hamm, P.; Helbing, J., Transient 2D-IR Spectroscopy of Thiopeptide Isomerization. *Journal of Physical Chemistry B* 2008, *112* (28), 8398-8405.

28. Bredenbeck, J.; Helbing, J.; Hamm, P., Labeling Vibrations by Light: Ultrafast Transient 2D-IR Spectroscopy Tracks Vibrational Modes During Photoinduced Charge Transfer. *Journal of the American Chemical Society* 2004, *126* (4), 990-991.

29. Xiong, W.; Laaser, J. E.; Paoprasert, P.; Franking, R. A.; Hamers, R. J.; Gopalan, P.; Zanni, M. T., Transient 2D IR Spectroscopy of Charge Injection in Dye-Sensitized Nanocrystalline Thin Films. *J. Am. Chem. Soc.* 2009, *131* (50), 18040.

30. King, J. T.; Baiz, C. R.; Kubarych, K. J., Solvent-Dependent Spectral Diffusion in a Hydrogen Bonded "Vibrational Aggregate". *Journal of Physical Chemistry A* 2010, *114* (39), 10590-10604.

31. Jansen, T. L. C.; Cringus, D.; Pshenichnikov, M. S., Dissimilar Dynamics of Coupled Water Vibrations. *J. Phys. Chem. A* 2009, *113* (22), 6260-6265.

32. Zhong, Q.; Fourkas, J. T., Optical Kerr Effect Spectroscopy of Simple Liquids. *J. Phys. Chem. B* 2008, *112* (49), 15529-15539.

33. Frisch, M. J.; Trucks, G. W.; Schlegel, H. B.; Scuseria, G. E.; Robb, M. A.; Cheeseman, J. R.; Scalmani, G.; Barone, V.; Mennucci, B.; Petersson, G. A.; Nakatsuji, H.; Caricato, M.; Li, X.; Hratchian, H. P.; Izmaylov, A. F.; Bloino, J.; Zheng, G.; Sonnenberg, J. L.; Hada, M.; Ehara, M.; Toyota, K.; Fukuda, R.; Hasegawa, J.; Ishida, M.; Nakajima, T.; Honda, Y.; Kitao, O.; Nakai, H.; Vreven, T.; Montgomery Jr., J. A.; Peralta, J. E.; Ogliaro, F.; Bearpark, M. J.; Heyd, J.; Brothers, E. N.; Kudin, K. N.; Staroverov, V. N.; Kobayashi, R.; Normand, J.; Raghavachari, K.; Rendell, A. P.; Burant, J. C.; Iyengar, S. S.; Tomasi, J.; Cossi, M.; Rega, N.; Millam, N. J.; Klene, M.; Knox, J. E.; Cross, J. B.; Bakken, V.; Adamo, C.; Jaramillo, J.; Gomperts, R.; Stratmann, R. E.; Yazyev, O.; Austin, A. J.; Cammi, R.; Pomelli, C.; Ochterski, J. W.; Martin, R. L.; Morokuma, K.; Zakrzewski, V. G.; Voth, G. A.; Salvador, P.; Dannenberg, J. J.; Dapprich, S.; Daniels, A. D.; Farkas, Ö.; Foresman, J. B.; Ortiz, J. V.; Cioslowski, J.; Fox, D. J. *Gaussian 09*, Gaussian, Inc.: Wallingford, CT, USA, 2009.

34. Anna, J. M.; Kubarych, K. J., Watching Solvent Friction Impede Ultrafast Barrier Crossings: A Direct Test of Kramers Theory. *Journal of Chemical Physics* 2010, *133* (17).

35. Maroncelli, M., Continuum Estimates of Rotational Dielectric Friction and Polar Solvation. *Journal of Chemical Physics* 1997, *106* (4), 1545-1555.

36. Heitele, H., Dynamic Solvent Effects on Electron-Transfer Reactions. *Angew. Chem. Int. Ed.* 1993, *32* (3), 359-377.

37. Maroncelli, M.; Macinnis, J.; Fleming, G. R., Polar-Solvent Dynamics and Electron-Transfer Reactions. *Science* 1989, *243* (4899), 1674-1681.

38. Anna, J. M.; Nee, M. J.; Baiz, C. R.; McCanne, R.; Kubarych, K. J., Measuring Absorptive Two-Dimensional Infrared Spectra Using Chirped-Pulse Upconversion Detection. *J. Opt. Soc. Am. B* 2010, *27* (3), 382-393.

39. Perry, D. S.; Bethardy, G. A.; Wang, X. L., The Effect of the Torsional Barrier Height on the Acceleration of Intramolecular Vibrational-Relaxation (IVR) by Molecular Flexibility. *Berichte Der Bunsen-Gesellschaft-Physical Chemistry Chemical Physics* 1995, *99* (3), 530-535.

Chapter 3

Solvent-Dependent Dynamics of a Series of Rhenium Photo-Activated Catalysts Measured with Ultrafast 2DIR

The work presented in this chapter has been published in the following paper:

L. M. Kiefer and K. J. Kubarych, "Solvent-Dependent Dynamics of a Series of Rhenium Photoactivated Catalysts Measured with Ultrafast 2DIR", J. Phys. Chem. A, **119**, 959 (2015)

3.1 INTRODUCTION

A promising solution to the increases in greenhouse gas emissions is to use sunlight to power the photocatalytic reduction of CO_2, thus removing the gas while regenerating useful chemicals. Over the past three decades, much research has focused on the Lehn catalyst, a rhenium-based photo-initiated CO_2 reduction catalyst. It has been investigated by virtually all analytical methods in an effort to unveil aspects of the catalytic reduction of CO_2 to CO[1-17]. Efforts have concentrated on the possible mechanisms and improving the efficiency of the catalyst *fac*-Re(4,4'-R_2-bpy)$(CO)_3$X by replacing the axial ligand X, adding substituents R to the bipyridine, or by changing the solvent conditions[18-20]. The catalytic efficiency, often measured by turn-over number, turn-over frequency, or quantum yield has been shown to depend on the substituents (R) for a fixed choice of monodentate axial ligand (X). The turn-over-frequency of the catalysis also depends on whether the complex is photo-activated with a sacrificial electron donor, or if it is electrochemically reduced. Kubiak *et al*. find that when the catalysis is conducted electrochemically, the t-butyl substituted rhenium compound, *fac*-Re(4,4'-*tert*-butyl-bpy)$(CO)_3$X,

performs best when chloride is the halide ligand[5]. Under the conditions of photo-initiation, and in the presence of a sacrificial electron donor (TEOA), Alberto et al. find that the unsubstituted, *fac*-$Re(bpy)(CO)_3X$ is most efficient over a long period when bromide is the halide ligand[21]. Determining the best combination of substituent/monodentate ligand is a difficult combinatorial challenge, and has not been fully explored. The catalysis is also dependent on X, and both electrochemically and photo-induced catalysis experiments report that SCN^- and $P(OEt)_3$ produce the highest quantum yields[4, 22]. Most of the catalysis is conducted in the solvents tetrahydrofuran (THF), acetonitrile (CH_3CN), dimethylformamide or a combination of two of them[10, 23]. Clearly, even optimizing this small complex involves a rather large design space.

Because the electronic excited state plays a crucial role in the photo-initiated catalysis, we recently investigated the spectral dynamics of the electronic excited state and showed how it differs from the electronic ground state[24]. Relative to the singlet (S_0) ground electronic state, we observed a three-fold slowdown of solvation dynamics in the ^{3}MLCT state. This result was attributed to multiple factors, one of them being dielectric friction arising from the coupling of the molecular dipole moment to the solvating continuum dielectric medium. Performing DFT calculations, we found the S_0 state to have a permanent dipole moment of 14.1 D, which decreases to 5.8 D in the ^{3}MLCT state. This pronounced change would lead to a decreased dielectric friction in the ^{3}MLCT state, contributing to the slowdown in the dynamics. Based on theoretical extensions of the original Nee-Zwanzig dielectric friction by van der Zwan and Hynes, as well as by Maroncelli[25, 26], we would predict a six-fold slowdown in dynamics, which qualitatively agrees with our results. The change in permanent dipole moment between the electronic states inspired our current investigation: how much does the dipole moment alone contribute to spectral diffusion? Since it is straightforward to modify the complex and alter the dipole moment, we synthesized a series of derivatives in order to determine what effect, if any, a change in charge distribution would have on the sensed solvation dynamics. The second goal of this study was to determine the role of the solvent in altering the spectral diffusion times in molecules that are similar, but which contain slight differences in the local electron densities at or near the carbonyl probes induced by distant substitutions on the bipyridine ring. Finally, we investigate the spectral dynamics of a series

of rhenium-bipyridyl catalysis in multiple aprotic solvents, in order to assess the degree to which these intramolecular modifications alter the relative changes in solvation dynamics.

3.2 EXPERIMENTAL METHODS

We synthesized the molecules *fac*-Re(4,4'-R_2-bpy)$(CO)_3Cl$, where R=H (**ReCl**), methyl (**DMB**), *tert*-butyl (***t*-Butyl**), and carboxylic acid (**COOH**), as well as the related complex Re(1,10-

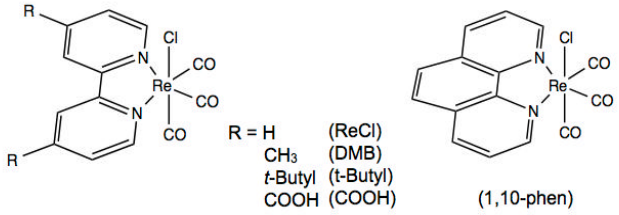

Figure 3.1: Structures of rhenium photocatalysts involved in this study. Abbreviations used in the text are given in parentheses.

phenanthroline)$(CO)_3Cl$ (**1,10-phen**) according to previously published methods (**Figure 3.1**)[5, 27]. The substituents on the bipyridine were selected for the changes they induce in the electron density *trans* to the equatorial carbonyls as well as possible steric effects due to the bulkier substituents. It is noteworthy that we only selected substituents that are symmetric on the bipyridine, and that asymmetric substitutions, such as only at the 4' position on the bipyridine, may produce different results. These studies are left to future investigations. The solvent set of dimethyl sulfoxide (DMSO), THF and CH_3CN was selected because they are aprotic, have different polarities and are relevant in multiple catalytic and photo-physical studies[28, 29].

2DIR Spectroscopy. This study focuses on the spectral dynamics of rhenium-bipyridine compounds in multiple polar solvents using two-dimensional IR (2DIR) spectroscopy. Our 2DIR setup has been thoroughly described elsewhere[30]. Briefly, we generate infrared light using 800 nm pulses from a regenerative amplifier that pumps two independent optical parametric amplifiers (OPA). The light generated in the OPAs drives two separate GaSe difference frequency generating (DFG) crystals, resulting in ~2000 cm^{-1} (125 cm^{-1} fwhm) light. This infrared light is split into multiple beams: two used to pump the molecule into an vibrationally excited state, one that is used to probe the sample and another pulse to interfere with the emitted signal for heterodyne detection. In our

experimental set-up, we used a non-collinear geometry, so that the emitted signal is in a background-free direction. We perform a rephasing (photon echo) and nonrephasing experiment for each waiting time delay (t_2) between the pump pulses and the probe pulse. A rephasing experiment has the phase matching conditions $\mathbf{k_r=-k_1+k_2+k_3}$, and nonrephasing $\mathbf{k_n=+k_1-k_2+k_3}$. We scan the time between the two pump pulses and then Fourier transform the signal over this scanning time to obtain the excitation frequencies and directly detect, via chirped pulse upconversion, the emitted frequencies. To obtain a frequency fluctuation correlation function (FFCF, $C(t_2)=\langle\delta\omega(0)\delta\omega(t_2)\rangle$, where $\delta\omega(t_2)=\omega(t_2)-\langle\omega\rangle$), an observable unique to 2DIR, we subtract the diagonal peak amplitudes of the nonrephasing experiment (A_n) from those of the rephasing experiment (A_r) at each waiting time (t_2) (**Eq 3.1**). This measure is referred to as the inhomogeneity index $I(t_2)$, and is proportional to the FFCF. The FFCF is a measure of frequency memory, which reports the time scale on which a vibration retains the same transition frequency it had when it was initially excited. The FFCF decays due to "spectral diffusion" of the vibration through its inhomogeneously broadened band by sampling multiple solvent configurations.

$$I(t_2)=\frac{A_r(t_2)-A_n(t_2)}{A_r(t_2)+A_n(t_2)} \qquad (3.1)$$

3.3 RESULTS AND DISCUSSION

The rhenium catalyst *fac*-Re(4,4'-R_2-bpy)$(CO)_3$Cl has three carbonyl vibrational stretching modes: an out-of-phase symmetric mode [A'(2)], an asymmetric mode primarily among the two equatorial carbonyls [A"], and an in-phase symmetric mode [A'(1)]. Though we investigated all three modes, we report detailed analyses of the lowest frequency A'(2) mode in the main text, with the full set of results available in the Supplemental Information (SI).

Linear IR Spectra are Substituent and Solvent Dependent. FTIR spectra of the five complexes in each of the three solvents DMSO, THF and CH_3CH, are shown in **Fig. 3.3A-C**. There are slight systematic frequency shifts which generally follow the trend that COOH > 1,10-Phen > ReCl ≥ DMB ≥ t-butyl. The frequencies are also solvent dependent, though generally the ordering is preserved in each solvent. Solvent-dependent frequencies are ordered as CH_3CN > THF > DMSO, which is

consistent with the relative solvent donicity. The spectral data for all three vibrational stretching modes, including peak positions and widths, are summarized in Table 1.

Spectral Diffusion is Solvent Dependent. To determine the dynamics associated with solvation, we analyzed the decays of the FFCFs obtained from 2DIR spectroscopy (**Figure 3.2**). **Figure 3.3D-F** shows the correlation function decays for the A'(2) mode of each of the five complexes in the three

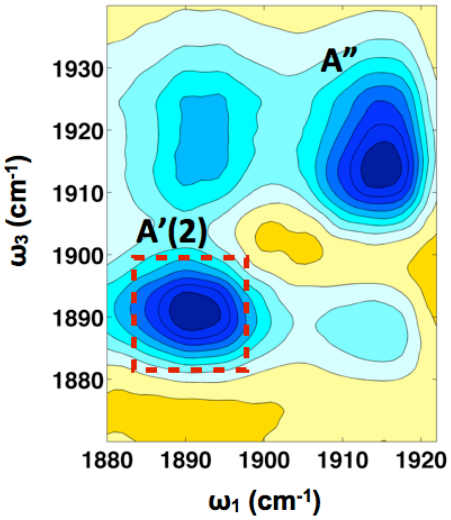

Figure 3.2: Absorptive 2DIR spectrum of the two low-frequency carbonyl stretching modes, A’(2) and A” of *fac*-Re(4,4’-dimethyl-bpy)$(CO)_3Cl$ in THF (t_2 = 22 ps). The peak analyzed in the main text, A’(2), is highlighted in red.

solvents. Surprisingly, we do not observe significant differences in the FFCF decays for the complexes within a particular solvent. Changing solvent, however, does affect the spectral diffusion dynamics essentially identically in the five solutes. All complexes exhibit similar A’(2) mode spectral diffusion times (~4 ps) in DMSO (**Table 3.1**). Likewise, in THF, the spectral diffusion times for this same mode are all near 2.6 ps, with the exception of the unsubstituted Re(bpy)$(CO)_3Cl$. The cause of this discrepancy is unknown. The spectral diffusion times of the A’(2) mode of the complexes in CH_3CN are all roughly 1.4 ps; COOH could not produce reliable results due to scattering. Multiple attempts were made to prevent scattering with this complex, but all methods failed in CH_3CN. These correlation functions exhibit a clear solvent dependence that is much more pronounced than any influences caused by the small changes in electron density imposed by the substitutions, or the steric effects of some of the bulkier substituents distal to the carbonyls. The decrease in the FFCF decay times of the solvents DMSO (~4 ps) > THF (~ 2.6 ps) >

CH_3CN (~1.4 ps) agree with the trend in solvation times reported by Maroncelli et al. determined by dynamic Stokes shift measurements using coumarin 153 as a probe: DMSO (2.0 ps) > THF (0.94 ps) > CH_3CN (0.26 ps)[31]. The unsubstituted Re complex was also studied in dimethylformamide (DMF; DN = 26.6); its A'(2) mode has an FFCF decay time of ~3.3 ps, consistent with the donicity trend. It is worth noting that both low-frequency mode FFCFs decay with essentially the same time constants, whereas the high-frequency A'(1) mode often shows FFCFs decays having different time constants than the other two modes; nevertheless, all three modes exhibit similar time scale decays among the substituted variations. This phenomenon of coupled vibrational modes exhibiting dissimilar dynamics has been observed before in the case of water molecules in

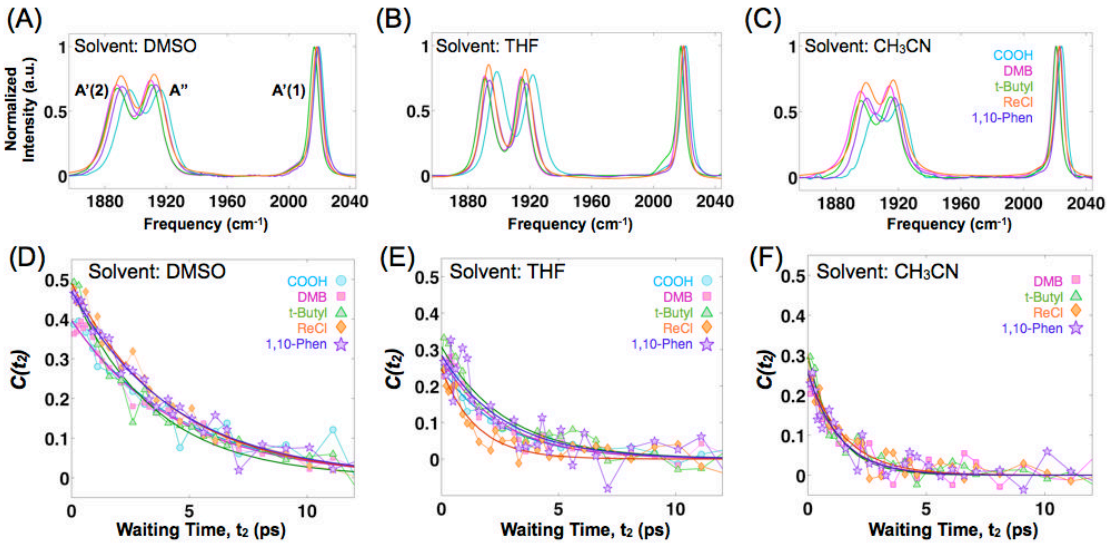

Figure 3.3: The FTIR Spectra of COOH (cyan, circle), DMB (magenta, square), t-Butyl (green,triangle), ReCl (orange, diamond) and 1,10-phen (purple, star) in the solvents DMSO (A), THF (B) and CH_3CN (C); The frequency-fluctuation correlation functions, $C(t_2)$, of the A'(2) vibrational stretching mode of COOH, DMB, t-Butyl, ReCl, and 1,10-phen in the solvents DMSO (D), THF (E) and CH_3CN (F). The FFCF was not obtainable for COOH in the solvent CH_3CN.

acetonitrile by Pshenichnikov et al.[32]. We have also observed similar behavior in other metal carbonyl complexes[33].

The high degree of similarity among the FFCFs of all five complexes is somewhat surprising because the carbonyls themselves have slightly different electronic environments due to the substitutions on the bypiridine ring. The calculated permanent dipole moments for the electron donating substituted or unsubstituted bipryidine compounds are all very similar: (ReCl) 14.1 D,

(DMB) 15.5 D, (t-Butyl) 16.0 D, and (1,10-phen) 14.6 D. The only electron withdrawing substituted bipyridine compound, COOH, has a considerably smaller dipole moment of 8.1 D. While the differences in electron donating or electron withdrawing abilities of the substituents, even minor differences, are apparent in the FTIR, they do not seem to influence the fluctuations of solvent environment. These results suggest that the solvation sensed by the carbonyls is best viewed as being due to the immediately local solvent environment.

Solvent Dependence Correlates with Donor Number. To understand the observed solvent dependence of the spectral diffusion dynamics, we first considered a polarity trend, but find no significant correlation with typical measures of polarity, such as $E_T(30)$[34]. Polarity, however, is a macroscopic property and the carbonyls appear to be sensitive primarily to quite local dynamics, so we had to look more closely at the molecular chemical properties of the solvents. After performing FTIR experiments on the five complexes in DMSO, THF and CH_3CN, and fitting each carbonyl stretching band using a single Gaussian, we have found that the red-shift in the frequencies and the increase in correlation decay times correlate with an increase in the donicity, or donor number (DN) of the solvent (**Table 3.1**). The DN is a measure of nucleophilicity, or of how the solvent acts as a Lewis base[35]. Other studies report a correlation between the acceptor number (AN), a measure of a solvent's electrophilic properties[36], and spectral diffusion and/or solvatochromic frequency shifts[37, 38]. Massari et al. found that the FFCF decay times of oxy-bis(triphenylphosphene) iridium(I) (oxy-Vaska's complex) in benzene, chloroform, and DMF (all aprotic solvents) increased with the AN of the solvents, and found no correlation with the polarity. Khalil et al., however, used both aprotic and protic solvents, and correlated the FFCF decay times of the sodium nitroprusside nitrosyl stretching mode with the solvent AN, finding an anti-correlation with the polarity. Since the DN and AN are not inversely related[35], with our experimental results, we cannot simply state that there is also a trend in AN. Indeed, we find no such correlation when comparing the solvent acceptor numbers.

There is an evident solvatochromic blue-shift in the frequencies going from DMSO to THF to CH_3CN, but the extent of the blue-shift is mode-specific. For instance, the A'(2) modes of the five complexes all blue-shift by 4-5 cm^{-1} going from DMSO to THF, and blue-shift by 5-6 cm^{-1} going from THF to CH_3CN. The A" and A'(1) modes both follow this same trend, but to different degrees

(Table 3.1). We may view, microscopically, the nucleophilic properties of the solvent as individual molecules donating electron density to the carbonyls, which then pushes electron density back towards the metal center. This effect either increases the C–Re σ-bond character or decreases the Re–C π-back bonding character, depending on whether the ligand opposite of the carbonyls is a good π-acceptor or not[39]. If the ligand is a good π-acceptor, then the former applies. Since bpy is such a ligand, the σ-effect dominates and thus we observe a red-shifting the frequencies as the DN increases. Massari *et al*. also observe the same effect when using aprotic solvents where the electrophilicity of the solvent seemed to dominate the solvent-probe interactions. They found that with increased AN, and hence a more electrophilic interaction with the probe, the π-back bonding between the iridium metal center and the carbonyl probe weakened and the frequency of the mode blue-shifted.

Table 3.1. The FTIR center frequencies (fwhm, cm^{-1}), FFCF decay times (ps) of the A'(2) carbonyl stretching mode and solvent donor numbers (DN)[35].

		FTIR (cm^{-1})			FFCF Decay Times (ps)		
Mode	**Molecule**	**DMSO**	**THF**	**CH_3CN**	**DMSO**	**THF**	**CH_3CN**
	COOH	1896 (18.7)	1899 (13.6)	1905 (15.0)	3.6 ± 1.1	2.5 ± 0.6	N/A
	ReCl	1890 (19.9)	1894 (12.8)	1899 (18.4)	4.2 ± 0.4	1.3 ± 0.5	1.6 ± 0.4
A'(2)	1,10-phen	1891 (18.8)	1894 (20.6)	1899 (18.9)	4.4 ± 0.8	2.7 ± 1.1	1.3 ± 0.4
	DMB	1888 (19.8)	1891 (13.3)	1896 (16.2)	4.5 ± 0.7	2.5 ± 0.6	1.4 ± 0.5
	t-Butyl	1888 (19.6)	1891 (14.1)	1896 (16.5)	3.5 ± 0.7	2.7 ± 0.9	1.2 ± 0.3
	COOH	1917 (17.6)	1922 (11.2)	1922 (12.4)	3.5 ± 1.6	2.5 ± 0.9	N/A
	ReCl	1913 (17.1)	1917 (12.7)	1918 (16.0)	3.2 ± 0.5	1.5 ± 0.5	1.7± 0.7
A"	1,10-phen	1914 (17.2)	1917 (18.0)	1918 (16.1)	3.5 ± 0.6	2.8 ± 0.9	1.3 ± 0.4
	DMB	1910 (16.7)	1914 (12.9)	1915 (15.6)	3.8 ± 0.8	2.2 ± 0.6	2.7 ± 2.2
	t-Butyl	1911 (16.4)	1915 (13.3)	1915 (16.3)	3.6 ± 1.2	2.2 ± 0.5	1.2 ± 0.4
	COOH	2020 (8.3)	2021 (6.5)	2025 (6.0)	2.8 ± 1.0	2.4 ± 1.0	N/A
	ReCl	2018 (8.5)	2019 (6.3)	2023 (7.2)	4.5 ± 0.9	3.1 ± 0.8	1.7 ± 0.7
A'(1)	1,10-phen	2019 (9.3)	2020 (8.7)	2023 (6.1)	3.5 ± 1.2	2.3 ± 1.7	1.7 ± 1.4
	DMB	2017 (7.6)	2018 (5.8)	2021 (6.0)	2.4 ± 0.7	4.6 ± 1.8	0.9 ± 1.3
	t-Butyl	2017 (8.1)	2018 (8.1)	2021 (6.6)	3.5 ± 0.9	1.0 ± 0.6	2.4 ± 1.4
	Solvent DN (kcal mol^{-1})	*29.8*	*20.0*	*14.0*	*29.8*	*20.0*	*14.0*

To assess the degree to which any of the solvent dependencies could be linked to continuum dielectric properties, we performed DFT calculations on the Re(bpy)$(CO)_3$Cl molecule in the solvents THF, DMSO, and CH_3CN. We used the functional PBEO (PBE1PBE), the basis 6-31+G(d) (LanL2DZ pseudopotential for Re) and CPCM (polarizable conductor calculation model) method for the solvent[40]. The frequency calculation results are shown in **Figure 3.4(B)**. **Figure 3.4(A)** shows the experimental central frequencies of the three carbonyl stretching modes acquired from FTIR and fitted using one Gaussian for each mode. The center frequencies either

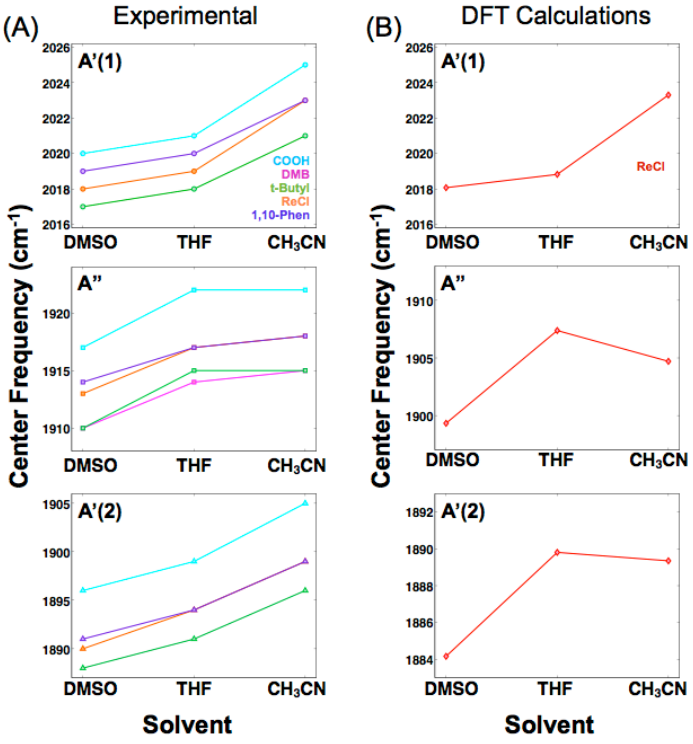

Figure 3.4: Experimental center frequencies of the A'(1) (A, top), A" (A, middle), and A'(2) (A, bottom) modes of COOH, DMB, t-Butyl, ReCl, and 1,10-phen in the solvents DMSO, THF and CH_3CN; DFT calculated center frequencies of the A'(1) (B, top), A" (B, middle), and A'(2) (B, bottom) modes of ReCl in the solvents DMSO, THF and CH_3CN using the CPCM solvent model.

increase or remain the same as the solvent DN decreases. The DFT calculated frequencies were scaled to reproduce the experimental A'(1) mode frequencies in the respective solvent. This mode was selected because it shows the most modest solvatochromic shift from solvent to solvent compared to the other two, and scaling factors are not transferable from solvent to solvent[41]. Using this technique, the DFT calculated frequencies decrease going from THF to CH_3CN, indicating that the polarizable conductor model does not accurately predict the observed solvatochromic

shift. This discrepancy implies that the solvatochromic shift is sensitive to the detailed molecular structure and electrostatic profile of the solvent shell. Future straightforward extensions of the present study will use QM/MM to compute vibrational frequencies for solvated clusters.

Finally, we address the apparent discrepancy between our ground electronic state series of rhenium bipyridyl carbonyl derivatives and the excited state study of the ReCl complex reported previously. The key finding from our previous work was to recognize that the spectral diffusion time scales slowed roughly three-fold in the ^{3}MLCT excited state relative to the S_0 ground state. Though we discussed several possible origins, we identified changes in the dielectric friction in

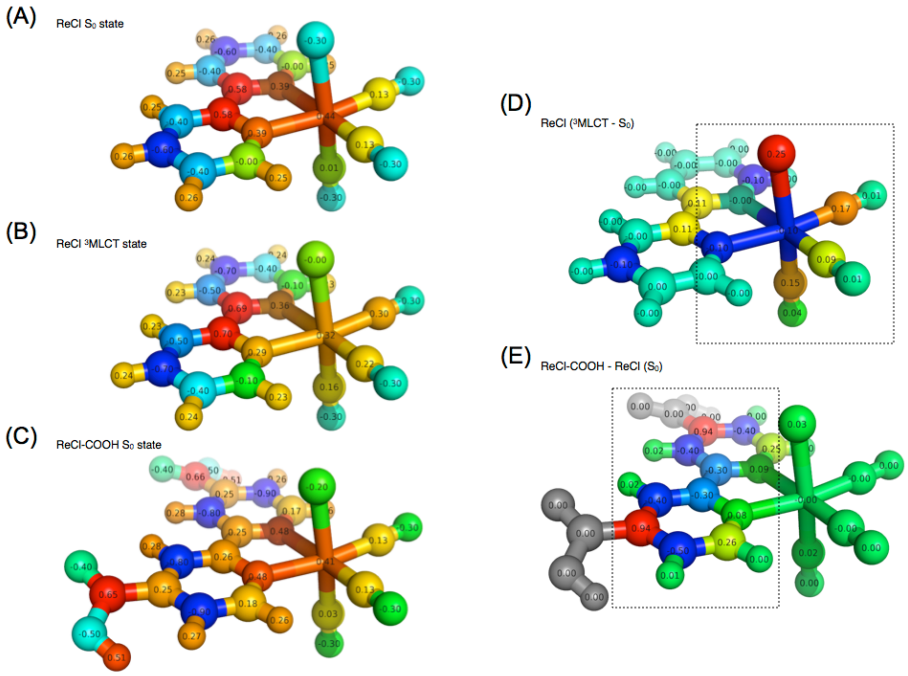

Figure 3.5: Mulliken charges obtained from DFT calculations of $Re(CO)_3(bpy)Cl$ (S_0 state; **(A)**), $Re(CO)_3(bpy)Cl$ (^{3}MLCT state; **(B)**), and $Re(CO)_3(4,4'$-di-COOH-bpy$)Cl$ **(C)**. The changes in partial charges between the ^{3}MLCT and S_0 states of $Re(CO)_3(bpy)Cl$ **(D)** and between $Re(CO)_3(4,4'$-di-COOH-bpy$)Cl$ and $Re(CO)_3(bpy)Cl$ **(E)**. In (D) and (E) the dashed box indicates the sites where charges change the most.

particular, since there was clear evidence from the DFT computational results for a smaller molecular dipole moment in the excited state. In the present case, however, the carboxylic acid derivative also has smaller overall molecular dipole moment, and would have been expected to exhibit slower spectral diffusion dynamics based on the dielectric friction argument. In the two solvents (DMSO and THF) where we were able to obtain reliable results, we find that the time

scales are essentially indistinguishable from the other derivatives. The central frequencies, which shift only about 5-6 cm^{-1} relative to ReCl, indicate that it is rather misleading to consider the global molecular dipole moment, since it certainly is highly influenced by the polar carboxylic acid groups. In ReCl, the $S_0 \rightarrow {}^3$MLCT frequency shifts are 20-40 cm^{-1}, indicating significant changes to the electron density, and by extension, the electrostatic profile of the CO region of the molecule. Indeed, in comparing the partial charges for ReCl (S_0), ReCl (^{3}MLCT), and the COOH derivative, we see clearly that there are virtually no changes except local to the carboxylic acid groups (**Fig. 3.5**). In other words, the spectral diffusion difference between the S_0 and ^{3}MLCT states is at least partially due to the change in dielectric friction because the underlying changes in charge distribution occur at the sites of the CO, which are directly coupled to the solvent. Changes in charge distribution distant from the carbonyls, on the other hand, do not affect the solvent motion at the probe sites. In this way, vibrational spectroscopy provides a measure of dynamics with an effective spatial resolution that is to some degree higher than what would be possible with electronic spectroscopy involving highly delocalized states.

3.4 CONCLUSION

We report the spectral dynamics of the A'(2) carbonyl stretching mode of multiple variations of the photo-catalyst *fac*-Re(R_2-bpy)$(CO)_3$Cl in the solvents DMSO, THF and CH_3CN. Among all of the variations, we observe similar dynamics within the same solvent. The spectral diffusion times therefore reflect the time scales of solvation dynamics sensed by the carbonyl stretching modes, which seem to depend only on the solvent, and not on the permanent molecular dipole moment or steric effects *trans* to the equatorial carbonyls. While the molecular electrostatics and intramolecular electronic structure may contribute, they must do so to a much smaller extent than the solvent. In recent work, we saw that the dipole moment change from a ^{3}MLCT T *fac*-Re(bpy)$(CO)_3$Cl in THF caused a pronounced change in the spectral diffusion. It is evident that the carbonyls are affected much more strongly by the photo-induced charge transfer, than by the addition of electron withdrawing substituents to the bipyridine. Although there are associated changes in the overall dipole moments, the induced shifts of the carbonyl vibrations are only a few wavenumbers, compared with shifts of tens of wavenumbers in the ^{3}MLCT excited

state. These results highlight the highly local nature of the carbonyl vibrational probes, which are essentially decoupled from the electrostatics of the distal bipyridine substituents.

We find that for the A'(2) mode, as the nucleophiliciy of the solvent increases, so does the FFCF decay time, which also correlates with an increased solvatochromic red-shift. The red shift can be explained by the solvent's nucleophilic character, pushing the electron density back towards the Re metal center and weakening the C≡O bond. In the future, we plan to study this series of complexes and solvents in the quasi-equilibrated ^{3}MLCT excited state using transient 2DIR, where we will compare the relative importance of substituent and solvent effects on the dynamics of the catalytically important photo-initiated state.

REFERENCES

1. Cannizzo, A.; Blanco-Rodríguez, A. M.; El Nahhas, A.; Šebera, J.; Záliš, S.; Vlček, A., Jr.; Chergui, M., Femtosecond Fluorescence and Intersystem Crossing in Rhenium(I) Carbonyl-Bipyridine Complexes. *J. Am. Chem. Soc.* 2008, *130*, 8967-8974.

2. Takeda, H.; Koike, K.; Inoue, H.; Ishitani, O., Development of an Efficient Photocatalytic System for CO_2 Reduction using Rhenium(I) Complexes Based on Mechanistic Studies. *J. Am. Chem. Soc.* 2008, *130*, 2023-2031.

3. Morris, A. J.; Meyer, G. J.; Fujita, E., Molecular Approaches to the Photocatalytic Reduction of Carbon Dioxide for Solar Fuels. *Acc. Chem. Res.* 2009, *42*, 1983-1994.

4. Grills, D. C.; Fujita, E., New Directions for the Photocatalytic Reduction of CO_2: Supramolecular, $scCO_2$ or Biphasic Ionic Liquid-$scCO_2$ Systems. *J. Phys. Chem. Lett.* 2010, *1*, 2709-2718.

5. Smieja, J. M.; Kubiak, C. P., Re(bipy-tBu)$(CO)_3Cl^-$Improved Catalytic Activity for Reduction of Carbon Dioxide: IR-Spectroelectrochemical and Mechanistic Studies. *Inorg. Chem.* 2010, *49*, 9283-9289.

6. Vlček, A., Jr., Ultrafast Excited-State Processes in Re(I) Carbonyl-Diimine Complexes: From Excitation to Photochemistry. In *Top. Organomet. Chem.*, 2010; Vol. 29, pp 73-114.

7. El Nahhas, A.; Consani, C.; Blanco-Rodríguez, A. M.; Lancaster, K. M.; Braem, O.; Cannizzo, A.; Towrie, M.; Clark, I. P.; Záliš, S.; Chergui, M.; Vlček, A., Jr., Ultrafast Excited-State Dynamics of

Rhenium(I) Photosensitizers [Re(Cl)(CO)$_3$(N,N)] and [Re(imidazole)(CO)$_3$(N,N)]$^+$: Diimine Effects. *Inorg. Chem.* 2011, *50*, 2932-2943.

8. Takeda, H.; Koike, K.; Morimoto, T.; Inumaru, H.; Ishitani, O., Photochemistry and Photocatalysis of Rhenium(I) Diimine Complexes. In *Advances in Inorganic Chemistry, Vol 63: Inorganic Photochemistry*, VanEldik, R.; Stochel, G., Eds. 2011; Vol. 63, pp 137-186.

9. Sato, S.; Matubara, Y.; Koike, K.; Falkenstrom, M.; Katayama, T.; Ishibashi, Y.; Miyasaka, H.; Taniguchi, S.; Chosrowjan, H.; Mataga, N.; Fukazawa, N.; Koshihara, S.; Onda, K.; Ishitani, O., Photochemistry of *fac*-Re(bpy)(CO)$_3$Cl. *Chem. Eur. J.* 2012, *18*, 15722-15734.

10. Smieja, J. M.; Benson, E. E.; Kumar, B.; Grice, K. A.; Seu, C. S.; Miller, A. J. M.; Mayer, J. M.; Kubiak, C. P., Kinetic and Structural Studies, Origins of Selectivity, and Interfacial Charge Transfer in the Artificial Photosynthesis of CO. *Proc. Natl. Acad. Sci. USA* 2012, *109*, 15646-15650.

11. El Nahhas, A.; van der Veen, R. M.; Penfold, T. J.; Pham, V. T.; Lima, F. A.; Abela, R.; Blanco-Rodríguez, A. M.; Záliš, S.; Vlček, A., Jr.; Tavernelli, I.; Rothlisberger, U.; Milne, C. J.; Chergui, M., X-ray Absorption Spectroscopy of Ground and Excited Rhenium-Carbonyl Diimine-Complexes: Evidence for a Two-Center Electron Transfer. *J. Phys. Chem. A* 2013, *117*, 361-369.

12. Machan, C. W.; Sampson, M. D.; Chabolla, S. A.; Dang, T.; Kubiak, C. P., Developing a Mechanistic Understanding of Molecular Electrocatalysts for CO_2 Reduction using Infrared Spectroelectrochemistry. *Organometallics* 2014, *33*, 4550-4559.

13. Liard, D. J.; Busby, M.; Matousek, P.; Towrie, M.; Vlček, A., Jr., Picosecond Relaxation of ^{3}MLCT Excited States of [Re(Etpy)(CO)$_3$(dmb)]$^+$ and [Re(Cl)(CO)$_3$(bpy)] as Revealed by Time-Resolved Resonance Raman, UV-vis, and IR Absorption Spectroscopy. *J. Phys. Chem. A* 2004, *108*, 2363-2369.

14. Dattelbaum, D. M.; Omberg, K. M.; Schoonover, J. R.; Martin, R. L.; Meyer, T. J., Application of Time-Resolved Infrared Spectroscopy to Electronic Structure in Metal-to-Ligand Charge-Transfer Excited States. *Inorg. Chem.* 2002, *41*, 6071-6079.

15. Johnson, F. P. A.; George, M. W.; Hartl, F.; Turner, J. J., Electrocatalytic Reduction of CO_2 Using the Complexes [Re(bpy)(CO)$_3$L]^n (n=+1, L=P(OEt)$_3$, CH_3CN; n=0, L=Cl^-, Otf^-; bpy=2,2'-bipyridine; Otf^-=CF_3SO_3) as Catalyst Precursors: Infrared Spectroelectrochemical Investigation. *Organometallics* 1996, *15*, 3374-3387.

16. Sato, S.; Sekine, A.; Ohashi, Y.; Ishitani, O.; Blanco-Rodriguez, A. M.; Vicek, A.; Unno, T.; Koike, K., Photochemical Ligand Substitution Reactions of *fac*-Re(bpy)$(CO)_3$Cl and Derivatives. *Inorg. Chem.* 2007, *46*, 3531-3540.

17. Heydová, R.; Gindensperger, E.; Romano, R.; Sýkora, J.; Vlček, A., Jr.; Záliš, S.; Daniel, C., Spin-Orbit Treatment of UV-vis Absorption Spectra and Photophysics of Rhenium(I) Carbonyl-Bipyridine Complexes: MS-CASPT2 and TD-DFT Analysis. *J. Phys. Chem. A* 2012, *116*, 11319-11329.

18. Agarwal, J.; Fujita, E.; Schaefer, H. F.; Muckerman, J. T., Mechanisms for CO Production from CO_2 Using Reduced Rhenium Tricarbonyl Catalysts. *J. Am. Chem. Soc.* 2012, *134*, 5180-5186.

19. Riplinger, C.; Sampson, M. D.; Ritzmann, A. M.; Kubiak, C. P.; Carter, E. A., Mechanistic Contracts between Manganese and Rhenium Bipyridine Electrocatalysts for the Reduction of Carbon Dioxide. *J. Am. Chem. Soc.* 2014, *136*, 16285-16298.

20. Rodriguez, L.; Ferrer, M.; Rossell, O.; Duarte, F. J. S.; Santos, A. G.; Lima, J. C., Solvent Effects on the Absorption and Emission of Re(R_2bpy)$(CO)_3$X Complexes and their Sensitivity to CO_2 in Solution. *Journal of Photochemistry and Photobiology a-Chemistry* 2009, *204*, 174-182.

21. Kurz, P.; Probst, B.; Spingler, B.; Alberto, R., Ligand Variations in ReX(diimine)$(CO)_3$ Complexes: Effects on Photocatalytic CO_2 Reduction. *Eur. J. Inorg. Chem.* 2006, 2966-2974.

22. Takeda, H.; Ishitani, O., Development of Efficient Photocatalytic Systems for CO_2 Reduction using Mononuclear and Multinuclear Metal Complexes Based on Mechanistic Studies. *Coord. Chem. Rev.* 2010, *254*, 346-354.

23. Sullivan, B. P.; Meyer, T. J., Kinetics and Mechanism Of CO_2 Insertion into a Metal-Hydride Bond. A Large Solvent Effect and an Inverse Kinetic Isotope Effect. *Organometallics* 1986, *5*, 1500-1502.

24. Kiefer, L. M.; King, J. T.; Kubarych, K. J., Equilibrium Excited State Dynamics of a Photoactivated Catalyst Measured with Ultrafast Transient 2DIR. *J. Phys. Chem. A* 2014, *118*, 9853–9860.

25. Nee, T. W.; Zwanzig, R., Theory of Dielectric Relaxation in Polar Liquids. *J. Chem. Phys.* 1970, *52*, 6353-6363.

26. Maroncelli, M., Continuum estimates of rotational dielectric friction and polar solvation. *J. Chem. Phys.* 1997, *106*, 1545-1555.

27. Anfuso, C. L.; Ricks, A. M.; Rodriguez-Cordoba, W.; Lian, T. Q., Ultrafast Vibrational Relaxation Dynamics of a Rhenium Bipyridyl CO_2-Reduction Catalyst at a Au Electrode Surface Probed by Time-Resolved Vibrational Sum Frequency Generation Spectroscopy. *J. Phys. Chem. C* 2012, *116*, 26377-26384.

28. Benson, E. E.; Sampson, M. D.; Grice, K. A.; Smieja, J. M.; Froehlich, J. D.; Friebel, D.; Keith, J. A.; Carter, E. A.; Nilsson, A.; Kubiak, C. P., The Electronic States of Rhenium Bipyridyl Electrocatalysts for CO2 Reduction as Revealed by X-ray Absorption Spectroscopy and Computational Quantum Chemistry. *Angewandte Chemie-International Edition* 2013, *52*, 4841-4844.

29. El Nahhas, A.; Cannizzo, A.; van Mourik, F.; Blanco-Rodríguez, A. M.; Záliš, S.; Vlček, A., Jr.; Chergui, M., Ultrafast Excited-State Dynamics of $[Re(L)(CO)_3(bpy)]^n$ Complexes: Involvement of the Solvent. *J. Phys. Chem. A* 2010, *114*, 6361-6369.

30. Nee, M. J.; Baiz, C. R.; Anna, J. M.; McCanne, R.; Kubarych, K. J., Multilevel Vibrational Coherence Transfer and Wavepacket Dynamics Probed with Multidimensional IR Spectroscopy. *J. Chem. Phys.* 2008, *129*, 084503.

31. Horng, M. L.; Gardecki, J. A.; Papazyan, A.; Maroncelli, M., Subpicosecond Measurements of Polar Solvation Dynamics: Coumarin-153 Revisited. *J. Phys. Chem.* 1995, *99*, 17311-17337.

32. Jansen, T. L. C.; Cringus, D.; Pshenichnikov, M. S., Dissimilar Dynamics of Coupled Water Vibrations. *J. Phys. Chem. A* 2009, *113*, 6260-6265.

33. King, J. T.; Baiz, C. R.; Kubarych, K. J., Solvent-Dependent Spectral Diffusion in a Hydrogen Bonded "Vibrational Aggregate". *J. Phys. Chem. A* 2010, *114*, 10590-10604.

34. Reichardt, C., Solvatochromic Dyes as Solvent Polarity Indicators. *Chem. Rev.* 1994, *94*, 2319-2358.

35. Gutmann, V., Solvent Effects on the Reactivities of Organometallic Compounds. *Coord. Chem. Rev.* 1976, *18*, 225-255.

36. Mayer, U.; Gutmann, V.; Gerger, W., Acceptor Number - Quantitative Empirical Parameter for Electrophilic Properties of Solvents. *Monatsh. Chem.* 1975, *106*, 1235-1257.

37. Jones, B. H.; Huber, C. J.; Massari, A. M., Solvation Dynamics of Vaska's Complex by 2D-IR Spectroscopy. *J. Phys. Chem. C* 2011, *115*, 24813-24822.

38. Brookes, J. F.; Slenkamp, K. M.; Lynch, M. S.; Khalil, M., Effect of Solvent Polarity on the Vibrational Dephasing Dynamics of the Nitrosyl Stretch in an Fe-II Complex Revealed by 2D IR Spectroscopy. *J. Phys. Chem. A* 2013, *117*, 6234-6243.

39. Chadwick, I.; Diaz, C.; Gonzalez, G.; Santaana, M. A.; Yutronic, N., Electrochemical Oxidation of Monosubstituted Chromium Carbonyl-Complexes. Ligand and Solvent Effects. *Journal of the Chemical Society-Dalton Transactions* 1986, 1867-1871.

40. Frisch, M. J.; Trucks, G. W.; Schlegel, H. B.; Scuseria, G. E.; Robb, M. A.; Cheeseman, J. R.; Scalmani, G.; Barone, V.; Mennucci, B.; Petersson, G. A.; Nakatsuji, H.; Caricato, M.; Li, X.; Hratchian, H. P.; Izmaylov, A. F.; Bloino, J.; Zheng, G.; Sonnenberg, J. L.; Hada, M.; Ehara, M.; Toyota, K.; Fukuda, R.; Hasegawa, J.; Ishida, M.; Nakajima, T.; Honda, Y.; Kitao, O.; Nakai, H.; Vreven, T.; Montgomery Jr., J. A.; Peralta, J. E.; Ogliaro, F.; Bearpark, M. J.; Heyd, J.; Brothers, E. N.; Kudin, K. N.; Staroverov, V. N.; Kobayashi, R.; Normand, J.; Raghavachari, K.; Rendell, A. P.; Burant, J. C.; Iyengar, S. S.; Tomasi, J.; Cossi, M.; Rega, N.; Millam, N. J.; Klene, M.; Knox, J. E.; Cross, J. B.; Bakken, V.; Adamo, C.; Jaramillo, J.; Gomperts, R.; Stratmann, R. E.; Yazyev, O.; Austin, A. J.; Cammi, R.; Pomelli, C.; Ochterski, J. W.; Martin, R. L.; Morokuma, K.; Zakrzewski, V. G.; Voth, G. A.; Salvador, P.; Dannenberg, J. J.; Dapprich, S.; Daniels, A. D.; Farkas, Ö.; Foresman, J. B.; Ortiz, J. V.; Cioslowski, J.; Fox, D. J. *Gaussian 09*, Gaussian, Inc.: Wallingford, CT, USA, 2009.

41. Cappelli, C.; Silva, C. O.; Tomasi, J., Solvent Effects on Vibrational Modes: Ab-Initio Calculations, Scaling and Solvent Functions with Applications to the Carbonyl Stretch of Dialkyl Ketones. *J. Mol. Struc-Theochem* 2001, *544*, 191-203.

Chapter 4

Solvent Exchange in Preformed Photocatalyst-Donor Encounter Complexes Determines Efficiency

4.1 INTRODUCTION

Understanding catalytic reaction mechanisms is central to optimizing selectivity and efficiency. Fundamental processes including solvation, electron transfer, and diffusion certainly occur, but their specific contributions are often obscured using common experimental techniques. Photocatalysis is further complicated by the involvement of at least one excited electronic state, but the optical excitation can synchronize events in the photocycle, simplifying elucidation of the

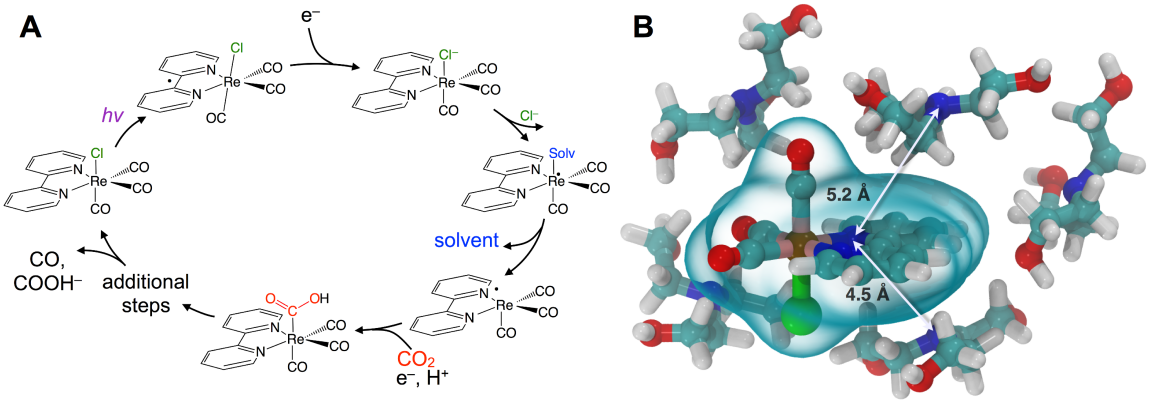

Figure 4.1: Rhenium bipyridyl photocatalysts for CO_2 reduction to CO and $COOH^-$. (A) The photocatalytic cycle starts with absorption of near-UV light, producing a metastable (~60 ns) ^{3}MLCT state that is reduced by electron transfer from an amine sacrificial donor. A solvent (or co-solvent) molecule substitutes the chloride and then dissociates leaving a radical, which subsequently binds CO_2 as a carboxylic acid. Further downstream steps lead to final production of CO or $COOH^-$. (B) Force-field optimized cluster of Re(**bpy**)$(CO)_3$Cl with five TEOA molecules, showing the donor-acceptor distance of roughly 5 Å.

earliest processes. Photoredox catalysis incorporates both light absorption and intermolecular charge transfer steps in addition to substrate binding and product release, so lessons learned in a given system should be generalizable.

We describe the structural dynamics of a rhenium complex, $Re(bpy)(CO)_3Cl$ (bpy = bipyridine), an effective CO_2 reduction photocatalyst, in solution conditions similar to those used to produce CO or $COOH^-$ from CO_2.[1-3] This family of complexes, first identified by Lehn *et al*., catalyzes the 2-electron/2-proton reduction of CO_2 through the sequence of steps outlined in **Fig. 4.1A**.[4-6] Near-UV light (~400 nm) excites the catalyst to a singlet charge transfer state (^{1}CT) state, which relaxes through a rapid (~0.2-1.0 ps) intersystem-crossing to a triplet metal-to-ligand charge transfer (^{3}MLCT) state.[7-8] Reduction by a sacrificial electron donor facilitates loss of the axial halide ligand, and the solvent or the electron donor itself coordinates to the Re center.[9] The CO_2 replaces the solvent (or donor) ligand, and there is some evidence that formation of a binuclear, CO_2-bridged dimer facilitates cleavage of a C–O bond.[2, 10-11]

Although this sequence of steps is supported by considerable evidence, key aspects of the molecular details are assumed without direct experimental support. In particular, the first reduction by the sacrificial donor is thought to take place following the formation of an encounter complex by diffusing through the solution. There is little reason to question this assumption, which is a basic ingredient in outer-sphere, intermolecular electron transfer. The long (~60 ns) lifetime of the activated ^{3}MLCT state permits relatively long-range diffusion before deactivation. The results we show here indicate that the encounter complex is actually *preformed* due to significant preferential interaction between the polar catalyst and donor amine. A simple force field optimization indicates that van der Waals contact between TEOA and the rhenium complex places the donor and acceptor within ~5 Å (**Fig. 4.1B**). We find evidence that the intrinsic ET time scale may be speed-limited by the distance dependence of electron tunneling. These findings suggest that the catalyst's efficiency could potentially be improved by increasing the yield of productive ET events.

Two-dimensional infrared (2D-IR) spectroscopy correlates excited and detected vibrational transitions, enabling decomposition of complex spectral bands into contributions from homogeneous dephasing and inhomogeneous frequency distributions arising from variations in

the local solvent environment.[12] The key observable is the time dependent loss of frequency correlation due to stochastic sampling of the frequencies within an inhomogeneously broadened band, which is known as spectral diffusion.[13] The decay of the frequency fluctuation correlation function (FFCF, $C(t)=\langle\delta\omega(0)\delta\omega(t)\rangle$) is the principal observable used to characterize the solvation structure and dynamics of the rhenium photocatalyst.

The FFCF offers a window into the solvation dynamics of the photocatalyst solute, revealing the time scale for solvent shell fluctuations. For a ternary mixture of the catalyst and two solvents, there is the possibility to observe the exchange of dissimilar species in the solvation shell of the vibrationally probed solute. Since solvent exchange is slower than the typical time scales of short range (i.e. librational) solvent motion, spectral diffusion can be slower in a mixture of solvents than in either solvent alone.[14] This exchange-induced slowdown of spectral dynamics has been observed in numerous time-resolved fluorescence studies of solvent mixtures, and we have identified the dynamical signature in 2D-IR spectroscopy.[15-16]

4.2 EXPERIMENTAL RESULTS

2DIR

Figure 4.2 displays absorptive 2D-IR spectra of the totally symmetric A'(1) carbonyl vibrational stretching mode (2019 cm^{-1}) of $Re(bpy)(CO)_3Cl$ at distinct waiting times (t_2 = 0.4, 5.1, and 14.1 ps) of the Re complex in pure tetrahydrofuran (THF), 20% triethanolamine (TEOA) in THF, and pure TEOA, highlighting the differences between the environments. The absorptive spectra depict both the $v = 0 \rightarrow v = 1$ (red, top) as well as the $v = 1 \rightarrow v = 2$ (blue, bottom) transitions. All analyses are performed on the fundamental $v = 0 \rightarrow v = 1$ transition. At early waiting times, it is clear that the Re complex in pure THF has very little inhomogeneous broadening based on the relatively narrow diagonal width. The solvent mixture induces a noticeable increase in inhomogeneous broadening, presumably reflecting the increased diversity of solvent environments. The FFCF indicates that in the 20%/80% TEOA/THF solution, frequency correlation persists even at longer waiting times compared with either of the two pure solvent cases.

In this series of experiments, we observe the A'(1) mode's spectral dynamics as a function of fraction of TEOA in THF (**Fig. 4.3A**). At low TEOA concentrations, there are gradual increases in

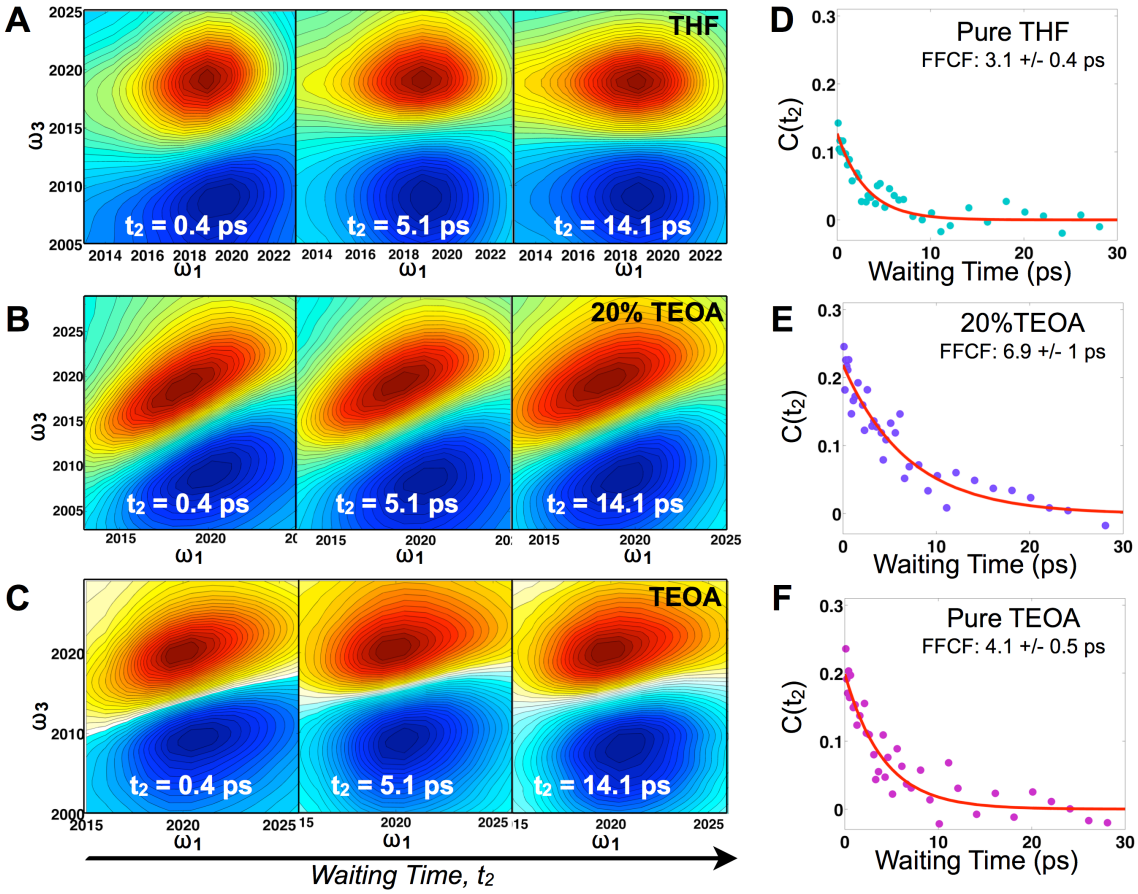

Figure 4.2: 2D-IR spectra of $Re(bpy)(CO)_3Cl$ in THF/TEOA solution. Absorptive 2D-IR spectra of the A'(1) CO stretching band in (A) THF, (B) 20% (v/v) TEOA in THF, (C) TEOA at three waiting times (0.4, 5.1 and 14.1 ps) illustrating the changes due to solvation dynamics. The inhomogeneous width is maximal in mixed solvent, and full decays of the FFCF (D-F) indicate that spectral fluctuations are slowest in the mixed solvent due to dissimilar solvent exchange.

the FFCF decay time relative to neat THF (3.1±0.5 ps). As the composition nears 20% TEOA (v/v), the correlation decay time increases to a maximum of 6.9±1 ps. At slightly higher TEOA concentrations, spectral diffusion becomes faster, ultimately reaching 4.1±0.5 ps in pure TEOA.

The spectral diffusion time constants of the mixtures depend on the relative contributions of fast libration-like solvent dynamics and the slower solvent exchange (**Fig. 4.3F**). Since we fit our FFCF decays to single exponentials with constant offsets, we measure a time scale that effectively mixes the two dynamical contributions. We have previously shown in water/dimethylformamide solutions that the solvent exchange time scale is predictable from mutual diffusion of the two

solvents.[14] The time scales reported here are consistent with the solvent exchange mechanism. The quantitative time scales are not intrinsically important, rather we view the introduction of a slow component as a signature of solvent exchange.[15-16] Absent preferential interactions, exchange of dissimilar solvent species should be maximal at 50% mole fraction in analogy to the maximal entropy of mixing at equal concentrations. Preferential solvation, on the other hand,

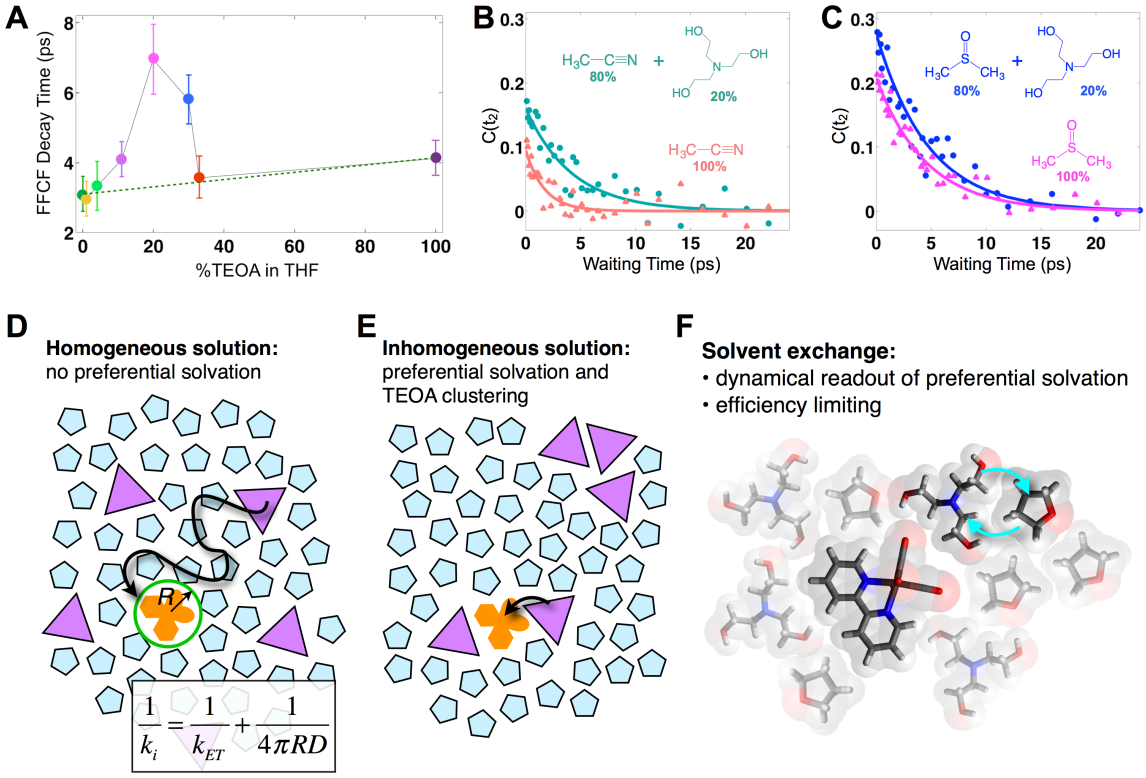

Figure 4.3: Solvent composition dependence. (A) Exponential time constants for spectral diffusion of the $Re(bpy)(CO)_3Cl$ symmetric CO stretch in various compositions of TEOA in THF, ranging from 0 to 100 % (v/v). Spectral diffusion is slowest at 20%, which corresponds to the maximal degree of solvent exchange. 20% composition yields the highest efficiency of CO production in active photocatalytic reactors (7). (B) 20% TEOA in acetonitrile also shows a pronounced slowdown, whereas (C) in DMSO, there is no significant composition dependence. In DMSO, $Re(bpy)(CO)_3Cl$ does not display evidence for preferential solvation by TEOA. Cartoons depicting (D) a homogeneous solution where the primary charge transfer would be expected to be diffusion controlled; (E) an inhomogeneous solution where preferential solvation and co-solvent clustering alter the local concentration; (F) dissimilar co-solvent exchange in the first solvation shell of the catalyst.

shifts the maximum towards lower concentration of the preferred species. We expect TEOA to preferentially solvate the highly polar (14.1 Debye) Re catalyst because TEOA is more polar than THF. We note that the spectral diffusion time scales change with increased concentration above 20% TEOA, and are anti-correlated with the solution's viscosity. Indeed, the viscosity of TEOA is two orders of magnitude higher than THF, yet we find very similar dynamical time scales in the

two neat solvents. Decoupling from viscosity is not unusual, however, and has been seen in several contexts such as simple liquids, glass forming liquids, and liquid crystals.[17-21]

To determine whether the composition dependent line shapes and dynamical slowdown are unique to THF, we performed 2D-IR experiments of $Re(bpy)(CO)_3Cl$ in 20%/80% TEOA/DMSO and in 20%/80% TEOA/CH_3CN and compared these results to those in the respective pure solvents (**Fig. 4.3B,C)**. The correlation decay times of the rhenium complex in the solvent mixtures exhibit a slowdown in CH_3CN (pure: 1.7 ± 0.3 ps; mixture: 4.2 ± 0.7 ps), but not in DMSO (pure: 4.5 ± 0.4 ps; mixture: 4.7 ± 0.5 ps). These results are consistent with the picture that emerges from the TEOA/THF data: we expect inhomogeneous (**Fig. 4.3E)**, preferential solvation by TEOA in CH_3CN, but not in DMSO, where we anticipate a largely homogeneous solution (**Fig. 4.3D)**. This expectation is based on spectroscopic studies using a solvation probe dye (betaine-30). Similar to the comparison of the diagonal line widths of the absorptive 2D spectra, the initial value of the FFCF, $C(t_2=0)$, is related to the inhomogeneity of the band.[22] We find that in all cases the solvent mixtures are more inhomogeneously broadened than the pure solvents reflected by the larger initial FFCF values.

UV-Vis and FTIR

We performed $E_T(30)$ experiments by combining ratios of TEOA/Solvent with betaine-30, or Reichardt's Dye, (2,6-diphenyl-4-(2,4,6-triphenyl-1-pyridinio)phenolate), and collected UV-Vis spectra of each mixture. Betaine-30 has been used in previous preferential solvation studies, and was used here to characterize preferential solvation of triethanolamine in the solvents used in this study, dimethyl sulfoxide (DMSO), tetrahydrofuran (THF) and acetonitrile (CH_3CN). Betaine-30 was selected because it is: (1) widely used to characterize solvent polarity, (2) has a large ground state dipole moment that also decreases in the electronic excited state, and (3) does not exhibit charge transfer complexation as we observed in the UV-Vis spectrum of the rhenium complex. The betaine-30 dye exhibits preferential solvation as evidenced by a peak shift of the maximum visible absorption band at low concentrations of the cosolvent, in this case, the TEOA. Both betaine-30 and the rhenium complex are alike in that they both undergo bathochromic spectral shifts within a solvent (i.e. $\mu_g > \mu_e$). $E_T(30)$ values were determined using the wavelength positions of the

absorption band maxima (λ_{max}) in the following equation:[23]

$$E_T(30)(kcal/mol) = \frac{28591\left(kcal \bullet nm \bullet mol^{-1}\right)}{\lambda_{\max}(nm)} \qquad (4.1)$$

Figure 4.4 depicts the maximum wavelength in the visible absorption spectra for the solvent combinations.

In the solvents THF and CH_3CN, a sharp shift in the spectrum is observed at a concentration of ~2% TEOA (v/v), while in the DMSO it only shifted slightly. This is the first indication that the

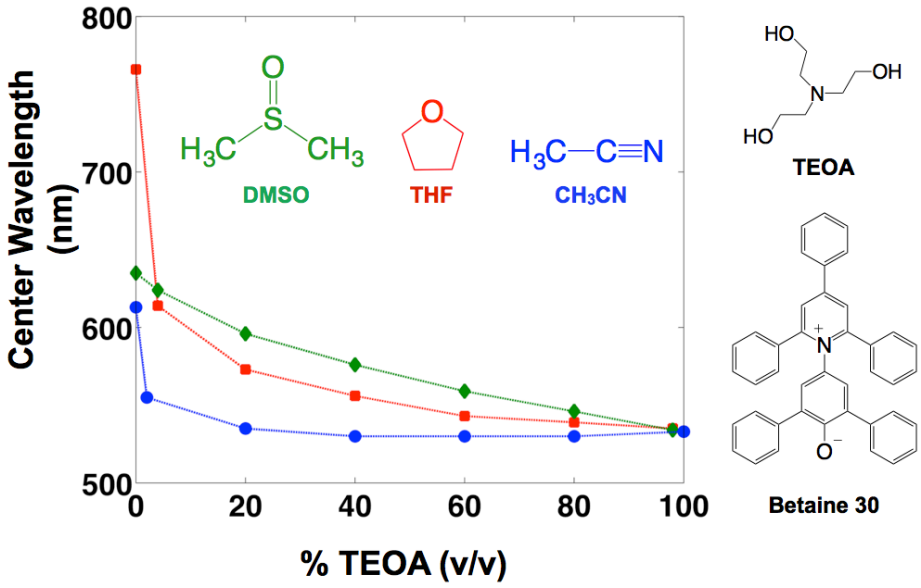

Figure 4.4: Wavelengths corresponding to betaine-30 absorption maxima in the visible absorption spectra for multiple ratios of TEOA:solvent, where the solvent = DMSO, THF or CH_3CN. The figure shows the structures of the solvents and betaine-30.

TEOA preferentially solvates betaine-30 in THF and CH_3CN, but not in DMSO, just as were observed in the 2DIR results. Upon further addition of TEOA, the DMSO showed an essentially linear shift in the spectrum, indicating no evidence of preferential solvation. When comparing properties of the solvents to rationalize these peak shifts, we first eliminated factors that were not responsible for the observed shift. The permanent dipole moment of the TEOA (μ = 3.48 D) is comparable to those of DMSO (μ = 3.90 D) and CH_3CN (μ = 3.44 D), but much larger than that of THF (μ = 1.7 D). Nevertheless, we observe preferential solvation when $\mu_{TEOA} < \mu_{SOLVENT}$. There is not a perceived

trend with the electrophilic properties (acceptor number, AN) for the three solvents: THF (AN = 8.0), CH_3CN (AN = 18.9) and DMSO (AN = 19.3). The solvents having the two lower values both exhibit preferential solvation of the TEOA, but the higher value of the two is very close to DMSO's value, and the AN must therefore be considered to contribute little, if at all. Both THF and CH_3CN have lower polarizability values (π* = 75 and 58, respectively) than DMSO (π* = 100), so this interaction may possibly influence the solvation preference. Finally, the donicities (DN = donor number) of the solvents show a similar same trend: both THF (DN = 20.0) and CH_3CN (DN = 14.1) have lower values than DMSO (DN = 29.9)[24]. Higher donor numbers correlate with stronger

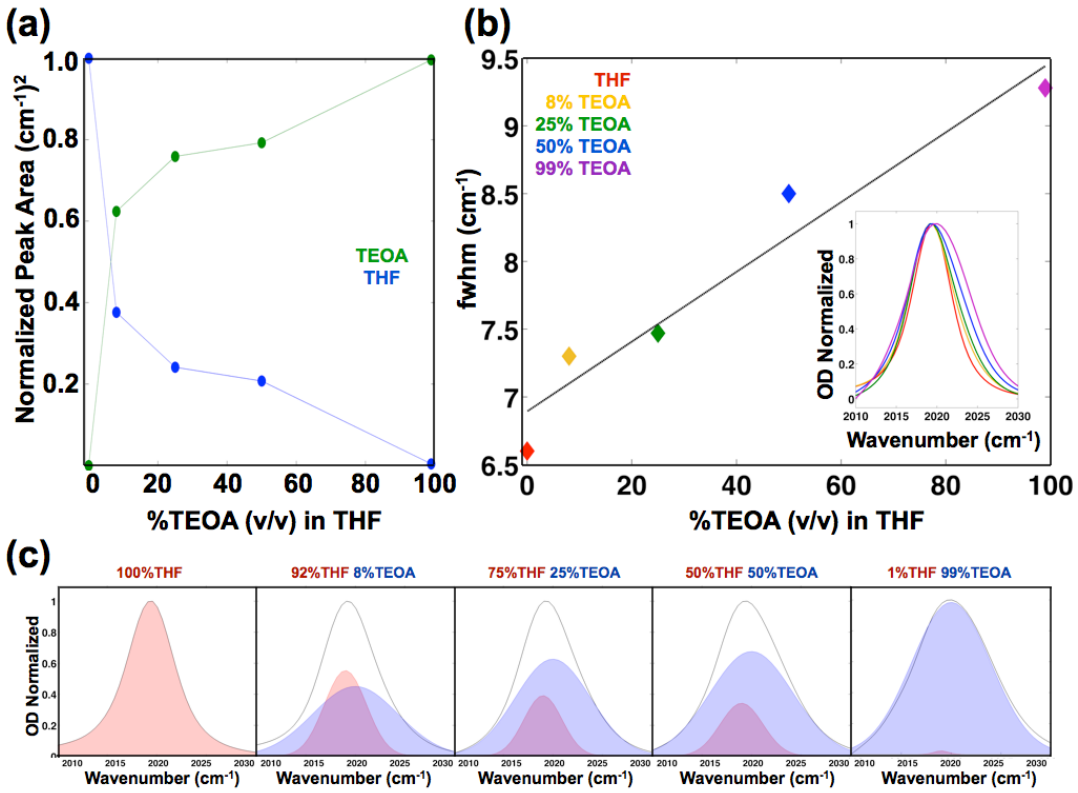

Figure 4.5: (a) individual peak areas of the A'(1) band of the solvent mixtures, fit to the peaks in the neat solvents, THF (blue) and TEOA (green); (b) fwhm of the A'(1) band in TEOA:THF mixtures; (c) plot of the individual gaussian fits of the A'(1) band in TEOA:THF mixtures, a plots showing fits used to obtain data in (a).

hydrogen bond acceptors, and these solvent DN's possibly indicate that hydrogen bonding between TEOA and DMSO may prevent preferential solvation of the solute chromophore.

Often FTIR experiments are indicators of preferential solvation through observation of a peak shift upon changes in solution composition. We conducted FTIR experiments on the mixtures,

but only observe a maximum blueshift of 1 cm^{-1} of the A'(1) band upon addition of TEOA in THF. The pronounced feature is the spectral broadening, which shows a linear dependence on %TEOA (**Fig. 4.5(b)**). With a peak shift of only 1 cm^{-1} and no deviation from linearity of the fwhm vs. %TEOA, there is little indication of preferential solvation from this analysis of the FTIR results. However, we considered an equilibrium of two species, fitting each band to a sum of two gaussians with their band positions fixed by the those found in the neat solvents, (THF: 2019 cm^{-1}, and TEOA: 2020 cm^{-1}). Allowing only the spectral width and the amplitudes to vary, comparison of the the areas of each peak indicates a strong signature of preferential solvation (**Fig. 4.5(c)**). A sharp change accompanies a small increase in volume %TEOA (**Fig. 4.5(a)**). Though capable of supporting our interpretation of preferential solvation in the solvent mixtures, neither the UV-Vis nor FTIR data report any unambiguous dynamical information that may be useful for the underlying photo-catalytic mechanism.

UV-Pump/IR-Probe and NMR Experiments

Although the 2D-IR results and the remarkably clear slowdown of spectral diffusion indicate that the TEOA sacrificial donor preferentially solvates the Re photocatalyst, definitive mechanistic insights must link the solvent structure to the catalytically essential primary electron transfer event. There have been many studies of Re photophysics using time-resolved IR spectroscopy as well as extensive spectroelectrochemical investigations,[25-26] but to-date there have been no ultrafast (i.e. sub-ns) transient IR absorption measurements of the photoinduced reduction by a sacrificial donor. The photophysics in the absence of the donor yields a substantial background, but following the initial 10-20 ps attributed to solvation and vibrational cooling of the ^{3}MLCT state, there is no significant dynamical evolution of the transient spectra. To isolate the reduced species, we employ a careful double-difference method, where we measure transient IR absorption spectra in the presence and absence of the TEOA donor using a flowing cell, leaving the beam alignment completely unchanged for the two samples. This approach enables us to measure the very small, ~50 OD, differences attributable to the weakly absorbing singly reduced species (**Fig. 4.6A**). The IR transitions of the reduced photocatalyst have been identified with spectroelectrochemistry, though with no information about the time dependence of its

formation.[27-28]

Integrating the double-difference spectra (i.e. ΔΔA) in the vicinity of 1996 cm^{-1}, characteristic of the singly reduced species (**Fig. 4.6B**) $[Re(bpy)(CO)_3Cl]^{\bullet -}$,[27] gives a signal that first appears

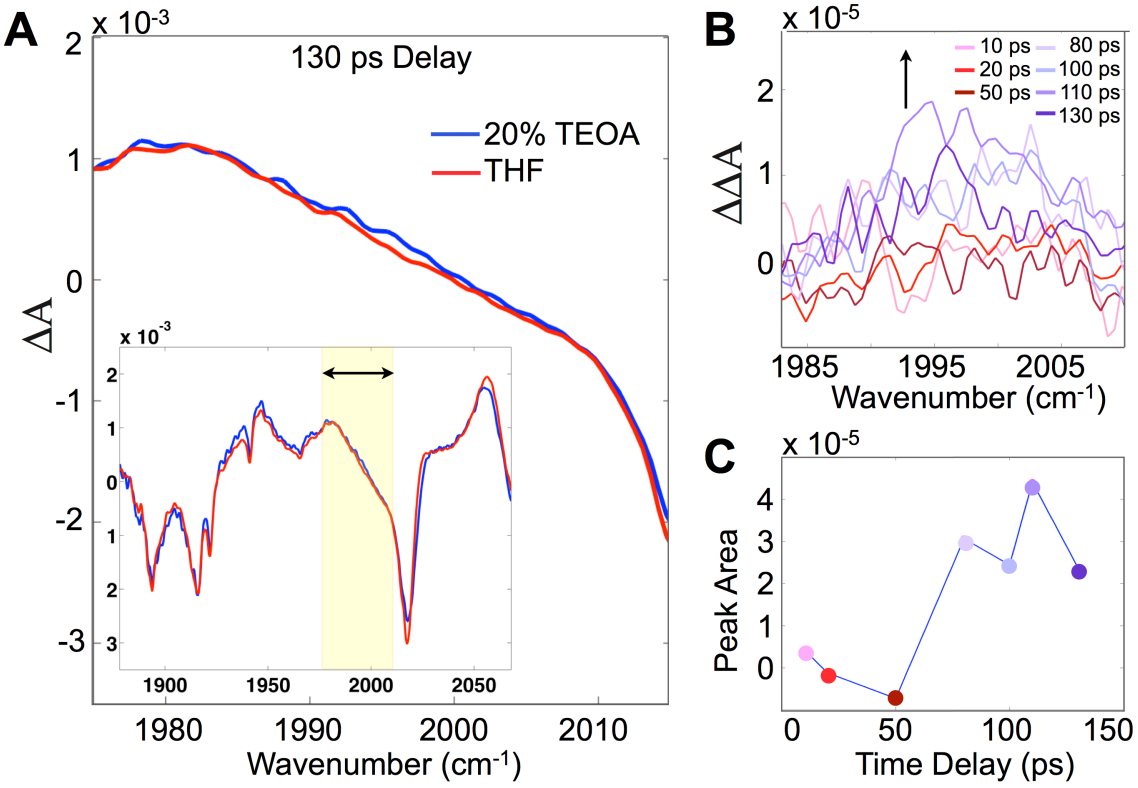

Figure 4.6: Transient IR absorption tracks the appearance of the singly reduced species. (A) Differential absorption (pump on – pump off) of $Re(bpy)(CO)_3Cl$ in 20% TEOA/THF solution in the carbonyl stretching band (inset), and zoomed to the region around 1996 cm^{-1}, corresponding to the singly reduced species. (B) Double-difference spectra at various time delays between the 400-nm pump and mid-IR probe showing the growth of the band. (C) Integrated singly-reduced band indicates a growth on a ~70 ps time scale, which is significantly faster than expected by diffusion.

between 50 and 80 ps following the 400 nm excitation. Taking the midpoint 65 ps to be a measure of the ET time scale (**Fig. 4.6C**), we can compare with a diffusion controlled prediction.

The picture of Collins-Kimball diffusion assisted electron transfer, which is schematically summarized in **Fig. 4.7**, depicts diffusion of quenchers to the region defined by the molecular geometry of the excited molecule. In the present study, the quencher is the amine electron donor. The time-derivative of the excited state photocatalyst follows conventional chemical kinetics:

$$\frac{d}{dt}A(t) = -k_i c A(t) \qquad (4.2)$$

where $A(t)$ is the concentration of electron acceptors, k_i is the time-independent rate constant, and c is the concentration of electron donors (TEOA) in solution. In the classical theory of bimolecular reactions due to Smoluchowski and later expanded by Collins and Kimball (CK), reactions occur once the electron donor reaches a contact region in the immediate vicinity of the

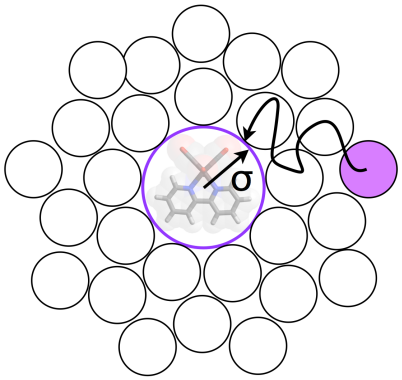

Figure 4.7: Cartoon indicating diffusion of an electron donor (filled purple) through solvent to contact the metastable ^{3}MLCT state of the photocatalyst, ReCl(bpy)(CO)$_3$. The reaction volume has a radius given by σ. The Collins-Kimball picture asserts that the reaction occurs with a kinetic rate constant (k_{ET}) once the donor and acceptor collide.

photocatalyst.[29-30] Typically the extent of that region is somewhat adjustable, but the simplest view is that the volume is spherical with radius σ, determined by the volume of the photocatalyst. In the case of highly viscous solution, the donor may linger in the vicinity of the photocatalyst, effectively enlarging the reaction layer. In the treatment of CK, the radius of the reaction volume R is simply set equal to σ.

Collins and Kimball derived an expression for the time-independent rate constant (k_i), which has been shown subsequently to be reliable for low-viscosity reaction solutions. The expression is:

$$\frac{1}{k_i} = \frac{1}{k_{ET}} + \frac{1}{4\pi RD} \qquad (4.3)$$

where k_{ET} is the kinetic rate constant for electron transfer and D is the diffusion constant of the electron donor in the reaction solution. It is evident from this formula that there is a maximum rate constant when the intrinsic electron transfer is significantly faster than the motional diffusion

contribution.

For the purposes of comparing directly to our time-domain experiments, we rewrite the rate constant as:

$$k_{obs} = k_i c = c\left(\frac{1}{k_{ET}} + \frac{1}{4\pi RD}\right)^{-1} \quad (4.4)$$

$$\tau_{obs} = 1/k_{obs} = \frac{1}{c}\left(\frac{1}{k_{ET}} + \frac{1}{4\pi RD}\right) \quad (4.5)$$

For infinite intrinsic k_{ET}, the ET time is given only by diffusion into the reaction volume:

$$\tau_{\min} = \frac{1}{4\pi cRD} \quad (4.6)$$

A finite k_{ET} would simply lead to a slower overall ET time scale. A quantitative estimate of this minimum reaction time can be made using the following values: c = 1.5 M, R = 4.0 Å, D = 62 Å^2/ns. This diffusion constant of TEOA was determined from DOSY NMR experiments of TEOA and THF in a TEOA/THF (20% TEOA v/v) solution. Briefly, it was determined from the peak intensity is given by:[31]

$$I = I_0 \exp\left[-D\gamma^2 g^2 \delta^2 \left(\Delta - \delta/3 - \tau/2\right)\right] \quad (4.7)$$

where D is the diffusion constant of the species corresponding to the chemical shift analyzed, γ is the gyromagnetic ratio, g is the gradient strength, and Δ, δ, and τ are time delays associated with the pulse sequence (values are given below). By varying the field gradient, it is possible to extract the diffusion coefficient. Fitting the following equation:

$$\ln\left[\frac{I}{I_0}\right] = -D\gamma^2 g^2 \delta^2 \left(\Delta - \delta/3 - \tau/2\right) \quad (4.8)$$

to a line allows us to determine D since the remaining values are set in the experiment or are

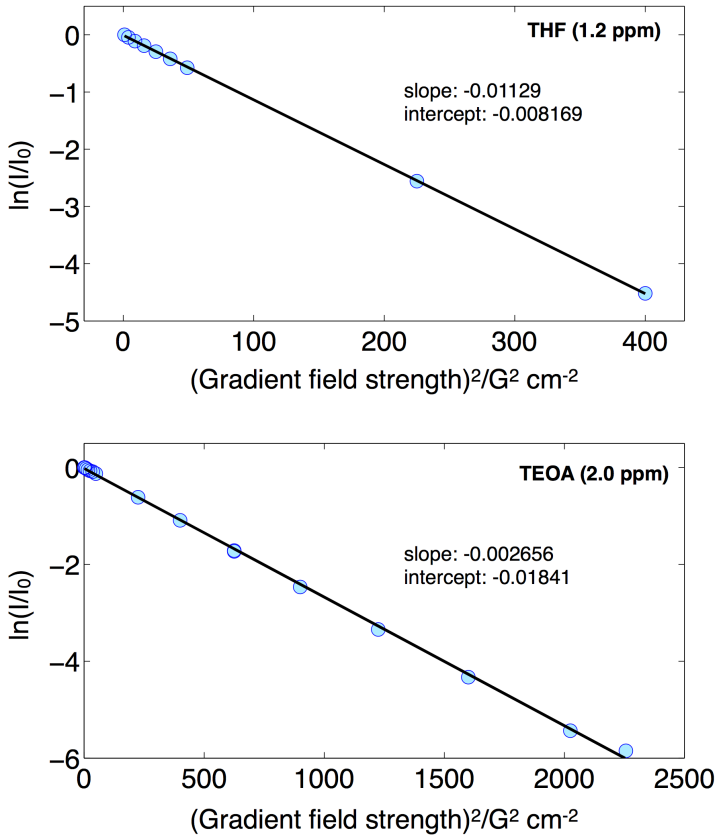

Figure 4.8: DOSY results and associated linear fits for a 20% (v/v) solution of TEOA in THF. (top) ln(I/I0) for the peak at a chemical shift of 1.2 ppm corresponding to THF; (bottom) ln(I/I0) for the peak at a chemical shift of 2.0 ppm corresponding to TEOA.

physical constants. The specific values are:

Δ = 150 ms

δ = 2000 s

τ = 200 s

γ = 26.75×10^{7} T^{-1} s^{-1} (T = tesla)

g = 50 G/cm at full gradient strength (G = gauss)

1 T = 10^{4} G

Figure 4.8 shows the measured data along with the linear fits and the fitting parameters. From the fits, we obtain D = 6.22×10^{-10} m^2/s for TEOA, and D = 2.64×10^{-9} m^2/s for THF. The radius is chosen from the molecular volume computed using DFT, which we found to be 168.111 (cm^3/mol), which is equal to 279.2 $Å^3$ for one molecule. The units of concentration must be

adapted to the formula, which needs to give units of time. *RD* has units of volume, and *c* has units of mol L^{-1}. 1 mol L^{-1} is 6.02×10^{23} molecules/(1000 cm^3), and 1 cm^3 = 10^{24} $Å^2$. Therefore, 1 M is 6.02×10^{-4} molecules/$Å^3$. Putting these values together we find a minimum time for the diffusion limited ET process to be:

$$\tau_{\min} = \left[4\pi \left(1.5 \times 6.02 \times 10^{-4} molecules / Å^3\right)\left(4Å\right)\left(62 Å^2 ns^{-1}\right)\right]^{-1} = 0.355 ns \quad (4.9)$$

or 355 ps. To achieve a time scale that is equal to our measured value of roughly 70 ps would require a reaction volume with radius of 20.3 Å, which is unphysically large. Moreover, any steric, orientational, or site-specific encounter requirements will necessarily reduce the rate of ET, further supporting the conclusion that we observe non-diffusive ultrafast electron transfer in the present Re/TEOA/THF photocatalyst system.

According to the Collins-Kimball treatment of diffusion controlled electron transfer,[30] given our sample conditions and our experimentally measured diffusion constant of TEOA in THF solution, the fastest possible time scale for the ET reaction is ~350 ps. Including a finite time scale intrinsic ET transfer rate, as well as steric and orientational contributions, the true diffusion controlled time scale must be considerably slower than this limiting value. Hence, our measured ET time scale is at least an order of magnitude faster than would be anticipated based on a diffusion controlled process, indicating that the TEOA must be in close proximity to the rhenium complex. Our result is generally consistent with a similar transient IR absorption study of $Re(bpy)(CO)_3Br$ acting as a photosensitizer for H_2 production found prompt reduction of the Re complex, followed by slow, diffusion controlled electron transfer to the cobalt catalyst.[32] Using the tunneling picture of electron transfer of Gray *et al*., our 50-80-ps ET time scale would put the TEOA within 7-9 Å of the rhenium complex.[33] Simple force field optimized geometries are consistent with this estimate, supporting the picture of the TEOA and the Re catalyst in van der Waals contact (**Fig. 4.1B**).

4.3 CONCLUSION

Rhenium bipyridyl complexes are currently the most effective known homogeneous

photocatalysts for CO_2 reduction.[2-3, 34] They notably combine the light absorbing photosensitizer with the catalytic center, reducing unproductive loss channels that are inevitable in multisite photosensitizer/catalyst constructs. Compared with other popular photocatalysts such as $[Ru(bpy)_3]^{2+}$, and $[Ir(ppy)_2(bpy)]^{+}$, the highly asymmetrical rhenium catalysts have large dipole moments. It is generally accepted that photocatalysts and photosensitizers must have long triplet state lifetimes so that charge transfer can occur before relaxation to the ground state. Nevertheless, Re-bpy complexes are more effective at oxidizing electron donors such as TEOA than is $[Ru(bpy)_3]^{2+}$ despite the Re complex's 10-100 fold shorter excited state lifetime.[35] Though some of this oxidizing ability is due to differences in thermodynamic driving force, our results suggest that preforming the encounter complex by virtue of the preferential solvation may be at least partly responsible. This alternative paradigm for photoredox catalysis provides guidance for tailoring the photocatalyst to the specific electrostatic nature of the substrates or other reagents. For the present case of photocatalytic reduction of CO_2, our findings suggest that the reaction performance may be limited by the actual electron transfer from the TEOA donor to the Re to generate the one-electron reduced species.

Preferential solvation is an essentially structural aspect of the photocatalytic process that nevertheless has been identified using a dynamical measurement since the natural timescale for solvent exchange is too fast to be observed using, for example, NOESY NMR. What is most striking about our observations is the correlation between the picosecond time scale solvent shell dynamics and the much slower overall catalytic reaction cycle. The solution composition where we find maximum solvent exchange coincides with the optimal conditions for CO production.[4-5] This experimental link between catalytic activity and maximal solvent exchange is consistent with the mechanistic step where the solvent or the donor coordinates to Re, but elevates the importance of the apparently rate determining dynamics of access to the catalyst. In that sense, the overall composite sequence of reduction by the donor and solvent/donor coordination is indeed diffusion controlled, but only the second process is actually diffusive. Since diffusion is essentially uncontrollable, our findings provide information necessary for catalyst optimization based on the specific sequence of molecular dynamics events, rather than the inevitably convoluted picture provided by kinetics.

4.4 METHODS

The 2DIR experiments use three mid-infrared pulses (500 nJ, ~100 fs) to generate a third-order nonlinear polarization that emits a fourth signal field in a background-free direction. The resultant signal was combined with a collinear reference field (500 nJ, ~100 fs) for heterodyne detection, upconverted to the visible by sum-frequency generation with a chirped 800-nm pulse, and detected using a spectrometer coupled to a CCD camera. The delay was scanned continuously between the two excitation pulses, and the resulting interferograms were Fourier transformed (resolution ~2 cm^{-1}) to obtain the excitation frequency axis in the 2DIR spectra; the detection frequency axis is obtained directly in the spectrometer. A detailed description of the technique is described in previous manuscripts.[36]

To obtain the spectral dynamics, two types of experiments were conducted: a rephasing (photon echo) and nonrephasing experiment, only differing from each other by their phase matching conditions, $k_{s,r} = -k_1+k_2+k_3$ and $k_{s,nr} = +k_1-k_2+k_3$ respectively. The dynamic observables obtained from these particular experiments are the vibrational lifetime, the inter- or intra-molecular vibrational redistribution time and the frequency-fluctuation correlation function (FFCF, $C(t)=\langle \delta\omega(0)\delta\omega(t)\rangle$), with this manuscript focusing on the latter. To obtain the FFCF, we calculate the Inhomogeneity Index ($I(t_2)$, Eq. **4.10**).[13]

$$I(t)=\frac{A_r - A_{nr}}{A_r + A_{nr}} \tag{4.10}$$

The peak amplitude from the nonrephasing (A_{nr}) experiment is subtracted from the peak amplitude of the rephasing experiment and the difference is normalized. This procedure is repeated for each waiting time delay (t_2). Since $I(t_2)$ is only proportional to the FFCF, we must use the following equation (**Eq. 4.11**) to calculate the FFCF:

$$C(t_2)=\sin\left[\frac{\pi I(t_2)}{2}\right] \tag{4.11}$$

This method of measuring the FFCF has been described previously by Tokmakoff *et al*. and by us.[13, 37]

REFERENCES

1. Hawecker, J.; Lehn, J. M.; Ziessel, R., Efficient Photochemical Reduction of CO_2 to CO by Visible Light Irradiation of Systems Containing $Re(bipy)(CO)_3X$ or $Ru(bipy)_3^{2+}$-Co^{2+} Combinations as Homogeneous Catalysts. *J. Chem. Soc., Chem. Commun.* **1983,** (9), 536-538.

2. Morris, A. J.; Meyer, G. J.; Fujita, E., Molecular Approaches to the Photocatalytic Reduction of Carbon Dioxide for Solar Fuels. *Acc. Chem. Res.* **2009,** *42* (12), 1983-1994.

3. Takeda, H.; Ishitani, O., Development of Efficient Photocatalytic Systems for CO_2 Reduction Using Mononuclear and Multinuclear Metal Complexes Based on Mechanistic Studies. *Coordination Chemistry Reviews* **2010,** *254* (3-4), 346-354.

4. Kutal, C.; Corbin, A. J.; Ferraudi, G., Further Studies of the Photoinduced Reduction of Carbon Dioxide Mediated by Tricarbonylbromo(2,2'-bipyridine)rhenium(I). *Organometallics* **1987,** *6* (3), 553-557.

5. Kutal, C.; Weber, M. A.; Ferraudi, G.; Geiger, D., A Mechanistic Investigation of the Photoinduced Reduction of Carbon Dioxide Mediated by Tricarbonylbromo(2,2'-bipyridine)rhenium(I). *Organometallics* **1985,** *4* (12), 2161-2166.

6. Vlček, A., Ultrafast Excited-State Processes in Re(I) Carbonyl-Diimine Complexes: From Excitation to Photochemistry. In *Photophysics of Organometallics*, Lees, A. J., Ed. 2010; Vol. 29, pp 73-114.

7. El Nahhas, A.; Cannizzo, A.; van Mourik, F.; Blanco-Rodriguez, A. M.; Zalis, S.; Vlček, A.; Chergui, M., Ultrafast Excited-State Dynamics of $[Re(L)(CO)_3(bpy)]^n$ Complexes: Involvement of the Solvent. *Journal of Physical Chemistry A* **2010,** *114* (22), 6361-6369.

8. Liard, D. J.; Busby, M.; Matousek, P.; Towrie, M.; Vlček, A., Picosecond Relaxation of ^{3}MLCT Excited States of $[Re(Etpy)(CO)_3(dmb)]^+$ and $Re(Cl)(CO)_3(bpy)$ as Revealed by Time-Resolved Resonance Raman, UV-vis, and IR Absorption Spectroscopy. *Journal of Physical Chemistry A* **2004,** *108* (13), 2363-2369.

9. Morimoto, T.; Nakajima, T.; Sawa, S.; Nakanishi, R.; Imori, D.; Ishitani, O., CO_2 Capture by a Rhenium(I) Complex with the Aid of Triethanolamine. *Journal of the American Chemical Society* **2013,** *135* (45), 16825-16828.

10. Agarwal, J.; Fujita, E.; Schaefer, H. F.; Muckerman, J. T., Mechanisms for CO Production from CO_2 Using Reduced Rhenium Tricarbonyl Catalysts. *Journal of the American Chemical Society* 2012, *134* (11), 5180-5186.

11. Hayashi, Y.; Kita, S.; Brunschwig, B. S.; Fujita, E., Involvement of a Binuclear Species with the Re-C(O)O-Re moiety in CO_2 Reduction Catalyzed by Tricarbonyl Rhenium(I) Complexes with Diimine Ligands: Strikingly Slow Formation of the Re-Re and Re-C(O)O-Re Species from $Re(dmb)(CO)_3S$ (dmb=4,4'-dimethyl-2,2'-bipyridine, S = solvent). *Journal of the American Chemical Society* 2003, *125* (39), 11976-11987.

12. Rosenfeld, D. E.; Gengeliczki, Z.; Smith, B. J.; Stack, T. D. P.; Fayer, M. D., Structural Dynamics of a Catalytic Monolayer Probed by Ultrafast 2D IR Vibrational Echoes. *Science* 2011, *334* (6056), 634-639.

13. Roberts, S. T.; Loparo, J. J.; Tokmakoff, A., Characterization of Spectral Diffusion from Two-dimensional Line Shapes. *Journal of Chemical Physics* 2006, *125* (8), 084502.

14. Dunbar, J. A.; Arthur, E. J.; White, A. M.; Kubarych, K. J., Ultrafast 2D-IR and Simulation Investigations of Preferential Solvation and Cosolvent Exchange Dynamics. *Journal of Physical Chemistry B* 2015, *119* (20), 6271-6279.

15. Agmon, N., The Dynamics of Preferential Solvation. *Journal of Physical Chemistry A* 2002, *106* (32), 7256-7260.

16. Nguyen, C. N.; Stratt, R. M., Preferential Solvation Dynamics in Liquids: How Geodesic Pathways through the Potential Energy Landscape Reveal Mechanistic Details about Solute Relaxation in Liquids. *Journal of Chemical Physics* 2010, *133* (12), 124503.

17. Brookes, J. F.; Slenkamp, K. M.; Lynch, M. S.; Khalil, M., Effect of Solvent Polarity on the Vibrational Dephasing Dynamics of the Nitrosyl Stretch in an Fe^{II} Complex Revealed by 2D IR Spectroscopy. *J. Phys. Chem. A* 2013, *117* (29), 6234-6243.

18. Jones, B. H.; Huber, C. J.; Spector, I. C.; Tabet, A. M.; Butler, R. L.; Hang, Y.; Massari, A. M., Correlating Solvent Dynamics and Chemical Reaction Rates using Binary Solvent Mixtures and Two-dimensional Infrared Spectroscopy. *Journal of Chemical Physics* 2015, *142* (21), 212441.

19. King, J. T.; Ross, M. R.; Kubarych, K. J., Ultrafast alpha-Like Relaxation of a Fragile Glass-Forming Liquid Measured Using Two-Dimensional Infrared Spectroscopy. *Phys. Rev. Lett.* 2012, *108* (15) .

20. Sokolowsky, K. P.; Bailey, H. E.; Fayer, M. D., New Divergent Dynamics in the Isotropic to Nematic Phase Transition of Liquid Crystals Measured with 2D IR Vibrational Echo Spectroscopy. *Journal of Chemical Physics* 2014, *141* (19), 194502.

21. Kiefer, L. M.; Kubarych, K. J., Solvent-Dependent Dynamics of a Series of Rhenium Photoactivated Catalysts Measured with Ultrafast 2DIR. *Journal of Physical Chemistry A* 2015, *119* (6), 959-965.

22. Kwak, K.; Park, S.; Finkelstein, I. J.; Fayer, M. D., Frequency-frequency Correlation Functions and Apodization in Two-dimensional Infrared Vibrational Echo Spectroscopy: A New Approach. *Journal of Chemical Physics* 2007, *127* (12), 124503.

23. Reichardt, C., Solvatochromic Dyes as Solvent Polarity Indicators. *Chemical Reviews* 1994, *94* (8), 2319-2358.

24. Gutmann, V., Solvent Effects on Reactivities of Organometallic Compounds. *Coordination Chemistry Reviews* 1976, *18* (2), 225-255.

25. Asbury, J. B.; Wang, Y.; Lian, T., Time-Dependent Vibration Stokes Shift During Solvation: Experiment and Theory. *Bulletin of the Chemical Society of Japan* 2002, *75* (5), 973-983.

26. Smieja, J. M.; Kubiak, C. P., Re(bipy-tBu)$(CO)_3$Cl-Improved Catalytic Activity for Reduction of Carbon Dioxide: IR-Spectroelectrochemical and Mechanistic Studies. *Inorganic Chemistry* 2010, *49* (20), 9283-9289.

27. Johnson, F. P. A.; George, M. W.; Hartl, F.; Turner, J. J., Electrocatalytic Reduction of CO_2 using the Complexes $[Re(bpy)(CO)_3L]^n$ (n=+1, L=$P(OEt)_3$, CH_3CN; n=0, L=Cl^-, Otf^-; bpy=2,2'-Bipyridine; Otf^-=CF_3SO_3) as Catalyst Precursors: Infrared Spectroelectrochemical Investigation. *Organometallics* 1996, *15* (15), 3374-3387.

28. Stor, G. J.; Hartl, F.; Vanoutersterp, J. W. M.; Stufkens, D. J., Spectroelectrochemical (Ir, UV/Vis) Determination of the Reduction Pathways for a Series of $[Re(CO)_3(\alpha\text{-diimine})L']^{0/+}$ (L'=Halide, Otf^-, THF, MeCN, n-PrCN, PPh_3, $P(OMe)_3$) Complexes. *Organometallics* 1995, *14* (3), 1115-1131.

29. Gladkikh, V. S.; Burshtein, A. I.; Tavernier, H. L.; Fayer, M. D., Influence of Diffusion on the Kinetics of Donor-acceptor Electron Transfer Monitored by the Quenching of Donor Fluorescence. *Journal of Physical Chemistry A* **2002,** *106* (30), 6982-6990.

30. Collins, F. C.; Kimball, G. E., Diffusion-Controlled Reaction Rates. *Journal of Colloid Science* **1949,** *4* (4), 425-437.

31. Stejskal, E. O.; Tanner, J. E., Spin Diffusion Measurements: Spin Echoes in the Presence of a Time-Dependent Field Gradient. *J. Chem. Phys.* **1965,** *42* (1), 288.

32. Probst, B.; Kolano, C.; Hamm, P.; Alberto, R., An Efficient Homogeneous Intermolecular Rhenium-Based Photocatalytic System for the Production of H_2. *Inorg. Chem.* **2009,** *48* (5), 1836-1843.

33. Gray, H. B.; Winkler, J. R., Electron Tunneling Through Proteins. *Quarterly Reviews of Biophysics* **2003,** *36* (3), 341-372.

34. Takeda, H.; Koike, K.; Inoue, H.; Ishitani, O., Development of an Efficient Photocatalytic System for CO_2 Reduction Using Rhenium(I) Complexes Based on Mechanistic Studies. *Journal of the American Chemical Society* **2008,** *130* (6), 2023-2031.

35. Reithmeier, R.; Bruckmeier, C.; Rieger, B., Conversion of CO_2 via Visible Light Promoted Homogeneous Redox Catalysis. *Catalysts* **2012,** *2* (4), 544-571.

36. Nee, M. J.; Baiz, C. R.; Anna, J. M.; McCanne, R.; Kubarych, K. J., Multilevel Vibrational Coherence Transfer and Wavepacket Dynamics Probed with Multidimensional IR Spectroscopy. *Journal of Chemical Physics* **2008,** *129* (8), 084503.

37. Kiefer, L. M.; King, J. T.; Kubarych, K. J., Dynamics of Rhenium Photocatalysts Revealed Through Ultrafast Multidimensional Spectroscopy. *Accounts of Chemical Research* **2015,** *48* (4), 1123-1130.

Chapter 5

NOESY-Like 2D-IR Spectroscopy Reveals Non-Gaussian Dynamics

The work presented in this chapter has been published in the following paper:

L. M. Kiefer, K. J. Kubarych, "NOESY-Like 2D-IR Spectroscopy Reveals Non-Gaussian Dynamics", J. Phys. Chem. Lett., 7, 3819 (2016)

5.1 INTRODUCTION

Two-dimensional optical spectroscopy has many conceptual analogies with nuclear magnetic resonance. Though nearly all of the molecular details differ, there are so many

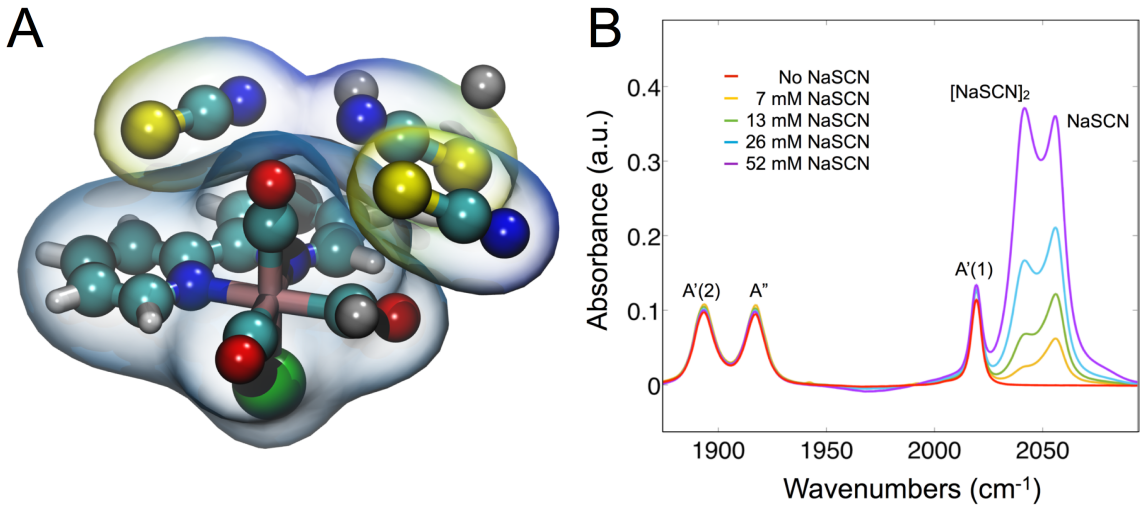

Figure 5.1: (A) $ReCl(bpy)(CO)_3$, a CO_2 reduction photocatalyst solvated by three NaSCN ion pairs. Though it was generated by force-field (UFF) energy minimization, this structure should be viewed as a cartoon since there was no solvent included. (B) FTIR spectra of various solutions of $ReCl(bpy)(CO)_3$ (1.5 mM) and NaSCN in THF.

similarities that we should explore new technical and conceptual advances using established NMR approaches as inspiration.[1] Energy transfer processes, both intra- and intermolecular, are ubiquitous in infrared and visible spectroscopy, and have been used to determine couplings, orientations, distances,[2-5] and to understand phenomena such as heat dissipation in peptides,[6] as well as photosynthetic energy harvesting.[7, 8] In NMR, "energy transfer" is associated with the nuclear Overhauser effect (NOE) describing the transfer of magnetic polarization through a dipole-dipole interaction, which has the same $1/R^6$ distance dependence one encounters in electronic or vibrational energy transfer. In practice, the simplest 2D NOESY spectroscopy consists of three $\pi/2$ pulses, separated by adjustable time delays, which is the same sequence used in two-dimensional optical spectroscopy. A key aspect of NOESY is that although the distance dependence is due to the dipole-dipole coupling, the amplitudes and signs of the cross peaks are determined by the time scales of motional fluctuations.[9, 10]

Both the NOE and optical Förster resonant energy transfer (FRET) typically follow the same $1/R^6$ distance dependent law, which is the essence of the pronounced structural sensitivity.[1] Optical 2D spectroscopy operates in the perturbative regime where three field-matter interactions induce a polarization that serves as the source of the emitted signal field. FRET is described as the simultaneous emission from the donor and excitation of the acceptor, which is second order in perturbation theory, raising the net nonlinearity of the pathway to fifth order. Further, since the energy transfer can only occur following donor excitation, there are effectively two waiting time periods, one before, and one after the energy transfer event. With respect to low-frequency dynamical fluctuations, third-order 2D spectroscopy is one-dimensional, providing only the one time-interval correlation function (i.e. $C(t)=\langle\delta\omega(0)\delta\omega(t)\rangle$). It has now been well established that fifth-order, 3D spectroscopy is required to sense non-Gaussian spectral dynamics during the waiting time.[11-13] The question we seek to address is the following: can the increased nonlinearity and additional evolution period bring a new dynamical window to an experiment where only three fields are delivered experimentally? Using a photocatalytic transition metal complex in solution with NaSCN co-solute (**Fig. 5.1**), we find that apparently the answer is yes, the intermolecular energy transfer filters dynamics that are difficult or impossible to observe from the spectral dynamics of either the donor or acceptor alone. At the same time, we are able to establish

definitively the preferential interaction between the polar $ReCl(bpy)(CO)_3$ photocatalyst and the NaSCN co-solute.

Within the framework of Gaussian statistics, linear response holds due to the harmonic nature of the potential of mean force underlying the solvation dynamics.[11] A Gaussian ensemble cannot exhibit frequency-dependent dephasing arising either from homogeneous, collisional dynamics or heterogeneous spectral diffusion. Analogously to how nonlinear spectroscopy requires anharmonicity, linear response will fail when the potential governing fluctuations is anharmonic. In a donor-acceptor system subject to Gaussian statistics, the dynamics of the acceptor after receiving energy from the donor should be identical to the equilibrium fluctuations of the acceptor in the absence of the donor or an energy transfer event. Since rapid energy transfer places constraints on the relative distance, orientation, and energy level fluctuations of both the donor and acceptor, we might expect energy transfer to be especially sensitive to non-Gaussian fluctuations. In the present system, we observe a non-equilibrium frequency shift of the NaSCN energy acceptor that is faster than the equilibrium fluctuations of the same acceptor species in the absence of energy transfer.

5.2 NaSCN AS A PROBE OF PREFERENTIAL INTERACTIONS

Our previous investigations into the dynamics of rhenium photocatalysts have highlighted the significance of electrostatics in determining the solvation dynamics on the ground singlet (S_0) and triplet metal-to-ligand charge transfer (^{3}MCLT) excited electronic states. We found the time scale of spectral diffusion as determined with equilibrium and transient 2D-IR spectroscopy to correlate with the solvent's donicity, which is a measure of the solvent's tendency to solvate electron deficient solutes.[14, 15] We attributed slower excited state spectral diffusion dynamics to the substantially reduced molecular dipole moment, which reduces the frictional coupling to the solvent.[16, 17] In general, a microscopic description of chemical reactions should include the effects of preferential solvation, since most solution phase reactions involve the interaction of more than two species.

As another probe of preferential solvation, we introduce here NaSCN contact ion pairs, which we have used previously as solvent-shell probes to study intramolecular electron transfer

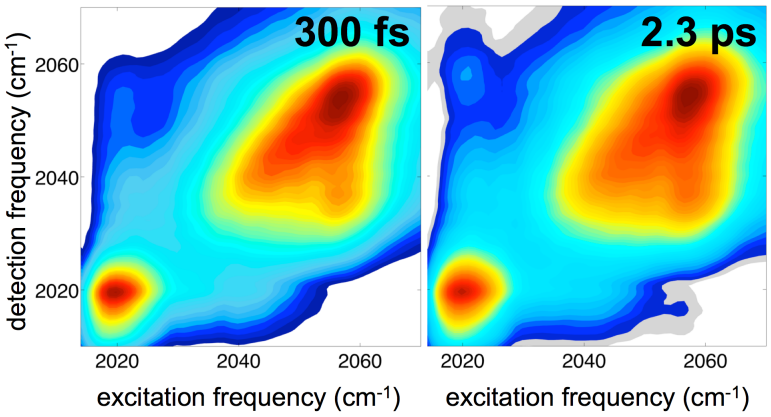

Figure 5.2: Absolute value rephasing spectra of ReCl(bpy)$(CO)_3$ (1.9 mM) and NaSCN (17 mM) in THF solution at two different waiting times. Even at 300 fs, there is a clear indication of cross peaks between the Re carbonyl stretch and both the monomer and dimer contact ion pairs, indicating rapid energy transfer.

in betaine-30 via a dynamical Stark effect.[18] Since the 14.1 Debye (D) ground state dipole moment of ReCl(bpy)$(CO)_3$ is similar to that of betaine-30 (17 D), we anticipated that in a relatively low polarity solvent such as THF, the NaSCN contact pairs would preferentially solvate the organometallic complex. The close lying symmetric stretch of the three CO ligands is within a few

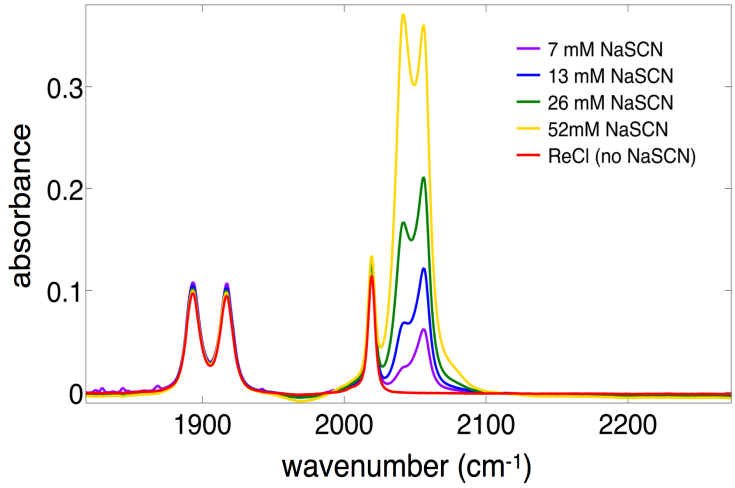

Figure 5.3: FTIR spectra of Re(bpy)$(CO)_3$Cl (1.5 mM) with multiple concentrations of NaNCS in THF used in this study, showing no evidence of a Re-SCN band at 2098 cm^{-1}.

10s of wavenumbers of the CN stretches of NaSCN (i.e. monomer) and $(NaSCN)_2$ (i.e. dimer), which should facilitate picosecond timescale energy transfer if the two species do in fact preferentially associate in solution.

The details of our specific experimental setup are described elsewhere.[19] Figure 5.2 shows 2D-IR absolute value rephasing spectra at waiting times of 0.3 and 2.3 ps, indicating clear energy transfer from the fully symmetric CO stretching mode of the $ReCl(bpy)(CO)_3$ to both the monomer and dimer NaSCN vibrations. Energy transfer on this short timescale indicates the close proximity between the species in solution, supporting the prediction of preferential interactions. The SCN^- ligand is not covalently bound to the Re metal center, as evidenced by the lack of a metal coordinated (i.e. Re-SCN) CN stretching band at 2098 cm^{-1} in the FTIR spectra (Figure 5.3).[20] Even at very low NaSCN concentration (17 mM), energy transfer cross peaks are evident under conditions where the majority species present is the monomer. We note that the monomer-dimer ratio exhibits a simple equilibrium constant except at very high salt concentrations. Due to the close spacing of the vibrational bands, cross peaks can appear in 2D spectra due to trivial overlap of spectral tails. We can exclude that these artifacts contribute to the dynamics discussed below, and a full description of this effect is given in a later section in this chapter.

5.3 UNEXPECTED SPECTRAL DYNAMICS OF THE ENERGY TRANSFER CROSS PEAKS

Intermolecular energy transfer has been observed in numerous contexts, especially in transient absorption and 2D-IR spectroscopy.[21-23] The cross peak amplitude is determined by the basic kinetics of donor-acceptor energy transfer, including both the transfer-less decay of the donor, and the decay of the acceptor.[24-26] Both the donor and acceptor vibrational lifetimes can be determined from the diagonal peak decays in the 2D spectrum assuming that the energy transfer is a small effect. Whatever the specific values for T_1 relaxation and the energy transfer rate constant, the expectation is that the cross peak amplitude increases and then decreases as a function of the waiting time. It is also possible to remove the effect of the vibrational relaxation by dividing by the acceptor diagonal peak amplitude as is often done in studies of intramolecular vibrational redistribution. Figure 5.4 shows the energy transfer kinetics as viewed through the integrated cross peak amplitudes; they display the expected time dependence. The energy transfer time constant from the Re complex donor to the accepting dimer was determined to be 3.6 ± 1.5 ps. We simulated the three peaks with zero coupling using SPECTRON to verify we are not seeing an artifact of spectral tail interference (details in a later section).[27] While the simulated

spectra do look similar to our measured spectra, the A'(1) → dimer and A'(1) → monomer cross peaks are more pronounced in the measured spectra. The simulations also do not produce a cross peak growth or a waiting time dependent blue-shift as observed in our experiment.

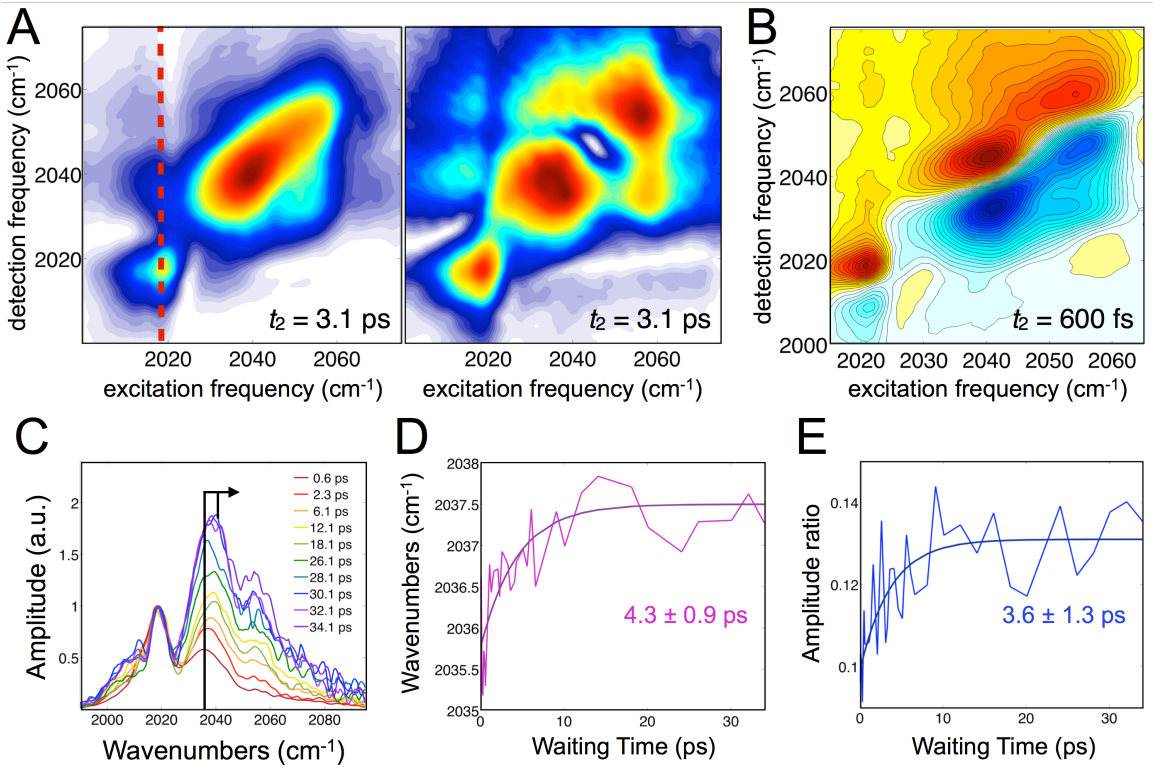

Figure 5.4: (A) Absolute value (left) rephasing and (right) nonrephasing spectra of $ReCl(bpy)(CO)_3$ (3.1 mM) and NaSCN (104 mM) in THF solution at a waiting time of 3.1 ps. (B) Absorptive 2D-IR spectrum shows cross peaks between the high frequency band of the Re complex at 2019 cm^{-1} and the two thiocyanate bands are evident in the spectrum at 600 fs waiting time. (C) Waiting time dependent slices of the rephasing spectra along the detection frequency axis, as indicated by the red dashed line in (A), normalized to the Re carbonyl band show a relative increase of the thiocyanate signal, as well as a pronounced blue shift. (D) Waiting time dependent peak position of the thiocyanate accepting mode shows a 4.3±0.9 ps evolution, which we attribute to spectral diffusion following energy transfer. (E) Ratio of the (2019 cm^{-1}, 2043 cm^{-1}) cross peak volume to the (2043 cm^{-1}, 2043 cm^{-1}) diagonal peak volume as a function of the waiting time. This ratio grows with a 3.6±1.3 ps time constant, reflecting the ultrafast intermolecular energy transfer from the carbonyl stretches of the rhenium complex to the solvating thiocyanate CN vibrations.

A closer look at the 2D spectra, however, reveals a striking feature that is not expected. It appears as though the cross peaks blue shift with increased waiting time. This shift allows one to view the spectral diffusion of the acceptor mode *after* the energy transfer process has occurred. Slices through the spectrum at the ReCl excitation frequency indicate two major features. The first is the diagonal peak belonging to totally symmetric A'(1) stretching band of the ReCl, and the

second is the cross peak corresponding to exciting ReCl followed by energy transfer to NaSCN. The lower frequency NaSCN band is due to the contact ion pair dimer, and the higher frequency band is attributed to the contact ion pair monomer.[28, 29] At even higher frequency, an ion triple is present in the mixture, but is not within the bandwidth of our experiment, and so is not present in the 2DIR spectra.

Fitting the slices along the detection frequency axis reveals the time dependent shift of the acceptor cross peak. To rule out the appearance of a peak shift due to amplitude changes in otherwise stationary bands, we attempted to fit the three bands with their respective center wavenumbers fixed but were unsuccessful, indicating that the peak shift is not due to the changes in amplitude of the involved peaks, and it is indeed from spectral diffusion. We extracted the peak center positions using three Gaussians, each constrained to ±7 cm^{-1} of the maxima of the FTIR

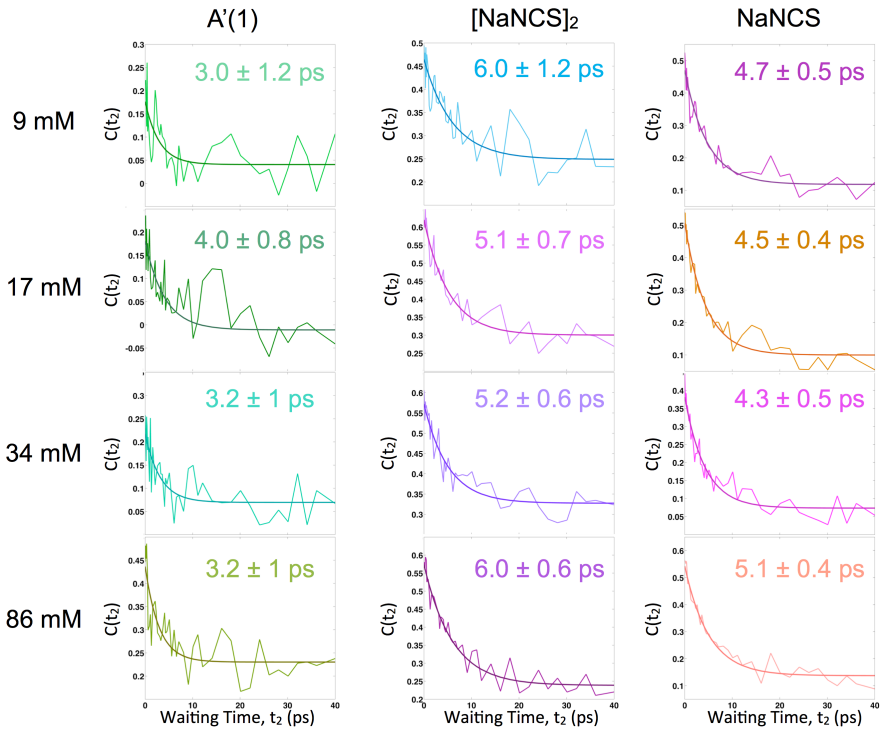

Figure 5.5: FFCFs of the A'(1) band of the $Re(bpy)(CO)_3Cl$, the $[NaNCS]_2$ and NaNCS bands at multiple concentrations of NaNCS in THF. The overall observed trend is that the A'(1) band is unaffected by the presence of the NaNCS and that the monomer has a faster correlation decay time than the dimer.

bands (Re complex: 2019 cm^{-1}; $(NaSCN)_2$: 2043 cm^{-1}; NaSCN : 2057 cm^{-1}) for each of the waiting times. A noticeable peak shift is observed in the cross peak from the Re A'(1) band to the dimer band with a time constant of 4.3±0.9 ps, a time that is different from either of the constituent

bands, which are reflected in the diagonal peaks. The FFCF of the Re A'(1) band decays with a 3.1±1 ps time constant, whereas the $(NaSCN)_2$ correlation function decays with a 5.2±0.8 ps time constant (**Fig. 5.5**). Interestingly, the time is similar to the spectral diffusion time of the single contact ion NaSCN pair (4.2±1 ps). We note that we performed the measurements at several NaSCN concentrations, ranging from 7 to 104 mM, and do not find significant differences in the spectral diffusion timescales, suggesting that the interaction between NaSCN and the rhenium complex induces substantial preferential solvation. The concentrations of the $ReCl(bpy)(CO)_3$ compound used in this study were between 1.4-3.1 mM in THF.

5.4 SIMULATION OF SPECTRA IN ABSENCE OF ENERGY TRANSFER

In 2D spectra, it is possible to observe features resembling cross peaks that result simply from the overlapping broad tails of two diagonal peaks. Typically, such features appear at the same or very similar location in the 2D spectrum where true cross peaks appear. To verify that our spectral observations are not obscured by these artifacts, we simulated rephasing and nonrephasing spectra for a three-component mixture using the SPECTRON[27] multidimensional spectroscopy code. We set the 0-1 transitions to be the experimental values determined by FTIR, and we set the anharmonicities equal to 7 cm^{-1} for the carbonyl stretch and 15 cm^{-1} for the two CN stretches of the monomer and dimer contact pairs. Next, we weighted the contributions of the three species to produce a linear absorption spectrum that closely matches the experimental FTIR for our experimental conditions. Finally, we computed the 2D spectra as a function of waiting time by changing the spectral weights with exponential decays as determined by our 2D measurements. The carbonyl stretch was set to decay with a 26 ps time constant, and the SCN stretches were set to decay with a 32 ps time constant. Using the simulated waiting time dependent spectra, we integrated the rephasing spectrum in the (2019 cm^{-1}, 2043 cm^{-1}) cross-peak region and divided that peak volume by the volume of the 2043 cm^{-1} diagonal peak (**Fig. 5.6**).

It is clear that several features of our 2D spectra resemble the simulated spectra, which simply confirms that we do have a mixture of species. The cross-peak to diagonal ratio, however, decreases as a function of waiting time, and does so on a very slow time scale. Fitting the decay to an exponential yields a time constant of 63 ps. Our experimental ratio increases with a 3 ps time

scale. Moreover, the absolute magnitude of the time evolution of the cross-peak to diagonal ratio is very small in the simulations, decreasing from 0.1965 to 0.187, which is less than 5%. The

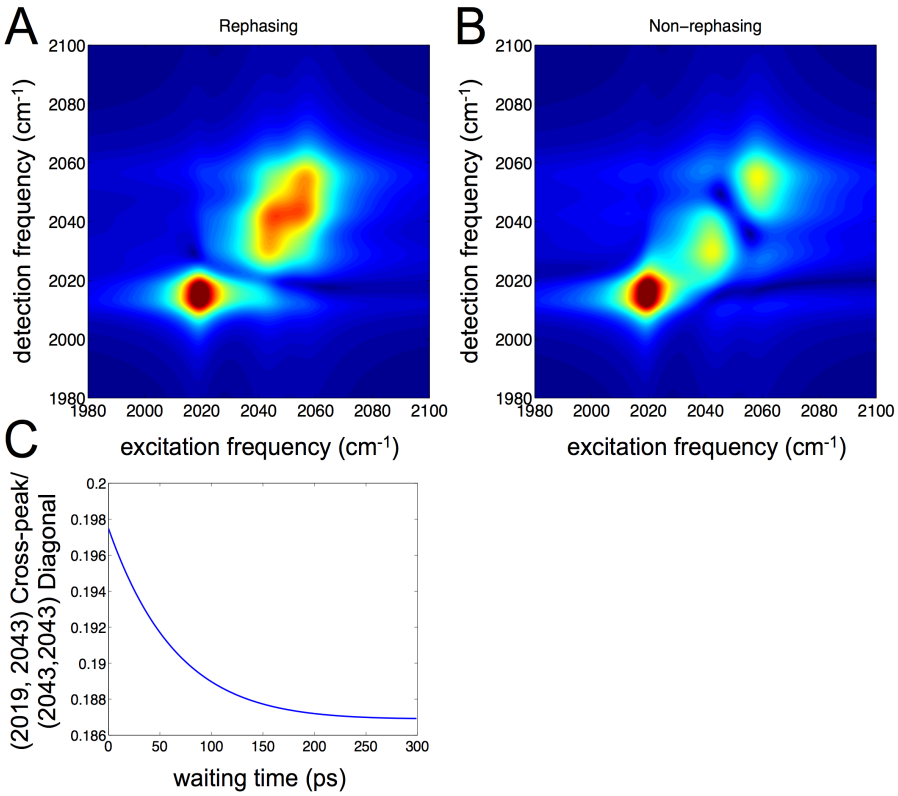

Figure 5.6: Simulated (A) rephasing and (B) nonrephasing spectra for a three-component mixture with vibrational Hamiltonian parameters corresponding to our experimental conditions. Many features of the 2D spectra resemble our measured spectra, but the increase in the cross peaks due to energy transfer are not. (C) The ratio of the (2019 cm^{-1}, 2043 cm^{-1}) cross peak volume to the (2043 cm^{-1}, 2043 cm^{-1}) diagonal peak volume for the rephasing spectrum. The decay of the ratio is very slow, and the magnitude of the change is less than 5% of the initial value. The experimental decay is shown in Fig. 5.3B of the main text; it *grows* by ~30% on a 3 ps time scale.

experimental ratio increases by roughly 30%. We also took vertical slices parallel to the detection axis using the simulated spectra to test whether the spectral shift could be due to the inherent overlapping spectra. The effect is quite small (**Fig. 5.7**), and we see in fact a red shift, rather than the blue shift observed in our measured data. At the positions of the 0-1 transitions of the monomer and dimer bands, there is essentially no spectral change.

5.5 DISCUSSION AND OUTLOOK

Intermolecular energy transfer selects those molecules that are optimally positioned to undergo rapid energy transfer. We expect to see a more pronounced cross peak from the A'(1)

band to the dimer band, evidenced by the upper cross peak in the 2DIR spectrum, largely due to the availability of multiple thiocyanate acceptors for each rhenium donor. After energy is

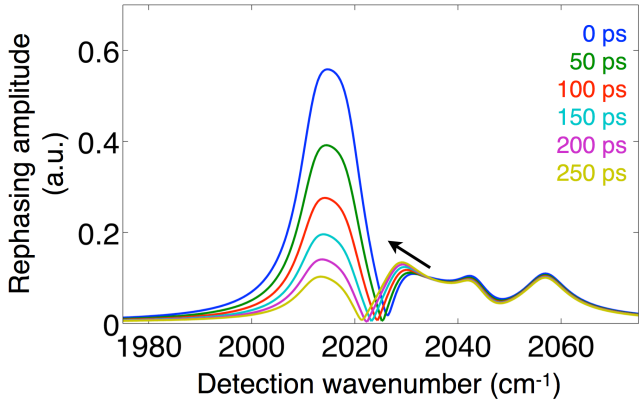

Figure 5.7: Vertical slices (along the detection frequency axis) for various simulated waiting times assuming a no-energy-transfer sum of three species. We observe slight spectral changes, most prominent in the 1-2 excited state absorption of the dimer, but they are red shifts. The experimental spectra exhibit blue shifts.

transferred to a lower energy subset of the NaSCN dimer band, the excited molecules then spectrally diffuse. The frequency shift occurs on a timescale that is coincidentally similar to that of the NaSCN contact ion pair, which may be indicative of the energy transfer from the Re complex to just one of the contact ion pairs in the dimer, possibly leading to the breakup of a dimer or other oligomer. The strong dependence of intermolecular vibrational energy transfer on the donor-acceptor energy gap, distance and relative orientation, serves to isolate those molecules that are best able to transfer energy, which in this case appear to be the lower-frequency subset of the dimer band.

How can energy transfer enhance the dynamical information content available in a third-order two-dimensional spectroscopy measurement? **Figure 5.8** shows a schematic representation of the pulse sequence, energy level diagrams of the donor and acceptor, as well as a cartoon indicating donor and acceptor energy level fluctuations. The dipole-dipole energy transfer process can be described using second-order perturbation theory, and hence increases the overall nonlinearity to fifth order, just as is the case for a three-dimensional spectroscopy method. The 3D spectrum has two waiting times (t_2 and $t_2^{'}$), and thus permits access to the two time interval correlation function of the frequency fluctuations: $C(t_2,t_2')=\langle\delta\omega(0)\delta\omega(t_2)\delta\omega(t_2+t_2')\rangle$.[11] A 2D

experiment with energy transfer can be thought of as being constructed from many 3D experiments averaged over a distribution of energy transfer times. With a large distribution of transfer times, the lack of synchronization should obscure the enhanced dynamical information.

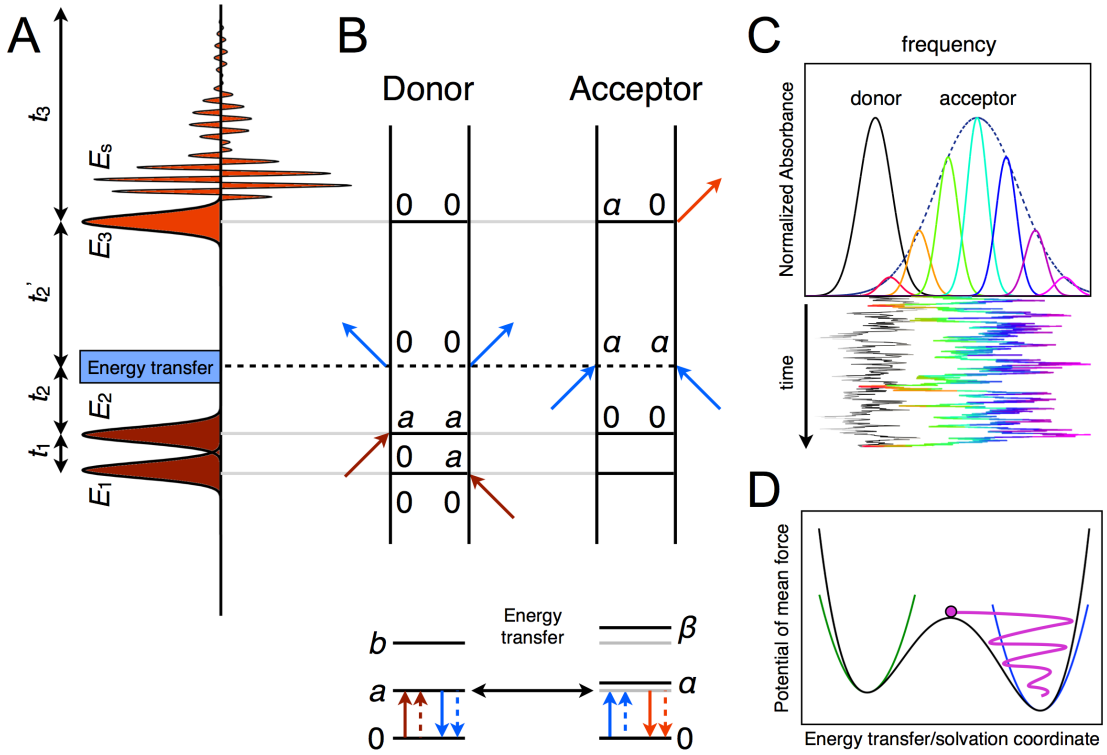

Figure 5.8: (A) 2D-IR pulse sequence explicitly indicating the energy transfer event shown together with (B) double-sided Feynman diagrams and wave matching energy level diagrams for the donor and acceptor. The energy transfer is a second-order process, which raises the effective nonlinearity of the experiment to fifth-order, and makes the spectral dynamics sensitive to the three time point correlation function of the frequency fluctuations: $C(t_2,t_2')=\langle\delta\omega(0)\delta\omega(t_2)\delta\omega(t_2+t_2')\rangle$. (C) Cartoon representation of the dephasing mechanism of energy transfer. Fluctuations of the donor and acceptor energies result in transient degeneracies where energy transfer can occur very rapidly. When the energy transfer is fast, the donor energy gap is transiently high frequency when the acceptor is transiently low frequency. Subsequent evolution results in a blue shift of the acceptor mode. (D) A schematic potential of mean force (PMF) showing a tagged subset (fuschia circle) prepared in the region between two stable basins. The relaxation of this subset samples the anharmonicity of the PMF, giving rise to non-Gaussian statistics.

If, on the other hand, the energy transfer is prompt, averaging over the timing of the events will preserve the filtered dynamics. For our case, where we find a 3 ps energy transfer time scale, for an exponential process, roughly 20% of the energy transfer events occur within the first 1 ps following excitation; 50% occur within the first 2 ps. Returning to the analogy with NOESY, it is important to note that the dipolar coupling that underlies NOESY orientationally averages to zero

in isotropic, fast tumbling systems, so it is only apparent when there are slow fluctuations due to conformational sampling or chemical exchange, for example.[10] In our case, we require the opposite dynamical condition: the energy transfer must be fast in order to avoid the time averaging that would destroy the synchronized spectral shift that contains the dynamical information. Vibrational energy transfer can probe catalyst aggregation between surface-bound molecules, and energy transfer may be significant for catalysis reaction dynamics.[30, 31] Though perhaps unusual in intermolecular vibrational energy transfer, rapid energy transfer is not uncommon in photosynthetic light harvesting,[32] where 2D electronic spectroscopy peak shape analysis may reveal sub-ensemble dynamics.

For a dynamical picture of vibrational energy transfer, we can represent the model that has been denoted the "dephasing mechanism" by Zheng *et al*.[2, 24] Here the stochastic fluctuations of donor and acceptor energies result in fleeting overlap, at which point the energy transfer is very rapid. Since it is most likely for this temporary resonance condition to be met during high-frequency excursions of the donor coincident with low-frequency fluctuations of the acceptor, we anticipate a general blue shift of the acceptor band following energy transfer. If the energy transfer were dictated by the spectral fluctuations of the donor and acceptor independently, the time scale for simultaneously fluctuating towards energy overlap must be slower than the spectral diffusion of the individual species since many fluctuations increase the donor-acceptor mismatch. Instead, we find a ~30% faster post-energy transfer spectral evolution, indicating that the successful energy transfer events are selected from a subset of the overall ensemble that exhibit fluctuations on a distinct time scale, which is a hallmark of non-Gaussian statistics.

Vibrational energy transfer has the potential to provide distance constraints that yield structural information in complex environments.[5] Beyond measuring distances, we find here that spectral evolution following ultrafast energy transfer can reveal not only preferential solvation, but can also highlight the dynamics of multi-molecular complexes. Given the changes in electrostatics in this rhenium photocatalyst, it is intriguing to imagine how a similar study on the metastable ^{3}MLCT state might reveal distinct energy transfer dynamics. This work helps to illustrate how inherent system dynamics can serve to enhance the nonlinearity of spectroscopic measurements, potentially revealing new information that survives ensemble averaging. Similar

phenomena are likely to be observed in natural and artificial light harvesting systems where energy transfer can occur on time scales faster than environmental structural dynamics.

REFERENCES

1. Scheurer, C.; Mukamel, S., Design Strategies for Pulse Sequences in Multidimensional Optical Spectroscopies. *J. Chem. Phys.* 2001, *115*, 4989-5004.

2. Chen, H.; Bian, H.; Li, J.; Wen, X.; Zhang, Q.; Zhuang, W.; Zheng, J., Vibrational Energy Transfer: An Angstrom Molecular Ruler in Studies of Ion Pairing and Clustering in Aqueous Solutions. *J. Phys. Chem. B* 2015, *119*, 4333-4349.

3. Woutersen, S.; Bakker, H. J., Resonant Intermolecular Transfer of Vibrational Energy in Liquid Water. *Nature* 1999, *402*, 507-509.

4. Thamer, M.; De Marco, L.; Ramasesha, K.; Mandal, A.; Tokmakoff, A., Ultrafast 2D IR Spectroscopy of the Excess Proton in Liquid Water. *Science* 2015, *350*, 78-82.

5. Jansen, T. L. C.; Knoester, J., Two-dimensional Infrared Population Transfer Spectroscopy for Enhancing Structural Markers of Proteins. *Biophys. J.* 2008, *94*, 1818-1825.

6. Botan, V.; Backus, E. H. G.; Pfister, R.; Moretto, A.; Crisma, M.; Toniolo, C.; Nguyen, P. H.; Stock, G.; Hamm, P., Energy Transport in Peptide Helices. *Proc. Natl. Acad. Sci. U. S. A.* 2007, *104*, 12749-12754.

7. Myers, J. A.; Lewis, K. L. M.; Fuller, F. D.; Tekavec, P. F.; Yocum, C. F.; Ogilvie, J. P., Two-Dimensional Electronic Spectroscopy of the D1-D2-cyt b559 Photosystem II Reaction Center Complex. *J. Phys. Chem. Lett.* 2010, *1*, 2774-2780.

8. Sundstrom, V.; Pullerits, T.; van Grondelle, R., Photosynthetic Light-Harvesting: Reconciling Dynamics and Structure of Purple Bacterial LH2 Reveals Function of Photosynthetic Unit. *J. Phys. Chem. B* 1999, *103*, 2327-2346.

9. Olejniczak, E. T.; Poulsen, F. M.; Dobson, C. M., Proton Nuclear Overhauser Effects and Protein Dynamics. *J. Am. Chem. Soc.* 1981, *103*, 6574-6580.

10. Ernst, R.; Bodenhausen, G.; Wokaun, A., *Principles of Nuclear Magnetic Resonance in One and Two Dimensions*. Clarendon Press: Oxford, 1987.

11. Hamm, P., Three-dimensional-IR Spectroscopy: Beyond the Two-point Frequency Fluctuation Correlation Function. *J. Chem. Phys.* 2006, *124*, 124506.

12. Garrett-Roe, S.; Hamm, P., What Can We Learn from Three-Dimensional Infrared Spectroscopy? *Acc. Chem. Res.* 2009, *42*, 1412-1422.

13. Bredenbeck, J.; Helbing, J.; Hamm, P., Solvation Beyond the Linear Response Regime. *Phys. Rev. Lett.* 2005, *95*, 083201.

14. Kiefer, L. M.; Kubarych, K. J., Solvent-Dependent Dynamics of a Series of Rhenium Photoactivated Catalysts Measured with Ultrafast 2DIR. *J. Phys. Chem. A* 2015, *119*, 959-965.

15. Gutmann, V., Solvent Effects on Reactivities of Organometallic Compounds. *Coord. Chem. Rev.* 1976, *18*, 225-255.

16. Kiefer, L. M.; King, J. T.; Kubarych, K. J., Equilibrium Excited State Dynamics of a Photoactivated Catalyst Measured with Ultrafast Transient 2DIR. *J. Phys. Chem. A* 2014, *118*, 9853-9860.

17. Kiefer, L. M.; King, J. T.; Kubarych, K. J., Dynamics of Rhenium Photocatalysts Revealed through Ultrafast Multidimensional Spectroscopy. *Acc. Chem. Res.* 2015, *48*, 1123-1130.

18. Baiz, C. R.; Kubarych, K. J., Ultrafast Vibrational Stark-Effect Spectroscopy: Exploring Charge-Transfer Reactions by Directly Monitoring the Solvation Shell Response. *J. Am. Chem. Soc.* 2010, *132*, 12784-12785.

19. Nee, M. J.; Baiz, C. R.; Anna, J. M.; McCanne, R.; Kubarych, K. J., Multilevel Vibrational Coherence Transfer and Wavepacket Dynamics Probed with Multidimensional IR Spectroscopy. *J. Chem. Phys.* 2008, *129*, 084503.

20. Rodriguez, A. M. B.; Gabrielsson, A.; Motevalli, M.; Matousek, P.; Towrie, M.; Sebera, J.; Zalis, S.; Vlček, A., Ligand-to-Diimine/Metal-to-Diimine Charge-Transfer Excited States of $Re(NCS)(CO)_3$(alpha-diimine) (alpha-diimine=2,2 '-bipyridine, di-Pr-i-N,N-1,4-diazabutadiene). A Spectroscopic and Computational Study. *J. Phys. Chem. A* 2005, *109*, 5016-5025.

21. Bian, H.; Wen, X.; Li, J.; Chen, H.; Han, S.; Sun, X.; Song, J.; Zhuang, W.; Zheng, J., Ion Clustering in Aqueous Solutions Probed with Vibrational Energy Transfer. *Proc. Natl. Acad. Sci. U. S. A.* 2011, *108*, 4737-4742.

22. Bian, H.; Li, J.; Wen, X.; Zheng, J., Mode-specific Intermolecular Vibrational Energy Transfer. I. Phenyl Selenocyanate and Deuterated Chloroform Mixture. *J. Chem. Phys.* 2010, *132*, 034505.

23. Kurochkin, D. V.; Naraharisetty, S. R. G.; Rubtsov, I. V., A Relaxation-Assisted 2D IR Spectroscopy Method. *Proc. Natl. Acad. Sci. U. S. A.* 2007, *104*, 14209-14214.

24. Chen, H.; Zhang, Q.; Guo, X.; Wen, X.; Li, J.; Zhuang, W.; Zheng, J., Nonresonant Energy Transfers Independent on the Phonon Densities in Polyatomic Liquids. *J. Phys. Chem. A* 2015, *119*, 669-680.

25. Chen, H.; Wen, X.; Guo, X.; Zheng, J., Intermolecular Vibrational Energy Transfers in Liquids and Solids. *Phys. Chem. Chem. Phys.* 2014, *16*, 13995-14014.

26. Bian, H.; Chen, H.; Li, J.; Wen, X.; Zheng, J., Nonresonant and Resonant Mode-Specific Intermolecular Vibrational Energy Transfers in Electrolyte Aqueous Solutions. *J. Phys. Chem. A* 2011, *115*, 11657-11664.

27. Zhuang, W.; Abramavicius, D.; Hayashi, T.; Mukamel, S., Simulation protocols for coherent femtosecond vibrational spectra of peptides. *J. Phys. Chem. B* 2006, *110*, 3362-3374.

28. Saar, D.; Petrucci, S., Infrared and Ultrasonic Spectra of Sodium Thiocyanate and Lithium Thiocyanate in Tetrahydrofuran. *J. Phys. Chem.* 1986, *90*, 3326-3330.

29. Firman, P.; Xu, M.; Eyring, E. M.; Petrucci, S., Thermodynamics of Dimerization of NaSCN in Some Acyclic Polyethers Studied by Infrared-Spectroscopy. *J. Phys. Chem.* 1992, *96*, 8631-8639.

30. Kraack, J. P.; Lotti, D.; Hamm, P., Ultrafast, Multidimensional Attenuated Total Reflectance Spectroscopy of Adsorbates at Metal Surfaces. *J. Phys. Chem. Lett.* 2014, *5*, 2325-2329.

31. Oudenhoven, T. A.; Joo, Y.; Laaser, J. E.; Gopalan, P.; Zanni, M. T., Dye aggregation identified by vibrational coupling using 2D IR spectroscopy. *J. Chem. Phys.* 2015, *142*.

32. Beljonne, D.; Curutchet, C.; Scholes, G. D.; Silbey, R. J., Beyond Forster Resonance Energy Transfer in Biological and Nanoscale Systems. *J. Phys. Chem. B* 2009, *113*, 6583-6599.

Chapter 6

Heterogeneous Polymer Flexibility Measured with Probe-Free, Site-Addressable Ultrafast Two-Dimensional Infrared Spectroscopy

6.1 INTRODUCTION

Many of the important aspects of polymer transport and rheological properties, in solution or in melts, derive from the fundamental motions of the atoms comprising the macromolecule.[1,2] Since the timescales of molecular motions are inherently ultrafast (10^{-15} to 10^{-12} s), direct experimental access has been a challenge. Spectroscopic probes, which potentially perturb the local dynamics, can be used to track overall diffusion,[3-5] but they do not provide site-specific information about the motion of the polymer chains themselves. Ideally, one would be able to probe the microscopic motional dynamics of each site of a polymer chain with ultrafast time resolution. However, due to the nature of a homopolymer, it is not straightforward to controllably insert spectroscopically distinct side chains for study with a method such as two-dimensional infrared (2D-IR) spectroscopy. One approach might be to use isotope labeled C=O units in a homopeptide, varying the location of the site label in order to spatially map the chain dynamics. Although there have been numerous applications of 2D-IR to peptides, they have generally been directed at problems with relevance to biology, rather than to polymer physics.[6-9] To-date, there have been no systematic studies of polymer dynamics using probe-free ultrafast

spectroscopy in conditions ranging from dilute solution to solid films. In this Letter we describe one approach to this long-standing problem using a novel metal-containing polymer (**Fig. 6.1**), wherein we leverage the chemically similar but spectroscopically distinct end-chain and inner-chain vibrational frequencies to elucidate differences in motional dynamics using 2D-IR.

The experimental findings are clear: (1) the chain ends appear to lose frequency correlation more slowly than do the inner chain sites, and (2) the degree to which the ends exhibit slower dynamics becomes reduced as the polymer is concentrated into a film. To test the basic timescale trend, we use a coarse-grained, Rouse-like model of the 8-mer consisting of harmonically-connected beads with sizes estimated using semi-empirical geometry optimization. Simulating the dynamics using a Langevin approach, we find that site-specific motional fluctuations are consistent with our measured 2D-IR spectral dynamics. The remarkable agreement between the simplified

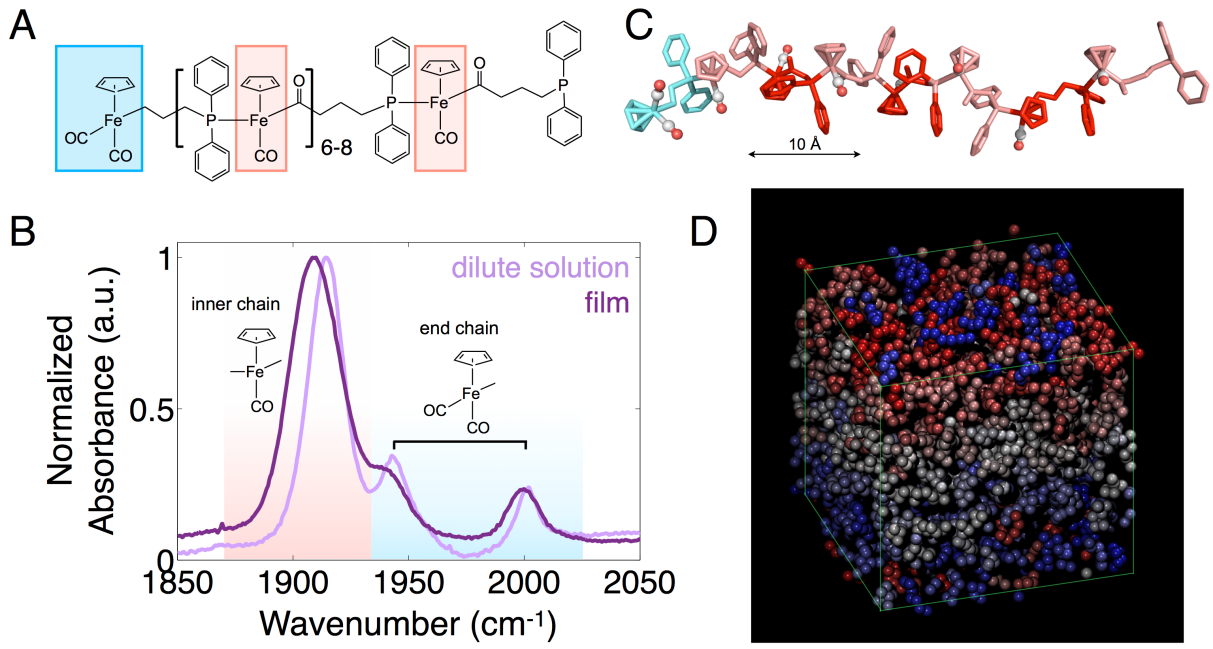

Fig. 6.1: (A) Structure of poly-FpP [poly-$(CpFe(CO)_2(CH_2)_3PPh_2)$] highlighting the chain end (blue) and inner chain (red) sites. (B) FTIR spectra of PFpP in dilute solution (light purple) and a solvent-free film (dark purple) show three bands (1914, 1944, and 2003 cm^{-1}) in the metal carbonyl CO stretching region. (C) Semi-empirical (PM6) energy minimized structure of the 8-mer; hydrogens are omitted and terminal carbonyls are shown as spheres. (D) Snapshot of a coarse grained simulation of a melt of 512 8-mers.

model and our relative dynamics timescales measured experimentally illustrate the powerful ability of 2D-IR spectroscopy to resolve polymer motion with site-addressability. At the same time,

the essentially quantitative agreement between measured and simulated dynamics timescales reinforces the general utility of simplistic models even for relatively short chains.

6.2 BACKGROUND ON 2D-IR AND METAL CARBONYLS, SPECTRAL DIFFUSION

The polymer system, described previously,[10] is synthesized using migration insertion polymerization (MIP) of the FpP ($CpFe(CO)_2(CH_2)_3PPh_2$, cyclopentadienylcarbonyl-diphenylphosphinobutanoyliron, Cp = cyclopentadienyl, Ph = phenyl) monomer.[11-13] Metal containing polymers are promising new elements in materials design due to the rich and versatile coordination of the transition metal centers, which can also serve functional roles in catalysis and electrochemistry. Previous experimental and computational studies have shown that polymers of FpP (PFpP) adopt linear chain topologies, and therefore are excellent models for studies of basic polymer dynamics.[12] Recent applications of polymers of FpP include formation of aqueous vesicles due to complex hydration interactions,[14,15] as well as a photoresist for electron beam lithography.[16]

To access the ultrafast site-specific dynamics of the polymer chain, we use two-dimensional infrared (2D-IR) spectroscopy to study the terminal CO stretches of the ligands bound to the iron centers. In several studies, ranging from membranes and proteins to simple liquids and the glass transition, we have shown that transition metal carbonyls act as robust dynamical sensors of their environment.[17-24] 2D-IR is a third-order nonlinear spectroscopy method that correlates excited transition frequencies with detected frequencies, and the dynamical evolution of the frequency correlation can be monitored by varying the time delay between excitation and detection on the femtosecond to picosecond timescale.[25] Briefly, three 100-fs, 0.3 μJ mid-IR pulses centered near 2000 cm^{-1} separated by time delays t_1 and t_2, generate a coherent signal in a background free direction. The signal and a reference local oscillator field derived from the third pulse are detected in a grating spectrometer following sum-frequency generation with a chirped 800-nm pulse, producing an upconverted visible spectral interferogram. The signal's phase and amplitude can be recovered by spectral interferometry,[26] and the spectrometer yields the detection frequency axis. Continuously scanning the coherence time delay the first two pulses (t_1) produces an oscillatory signal at each detected frequency, and Fourier transforming with respect to t_1 yields

the excitation frequency axis. Stepping the waiting time (t_2) produces a series of 2D-IR spectra from which we determine dynamical changes.

There is rich information contained in the full 2D-IR response, but we highlight here the aspects relevant to the present polymer study. Vibrational coupling typically results in splitting of excited vibrational states, and due to the common ground state, cross peaks appear in the 2D-IR spectrum reflecting the fact that excitation of one mode influences the transition probability of other coupled modes.[27] Cross peaks are only present among modes of the same molecular type, or which are in spatial proximity within a macromolecule.[28] The use of cross peaks enables the spectroscopic separation and assignment of heterogeneous mixtures. Condensed phase environments cause inhomogeneous broadening associated with slight variations in transition frequencies arising from microscopically distinct local environments. Hence, the 2D line shape is elongated along the frequency diagonal to an extent given by the range of these frequency variations. Dynamical evolution during the waiting time leads to stochastic sampling of the inhomogeneously broadened band through a process known as spectral diffusion. The time scale of spectral diffusion is a powerful observable directly obtained from 2D-IR spectra, and has been used to understand a wide range of challenging problems in condensed phase dynamics.

In the present study, we use the cross peaks to assign the carbonyl stretching bands of the end-chain site of the polymer or to the interior by virtue of the fact that the end contains an $Fe(CO)_2$ unit whereas the interior is a series of Fe(CO) units. The end chain dicarbonyls are coupled and produce two split vibrational bands that exhibit cross peaks in the 2D spectrum, whereas the monocarbonyls are uncoupled and do not show cross peaks to the two other bands.[27] We also performed density function theory (DFT) calculations on a truncated dimer, and the frequency analysis yields two higher frequency bands on the dicarbonyl unit, and one lower frequency band on the monocarbonyl site. With this assignment made, we use the spectral diffusion of the distinct modes to probe site-specifically the dynamics sensed at the end separately from the polymer interior.

Since the chemistry of the $Fe(CO)_2$ and Fe(CO) sites are nearly identical, and the polymer is dissolved in a good solvent (tetrahydrofuran, THF), we attribute the differences in spectral diffusion dynamics primarily to the motion of the polymer itself. Our experiments show that the

end chain sites exhibit markedly slower spectral diffusion than do the inner chain sites. Investigating the polymer in dilute and concentrated solutions as well as in a solvent-free film shows that the overall spectral dynamics slow as the solvent is removed, but that the site-specific differences in spectral diffusion become less pronounced. To rationalize these observations, we construct a simple coarse grained model of the polymer to simulate the motion of an isolated molecule and a film using a Langevin dynamics approach. Introducing a dynamical variable that quantifies site-specific motion we find excellent agreement with the experimental observation that the ends spectrally and motionally diffuse slower than the inner chain sites. The simulation also captures the decrease in dynamical heterogeneity in the film relative to the dilute case.

6.3 RESULTS OF 1D, 2D-IR, AND QUANTUM CHEMISTRY

The short polymer studied here PFpP, is an 8-mer with a cyclopentadienyl $Fe(CO)_2$ terminus, and cyclopentadienyl Fe(CO) inner-chain sites.[10] The one-dimensional FTIR spectrum (**Fig. 6.1**) of PFpP in THF solution shows three bands at 1914, 1944 and 2003 cm^{-1}, which shift and broaden slightly as a film. Typically, one finds that iron-monocarbonyls have lower transition frequencies than similar iron-dicarbonyls due to the stronger π-back bonding in the monomer case, which leads to a weaker CO bond with a lower force constant. In an 8-mer, there is a single dicarbonyl at the end-chain and seven inner-chain sites, so we expect a lower relative absorbance for the end-chain site than for the inner-chain sites. This spectral assignment is supported by DFT calculations performed on a truncated molecule consisting of the end-chain and one repeat unit.

The 2D-IR spectrum recorded at early waiting times (**Fig. 6.2**) also support the spectral assignments. The two higher frequency bands show a clear cross peak, whereas there is no cross peak between the lower frequency, 1914 cm^{-1} band and either of the other two bands at early waiting time delay. We note the missing upper-left cross peak is due to the asymmetric tuning of our excitation and detection pulses, which are derived from two independent optical parametric amplifiers. The cross peak between the 1944 and 2003 cm^{-1} bands confirms the dicarbonyl assignment, and the uncoupled monocarbonyl band is consistent with the large spatial separation between the repeat units. Analysis of the normal modes from the DFT calculations also shows that there is no coupling between the mono- and dicarbonyl sites.

One feature of the 2D-IR spectrum deserves comment. It is clear that the spectrum shown in Fig. 6.2 is distorted due to linear absorption of water vapor. This signal reshaping would make detailed line shape analysis problematic,[29] but since we employ an alternative method based on computing the inhomogeneity index from the magnitudes of the rephasing (i.e. echo) and non-rephasing (i.e. virtual echo) pulse orderings, and the absorption influences each identically, we are able to extract spectral diffusion dynamics despite the line shape distortion.[30,31]

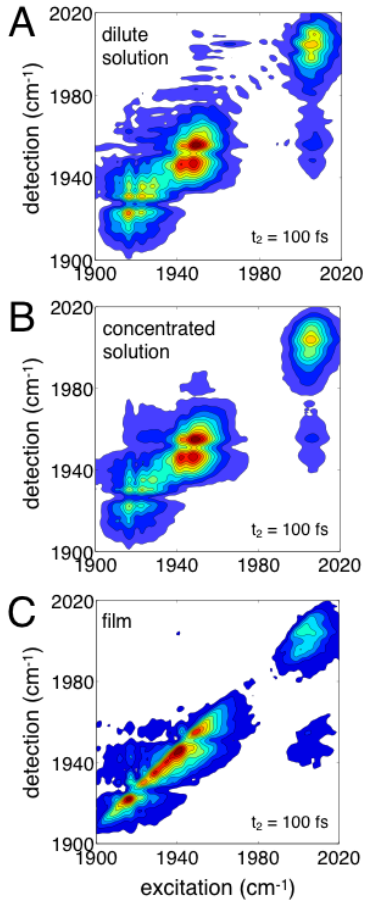

Fig. 6.2: 2D-IR absolute value rephasing spectra of PFpP in (A) dilute THF solution, (B) concentrated in THF solution, and (C) a solvent-free film. The cross peak between the two higher frequency bands confirms the dicarbonyl assignment of those coupled bands. As the solvent is depleted, the inhomogeneous broadening increases as evidenced by the diagonal spectral elongation.

From a series of 2D-IR spectra recorded at various waiting times ranging from 0.1 to 50 ps, we can extract the frequency fluctuation correlation function, $C(t)=\langle\delta\omega(0)\delta\omega(t)\rangle$, where $\delta\omega(t)=\omega(t)-\langle\omega\rangle$ is the fluctuation of the instantaneous frequency from its average $\langle\omega\rangle$. The picosecond timescale decay of this correlation function is due to spectral diffusion. By analyzing

separately the bands at 2003 cm^{-1} and 1914 cm^{-1} (**Fig. 6.3**), we can selectively monitor the dynamics probed at the end-chain and the inner-chain sites, respectively. For each experimental condition, ranging from dilute solution to a solvent-free film, the data indicate slower spectral diffusion at the end-chain relative to the inner-chain sites. Fitting the decays to single exponentials

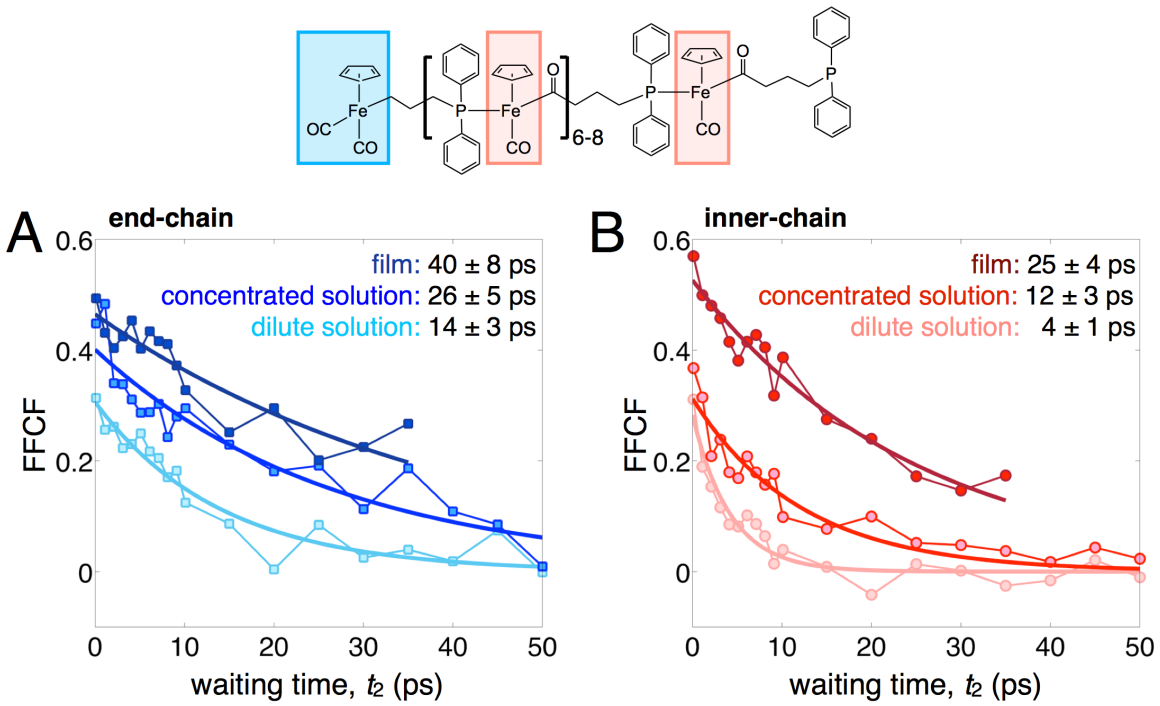

Fig. 6.3: Frequency fluctuation correlation function (FFCF) for bands corresponding to (A) end-chain (2003 cm^{-1}) and (B) inner-chain (1914 cm^{-1}) sites in the three solvent conditions show consistently slower dynamics at the ends relative to the inner chain sites. Whereas in dilute solution the ends are roughly 3-fold slower than the inner chain sites, in the film, the end chain is only about 1.5 times slower than the inner chain sites.

with static offsets gives time constants we can use to compare the different sites and solution conditions. The end-chain time scales range from 14±3 ps in dilute solution to 40±8 ps in the film, whereas the inner-chain dynamics range from 4±1 ps (dilute) to 25±4 ps (film). In the dilute case, the end-chain time scale is roughly three-fold slower, whereas in the film it is only 1.5 times slower. This finding of the relative dynamics time scales, and that they become less distinct in the film, is the central experimental observation of this work. From the data alone, we would conclude that the chain ends, being less constrained, are able to adopt a wider range of conformations than the inner chain sites. Assuming relatively similar intrinsic solvent dynamics, the time scale to sample these conformations should be slower than the more restricted conformational space sampled by

the inner chain sites. As the molecules are globally constrained in a film, the conformational freedom of the ends is reduced, and the time scale to sample the available conformations should be similar to the inner-chain sites.

6.4 DESCRIPTION OF THE ROUSE MODEL AND ANALYSIS

To test the picture inspired by the experiments, we generated a simple coarse grained model.[32] The sites are modeled as masses connected linearly with springs to adjacent sites with force constants taken to be equivalent to roughly two C-C bonds (k = 500 Å kcal/mol). The distance between the sites is set by the harmonic potential minimum location (7.0 Å) estimated from the semi-empirical geometry optimization. The masses are assigned using the inner-chain repeat unit mass (404.05 g/mol). The sites interact through a Lennard-Jones (L-J) potential with a range similar to the size of the repeat unit (10 Å), and cutoff of 15.5 Å. The energy minimized geometry of the full polymer was estimated using semi-empirical (PM6) quantum chemistry calculations.[12] The L-J potential was set to be almost entirely repulsive with a small attractive term (0.1 kcal/mol). In the coarse grained force field, there was also included a very small harmonic angle force constant (0.3 Å kcal/mol) that serves to straighten the polymer, producing a minimized geometry similar to that found using the semi-empirical calculations.[12] Overall, however, the findings presented here are not highly sensitive to variations of the force field parameters.

For the dilute simulation, a single polymer was simulated using Langevin dynamics with a friction coefficient having a damping time of 5.0 fs and a simulated temperature of 2000 K with so-called “shrink-wrap” boundary conditions. These parameters are somewhat arbitrary, and it is well known that Langevin simulations generally follow linear response, which links the temperature and the friction coefficient through the fluctuation-dissipation theorem.[33] Simulations used time steps of 1 fs and were run for several microseconds. All simulations were performed using the LAMMPS package (See Appendix).[34] The film simulations used an identical force field and friction, but included 512 polymer molecules in a simulation box with periodic boundary conditions. The film simulation was run for 60 ns following >500 ns of equilibration.

To compare the simulation results with the hypothesis based on experiment, we introduce a dynamical variable that can provide a site-specific measure of the motion of the chain elements. Taking the radius of gyration (R_g) as a starting point,

$$R_g^2 = \frac{1}{N}\sum_j \left(r_j - \langle r \rangle\right)^2 \tag{6.1}$$

we adopt the absolute site distance-to-the-mean, $R_j(t) = \left|r_j(t) - \langle r(t)\rangle\right|$, as a measure of site-specific motion. Here the angled brackets denote the center of mass, which naturally diffuses during the simulation. The correlation function of the fluctuations of $R_j(t)$ ($C_{jj}(t) = \langle \delta R_j(0)\delta R_j(t)\rangle$) gives the site-specific motional correlation. In the film simulation, we ensemble average the correlation functions of the 512 individual polymers.

6.5 RESULTS OF THE SIMULATIONS

The simulation results capture the trend observed experimentally. In the dilute case, the site distance fluctuation correlation functions decay more slowly at the chain ends than they do at the inner-chain sites. Since we find the decays not to be well described using single exponential functions, we chose to analyze the relaxation using average time constants computed by integrating the decays of the normalized correlation functions:

$$\langle \tau_j \rangle = \frac{1}{C_{jj}(0)}\int_0^\infty C_{jj}(t)\,dt \tag{6.2}$$

Figure 6.4 shows the normalized $C_{jj}(t)$ for the dilute and film conditions together with the site-dependent average relative decay constants. It is apparent that the chain ends relax slower than do the inner chain sites, and the film shows a smaller variation of relaxation than the dilute solution. Since the time scale of a Langevin simulation is set by the friction coefficient, we make no attempt to extract absolute time scales from the simulations. Rather, we analyze the relative time scales by dividing all of the average time constants by the minimum value, which should be more directly related to our experimentally determined relative spectral diffusion time scales. Indeed, the ratio of the end/inner decays is close to 3 for the dilute case, and it is markedly lower, 1.4, for the film. We note that the precise site-dependence is sensitive to the specific choice of force field parameters, but the overall trend of slower end fluctuations is not altered.

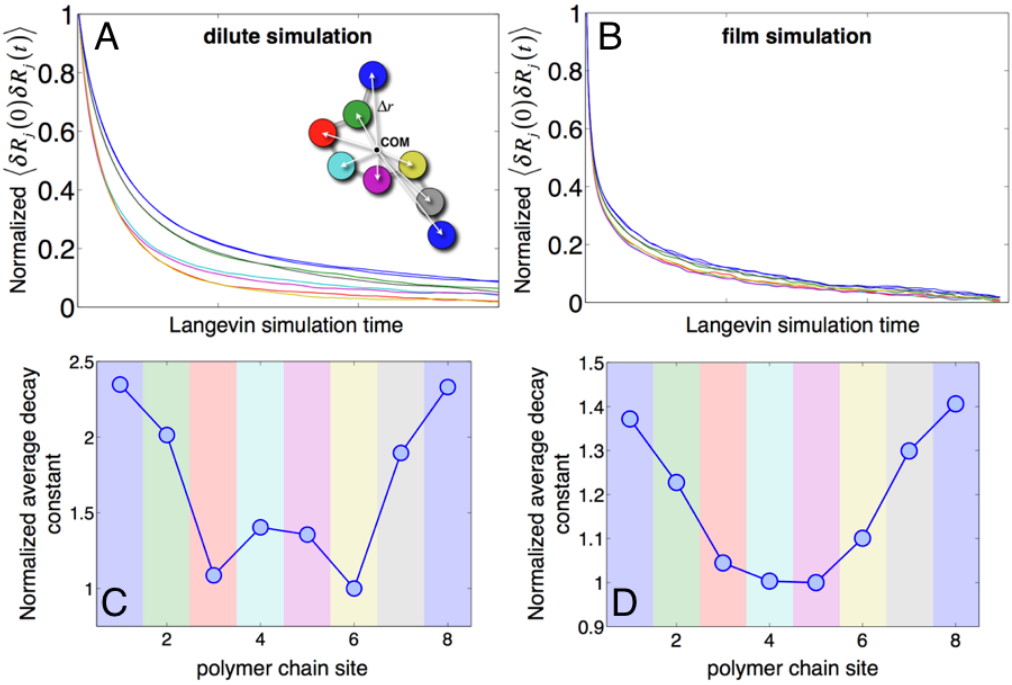

Fig. 6.4: Correlation functions of fluctuations of each site's distance to the polymer's center of mass for (A) the dilute, single polymer case and (B) the 512 molecule simulation of the film. Average decay constants of each site's correlation function normalized to the minimum decay constant for the (C) dilute and (D) film results. In both conditions, the fluctuations decay more slowly at the ends of the chain, but in the dense film conditions, the dynamical heterogeneity is markedly reduced relative to the dilute solution.

Taken together, the combination of ultrafast 2D-IR spectroscopy of a novel transition metal containing polymer with a coarse grained dynamics simulation shows that it is possible to address, in a largely site-specific manner, the heterogeneous dynamics of a short polymer chain in solution, both dilute and concentrated, as well as in a solvent-free film. The use of intrinsic vibrational transitions enables an effectively label-free approach, permitting spectroscopic access to the key end chain site distinct from the inner chain locations. Clearly it would be ideal to be able to probe each polymer site individually, but that would require isotope labeling that might be difficult to synthesize with monodispersity. The remarkable agreement between the experimental spectral diffusion and the coarse grained motional fluctuations provides both a molecular interpretation as well as, to some extent, a validation that such simple models do indeed capture the essential dynamics.

REFERENCES

[1] M. Bixon, J. Chem. Phys. **58**, 1459 (1973).

[2] J. G. Kirkwood and J. Riseman, J. Chem. Phys. **16**, 565 (1948).

[3] J. Kas, H. Strey, and E. Sackmann, Nature **368**, 226 (1994).

[4] T. T. Perkins, D. E. Smith, and S. Chu, Science **264**, 819 (1994).

[5] N. Tomczak, R. A. L. Vallee, E. M. H. P. van Dijk, M. Garcia-Parajo, L. Kuipers, N. F. van Hulst, and G. J. Vancso, Eur. Polym. J. **40**, 1001 (2004).

[6] H. S. Chung, Z. Ganim, K. C. Jones, and A. Tokmakoff, Proc. Natl. Acad. Sci. U. S. A. **104**, 14237 (2007).

[7] H. S. Chung, M. Khalil, A. W. Smith, Z. Ganim, and A. Tokmakoff, Proc. Natl. Acad. Sci. U. S. A. **102**, 612 (2005).

[8] C. Kolano, J. Helbing, M. Kozinski, W. Sander, and P. Hamm, Nature **444**, 469 (2006).

[9] P. Mukherjee, I. Kass, I. Arkin, and M. T. Zanni, Proc. Natl. Acad. Sci. U. S. A. **103**, 3528 (2006).

[10] X. Wang, K. Cao, Y. Liu, B. Tsang, and S. Liew, J. Am. Chem. Soc. **135**, 3399 (2013).

[11] K. Cao, B. Tsang, Y. Liu, D. Chelladural, W. P. Power, and X. Wang, Organometallics **33**, 531 (2014).

[12] K. Cao, J. Ward, R. C. Amos, M. G. Jeong, K. T. Kim, M. Gauthier, D. Foucher, and X. Wang, Chem. Commun. **50**, 10062 (2014).

[13] N. Lanigan, A. Assoud, and X. Wang, ACS Macro Letters **3**, 1281 (2014).

[14] N. Murshid and X. Wang, Chem. Eur. J. **21**, 19223 (2015).

[15] K. Cao, N. Murshid, L. Li, A. Lopez, K. C. Tam, and X. Wang, Macromolecules **48**, 7968 (2015).

[16] J. Zhang, K. Cao, X. S. Wang, and B. Cui, Chem. Commun. **51**, 17592 (2015).

[17] L. M. Kiefer and K. J. Kubarych, Journal of Physical Chemistry. A **119**, 959 (2015).

[18] L. M. Kiefer, J. T. King, and K. J. Kubarych, Acc. Chem. Res. **48**, 1123 (2015).

[19] J. A. Dunbar, E. J. Arthur, A. M. White, and K. J. Kubarych, J. Phys. Chem. B **119**, 6271 (2015).

[20] J. T. King, E. J. Arthur, C. L. Brooks, and K. J. Kubarych, J. Am. Chem. Soc. **136**, 188 (2014).

[21] D. G. Osborne, J. A. Dunbar, J. G. Lapping, A. M. White, and K. J. Kubarych, J. Phys. Chem. B **117**, 15407 (2013).

[22] J. T. King, M. R. Ross, and K. J. Kubarych, Phys. Rev. Lett. **108**, 157401 (2012).

[23] J. T. King and K. J. Kubarych, J. Am. Chem. Soc. **134**, 18705 (2012).

[24] J. T. King, E. J. Arthur, C. L. Brooks, and K. J. Kubarych, J. Phys. Chem. B **116**, 5604 (2012).

[25] P. Hamm and M. T. Zanni, *Concepts and Methods of 2D Infrared Spectroscopy* (Cambridge University Press, New York, 2011).

[26] L. Lepetit, G. Cheriaux, and M. Joffre, J. Opt. Soc. Am. B-Opt. Phys. **12**, 2467 (1995).

[27] O. Golonzka, M. Khalil, N. Demirdoven, and A. Tokmakoff, J. Chem. Phys. **115**, 10814 (2001).

[28] J. Asbury, T. Steinel, and M. Fayer, Chem. Phys. Lett. **381**, 139 (2003).

[29] K. Kwak, S. Park, I. Finkelstein, and M. Fayer, J. Chem. Phys. **127**, 124503 (2007).

[30] S. Roberts, J. Loparo, and A. Tokmakoff, J. Chem. Phys. **125**, 084502 (2006).

[31] D. G. Osborne and K. J. Kubarych, J. Phys. Chem. A **117**, 5891 (2013).

[32] T. Vettorel, G. Besold, and K. Kremer, Soft Matter **6**, 2282 (2010).

[33] R. Kubu, Rep. Prog. Phys. **29**, 255 (1966).

[34] S. Plimpton, J. Comput. Phys. **117**, 1 (1995).

Chapter 7

Ultrafast 2DIR Reveals Spectral Dynamics of Previously Unresolved NCS Bands in DSSC Dye N719

7.1 INTRODUCTION

A rise in the consumption of fossil fuels and the limited quantity on the earth have motivated many to invest future energy requirements on harvesting the energy from the sun. A popular motif for energy extraction are dye-sensitized solar cells because they have high efficiencies and low cost [1-4]. These molecules absorb over broad ranges of the suns emission spectrum and this results in an electronic excitation of the dye, leading to an electron injection into a conducting surface, such as TiO_2, generating an electric current. The popular light-harvesting molecules first discovered by Gratzel[1], have proven to be efficient light harvesting antennae, but reduce in efficiency at high loading due to possible aggregation. Though the structures of these dyes are very similar, often differing by only a functional group, the N719 dye (cis-bis(isothiocyanato)bis(2,2'-bipyridyl-4,4'-dicarb-oxylato)ruthenium(II) bis-tetrabutylammonium ($Ru(dcbpy)_2$ $(NCS)_2$ 2TBA))shows no aggregation, even at full dye coverage[5].

Recently, other groups have used 2DIR spectroscopy to investigate the N3 dye, and reported an inability to resolve the two CN stretching modes[6]. By simply performing independent rephasing and nonrephasing experiments, we can both resolve the two bands and observe their distinct inhomogeneities. What is generally reported are absorptive spectra, which can often mask the resolution of two energetically similar peaks. We find a strong solvent dependence on both the peak shapes and their underlying dynamics.

7.2 EXPERIMENTAL SETUP

The two-dimensional infrared spectroscopy (2DIR) experiments were conducted using three mid-IR pulses (~2000 cm^{-1}, 120 fs, 500 nJ) in a background free box car geometry. The time delay is scanned between the 2 pump pulses and a Fourier transform performed to generate an excitation frequency axis. A third probe pulse generates a signal from the sample that is directly detected in a spectrometer, creating a detection frequency axis. In our specific experimental setup, we combine the signal with a local oscillator reference pulse for heterodyne detection and mix these fields with a chirped pulse (centered at 800 nm) in a Mg doped lithium niobate crystal to upconvert our infrared signal to a visible signal. The time delay is scanned between the excitation and detection pulses to obtain dynamical information on the system. We perform both rephasing (photon echo) and nonrephasing experiments according to their respective phase matching conditions, $k_r=-k_1+k_2+k_3$ and $k_n=+k_1-k_2+k_3$, at each waiting time, t_2. These two experiments, independently, can reveal the vibrational lifetimes and intramolecular vibrational redistribution time constants. When the they are combined for each waiting time, the frequency-fluctuation correlation function (FFCF), an observable unique to 2DIR, is obtained. The FFCF is often referred to as spectral diffusion. To calculate the spectral diffusion, we first must calculate the inhomogeneity index $I(t_2)$:

$$I(t_2) = \frac{A_r(t_2) - A_n(t_2)}{A_r(t_2) + A_n(t_2)} \qquad (7.1)$$

where $A_r(t_2)$ and $A_n(t_2)$ are the rephasing and nonrephasing amplitudes of the diagonal peaks in the 2D spectra at the waiting time, t_2. A more detailed account of our experimental setup has been published previously[7].

We report the spectral dynamics of the dye-sensitized solar cell (DSSC) dye, N719. In these studies, the concentration of the N719 in DMF was 5 mM. The N719 dye was purchased from Aldrich, and the DMF from Sigma-Aldrich, both used as is. The titanium oxide (TiO_2) nanopowder (<100 nm(BET), 97%) used was doped with Mg (1%) and purchased from Aldrich. To prepare the N719-TiO_2 bound complex, 5 mM of N719 in DMF was combined with an excess of TiO_2 and the mixture heated to 80°C and stirred for 1 hour. The mixture was allowed to cool and the refrigerated for 24 hours and then filtered. We note that the S-bound has an IR stretching band

just a few wavenumbers higher than the symmetric stretch of the N-bound isomer and that the former has a much lower yield in the reaction outcome than the latter. It has been reported that heating converts the S-bound isomer to the N-bound isomer[8] and because we heated the sample, we are confident that the N719 was composed primarily of the N-bound isomers. Previous studies using 0.1 mM NaOH in H_2O as the solvent have shown N719 not to cluster at the concentration used in our study (5 mM, DMF). Similar dyes have been shown to aggregate at concentrations > 15 mM, however, N719 has not been shown to aggregate, even at full coverage on a TiO_2 surface.[5]

7.3 RESULTS

When fitting the asymmetric FTIR band corresponding to the CN stretching modes using Gaussians, we find it is composed of two peaks, one associated with an out of phase symmetric stretch and the other is a totally symmetric stretch, having frequencies of 2098 and 2105 cm^{-1}, respectively (**Fig. 7.1 A, B**). These values are in agreement with previous reports of the similar N3 dye CN stretching modes [6]. Our assignments of these modes are based on DFT calculations. The

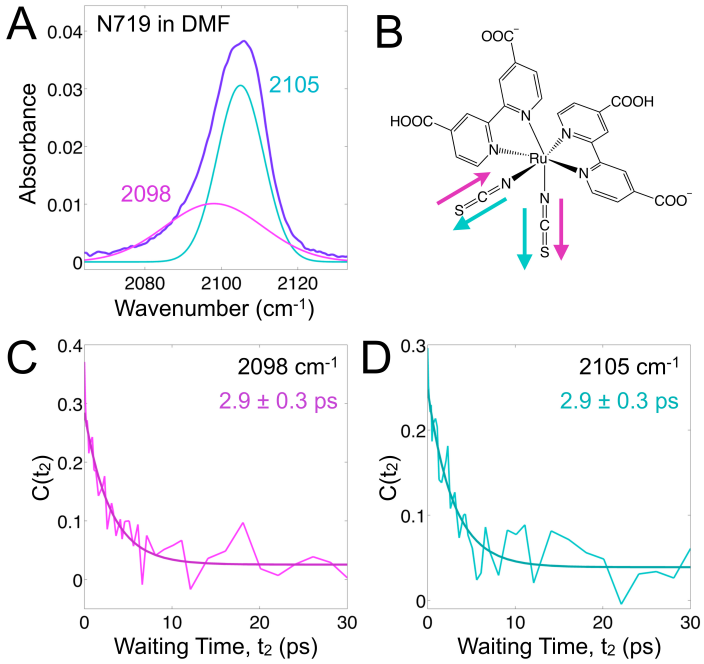

Figure 7.1: A) Deconvoluted FTIR of the asymmetric (2098 cm^{-1}) and symmetric (2105 cm^{-1}) CN vibrational stretches; B) Molecular structure of the N719 dye without the cation, bis-tetrabutylammonium, present; C) FFCF of the asymmetric mode and D) FFCF of the symmetric mode of the free particles in DMF.

full width half max (fwhm) of the fits are markedly different for the two modes: 30.3 cm^{-1} (2098 cm^{-1}) and 14.3 cm^{-1} (2105 cm^{-1}). This is consistent our previous observations of metal centers containing multiple oscillators: the symmetric, high frequency mode having less inhomogeneous broadening than the lower, out-of-phase symmetric mode[9]. The different inhomogeneities are also apparent in the FFCF. The y-intercept of the FFCF depicts the degree of inhomogeneity, allowing for a direct comparison between the two modes' dephasing mechanisms. **Figure 7.1 B and C** show the FFCF's of both modes, and clearly, the lower frequency mode has a larger (roughly 25%) valued y-intercept than the higher frequency mode (2098 cm^{-1}: 0.23 a.u.; 2105 cm^{-1}: 0.17 a.u.). Both modes, however, have the same spectral diffusion time of 2.9 ± 0.3 ps, and have a vibrational lifetime of 51 ± 2 ps.

The difference in the inhomogeneities of two coupled modes has been observed previously by Jansen *et al* in the case of the OH stretching modes of water in a water/acetonitrile mixture[10]. In their results, they find both the inhomogeneous broadening and spectral dynamics of the two modes to be different. In our experiments, we do not observe a difference in dynamics, only a difference in the inhomogeneous broadening. Due to their shared similar environment, we do not think that the number of specific solvent environments around the two SCN ligands is the reason behind the different inhomogeneous broadenings of the two modes. We do observe an increase in the homogeneous broadening along the anti-diagonal in the absorptive spectrum, which could be the reason the lower frequency mode is broader than the higher frequency counterpart in the linear spectrum deconvolution.

We also observe an anticorrelation between the 0→1 transition and its 1→2 transition of the higher frequency mode in the absorptive spectrum in that the diagonal peaks are along the diagonal and the excited state, off diagonal peaks appear to be aligned horizontally along the detection axis (**Fig. 7.2, 3rd panel**). The anharmonicity of the asymmetric stretch was determined to be 17 cm^{-1} and the anharmonicity of the totally symmetric stretch is 25 cm^{-1}(**Fig. 7.2, 3rd panel**). This band was determined not to be a cross peak for the following reasons: there is no cross peak apparent from the lower frequency mode to the higher frequency mode, the anharmonicity observed is consistent with metal-bound CN stretches, the sign is wrong for the lower peak if it were an actual cross-peak. Anti-correlations have been observed in other systems and imply that

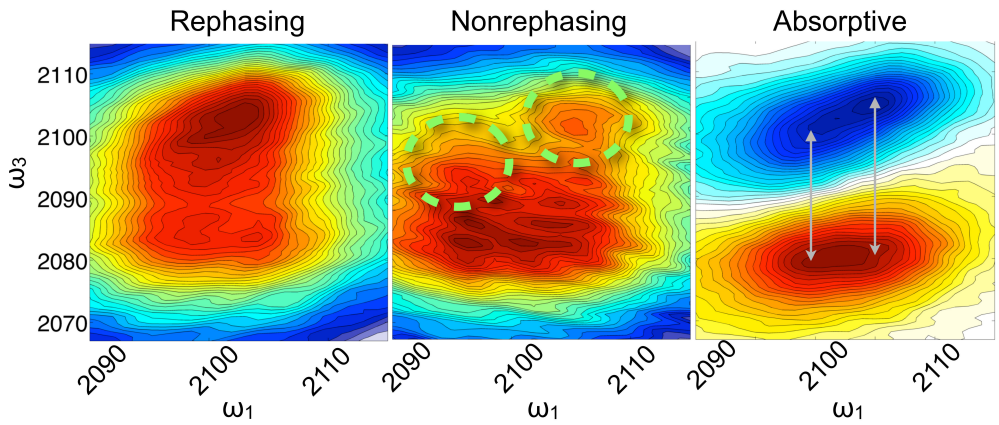

Figure 7.2: Absolute rephasing, absolute nonrephasing and absorptive spectra of the two CN stretching bands in DMF. The absolute nonrephasing clearly shows the resolved CN bands and the absorptive spectra shows that the modes have different inhomogeneous broadening (anti-diagonal linewidth) and different anharmonicities, with the lower frequency mode having an anharmonicity of 17 cm^{-1} and the higher frequency mode having an anharmonicity of 25 cm^{-1}.

either variations exist in the local mode coupling leading to the inhomogeneous broadening or that the local mode energies are directly anti-correlate[10-13]. N719 was also studied in the solvent DMSO, and had similar behavior as to that in DMF, except due to the low signal, the bands do not appear spectrally resolved in the nonrephasing spectrum. The FTIR bands were fitted to Gaussians centered at 2098 and 2107 cm^{-1}. Both modes were analyzed at the same time with spectral diffusion decay time of 3.9 ± 0.4 ps (**Fig. 7.3**). This is consistent with the higher the donicity (or donor number, DN) of the solvent, the longer spectral diffusion time, since $DN_{DMSO} = 29.8 > DN_{DMF} = 26.6$.

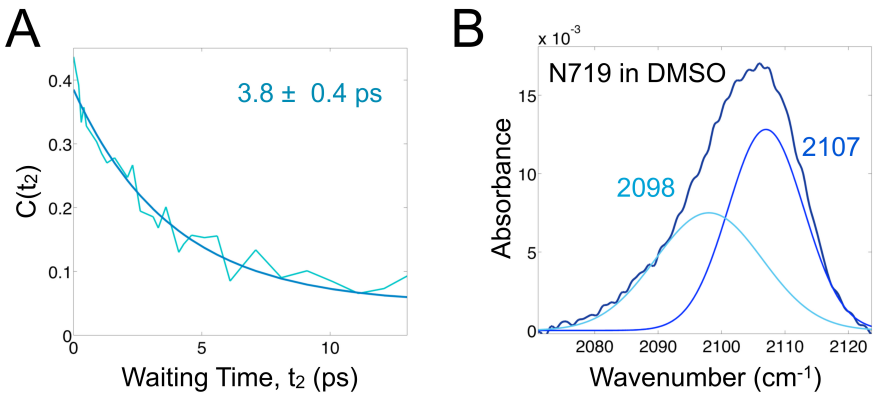

Figure 7.3: A) FFCF of N719 in DMSO; B) Deconvoluted FTIR spectrum of N719 in

The spectral diffusion decay time of the N719 bound to the TiO_2 nanoparticles is similar to that of the unbound species, having a decay time of 2.9 ± 0.3 ps. The FFCF of the high frequency band (2015 cm^{-1}) is depicted in **Figure 7.4** as well as UV-Vis spectra showing the differences between free N719 to TiO_2-bound N719. Interestingly, the vibrational lifetime is 20% faster for the bound species than the free species (bound: 41 ± 2 ps, free: 52 ± 2 ps). This faster lifetime can be attributed to more relaxation pathways offered by the TiO_2.

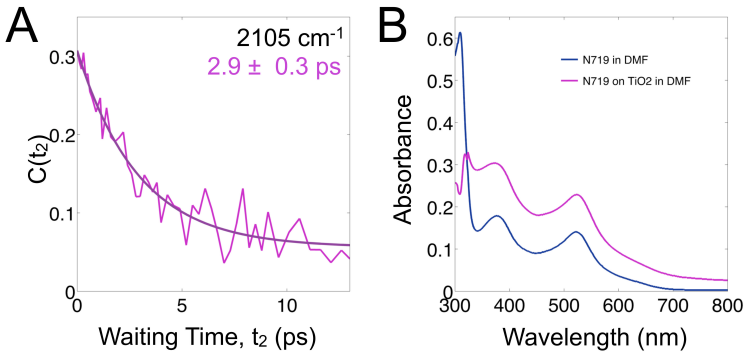

Figure 7.4: A) FFCF of high frequency band of TiO_2-bound N719; and B) UV-Vis of free N719 in DMF (blue) and TiO_2-bound N719 in DMF (pink).

REFERENCES

1. Desilvestro, J.; Gratzel, M.; Kavan, L.; Moser, J.; Augustynski, J., Highly Efficient Sensitization of Titanium-Dioxide. Journal of the American Chemical Society 1985, 107 (10), 2988-2990.

2. Gratzel, M., Recent Advances in Sensitized Mesoscopic Solar Cells. Accounts of Chemical Research 2009, 42 (11), 1788-1798.

3. Huang, W. K.; Cheng, C. W.; Chang, S. M.; Lee, Y. P.; Diau, E. W. G., Synthesis and Electron-Transfer Properties of Benzimidazole-Functionalized Ruthenium Complexes for Highly Efficient Dye-Sensitized Solar Cells. Chemical Communications 2010, 46 (47), 8992-8994.

4. Oregan, B.; Gratzel, M., A Low-Cost, High-Efficiency Solar-Cell Based on Dye-Sensitized Colloidal TiO_2 Films. Nature 1991, 353 (6346), 737-740.

5. Katoh, R.; Yaguchi, K.; Furube, A., Effect of Dye Concentration on Electron Injection Efficiency in Nanocrystalline TiO_2 Films Sensitized with N719 Dye. Chemical Physics Letters 2011, 511 (4-6), 336-339.

6. Fedoseeva, M.; Delor, M.; Parker, S. C.; Sazanovich, I. V.; Towrie, M.; Parker, A. W.; Weinstein, J. A., Vibrational Energy Transfer Dynamics in Ruthenium Polypyridine Transition Metal Complexes. Physical Chemistry Chemical Physics 2015, 17 (3), 1688-1696.

7. Nee, M. J.; Baiz, C. R.; Anna, J. M.; McCanne, R.; Kubarych, K. J., Multilevel Vibrational Coherence Transfer and Wavepacket Dynamics Probed with Multidimensional IR Spectroscopy. Journal of Chemical Physics 2008, 129 (8), 084503.

8. Kohle, O.; Ruile, S.; Gratzel, M., Ruthenium(II) Charge-Transfer Sensitizers Containing 4,4'-dicarboxy-2,2'-bipyridine. Synthesis, Properties, and Bonding Mode of Coordinated Thio- and Selenocyanates. Inorganic Chemistry 1996, 35 (16), 4779-4787.

9. Kiefer, L. M.; King, J. T.; Kubarych, K. J., Equilibrium Excited State Dynamics of a Photoactivated Catalyst Measured with Ultrafast Transient 2DIR. Journal of Physical Chemistry A 2014, 118 (42), 9853-9860.

10. Jansen, T. L. C.; Cringus, D.; Pshenichnikov, M. S., Dissimilar Dynamics of Coupled Water Vibrations. Journal of Physical Chemistry A 2009, 113 (22), 6260-6265.

11. Rubtsov, I. V.; Wang, J.; Hochstrasser, R. M., Dual Frequency 2D-IR of Peptide Amide-A and Amide-I Modes. Journal of Chemical Physics 2003, 118 (17), 7733-7736.

12. King, J. T.; Baiz, C. R.; Kubarych, K. J., Solvent-Dependent Spectral Diffusion in a Hydrogen Bonded "Vibrational Aggregate". Journal of Physical Chemistry A 2010, 114 (39), 10590-10604.

13. Thompson, D. E.; Merchant, K. A.; Fayer, M. D., Two-Dimensional Ultrafast Infrared Vibrational Echo Studies of Solute-Solvent Interactions and Dynamics. Journal of Chemical Physics 2001, 115 (1), 317-330.

Chapter 8

Conclusion

8.1 KEY CONCLUSIONS

The work presented in this thesis can be reduced to the following themes: **1.** Spectral dynamics of multiple key steps in the photocatalytic reaction of the CO_2 reduction catalyst $Re(bpy)(CO)_3Cl$ in multiple solvents (Chapters 2-4); **2.** Vibrational energy transfer between distinct molecules (Chapter 5); **3.** Site-specific dynamics within the polymer PfPp (Chapter 6) and **4.** Dynamics of spectrally resolved CN stretching modes of the N719 dye free and bound to TiO_2 (Chapter 7). We have found that using ultrafast multidimensional spectroscopy, it is possible to study multiple perspectives of a chemical reaction, ranging from electrostatics to preferential solvation. Though many intermediates in a chemical reaction may not be stable, for those that are, this work has shown the ability to understand of the roles of the contributing factors (i.e. solvent, electrostatics) through characterization of spectral dynamic differences at these important steps.

We have provided a method to isolate and study the dynamics of an electronic ground state species and a quasi-equilibrated electronic excited state, independently, instead of the conventional method of fluorescence, which reports the difference in energy between the states[1]. Equilibrium two-dimensional infrared spectroscopy was used to characterize the spectral dynamics in the electronic ground (S_0) state of the photocatalyst $Re(CO)_3(bpy)Cl$ in THF and transient two-dimensional infrared spectroscopy was used to characterize the quasi-equilibrated ^{3}MLCT excited state species[2]. The spectral diffusion of the ^{3}MLCT excited state was found to be three times slower than its ground state counterpart (S_0: ~1.4 ps; ^{3}MLCT: ~ 4.5 ps), and its

vibrational lifetime that nearly an order of magnitude faster (S_0: ~25 ps; ^{3}MLCT: ~3.2 ps). The difference in spectral dynamics was primarily attributed to both a change in solvent friction and in the catalyst's electronic structure, which considerably modified the catalyst's electrostatic profile.

The electrostatics of the ground state Re complex were then altered to see the effect on spectral dynamics by adding either electron withdrawing (COOH) or electron donating groups (CH_3, *tert*-butyl) on the bipyridine[3]. These modifications led to changes in the electrostatics that were much smaller than those resulting from the ^{3}MLCT and mainly affected the non-carbonyl atoms within the complex. Since the carbonyl probes' environment was unaffected, they did not exhibit changes in their spectral diffusion time constants. They did, however, collectively change when the solvents were changed, with a trend following an increase in spectral diffusion time with an increase in the donicity of the solvent. This result has implications towards the catalytic efficiency because the efficiency depends on the solvent[4-5]. The solvents used in this study were all aprotic polar solvents (DMSO, CH_3CN, THF) that were relevant to the catalysis reaction.

Further investigations of the solvent system that the catalytic reaction takes place in (80% Solvent/ 20% TEOA) were then conducted to understand the significance of the ratio that leads to optimal catalytic efficiency. The TEOA was found to preferentially solvate the Re complex, but not strongly. Equilibrium 2DIR experiments on multiple ratios of solvent:TEOA revealed a spectral dynamic slowdown that occurred at the very concentration which results in optimal catalytic efficiency. In the photocatalytic mechanism, the TEOA donates a sacrificial electron to the Re complex following its excitation to the ^{3}MLCT state, and a few steps later the solvent coordinates to the Re metal center, indicating that both solvents are intimately involved in the reaction[6]. We concluded that the "magic ratio" of the solvent:TEOA optimized the solvent exchange between the solvent shells, allowing for both the TEOA and solvent to readily participate in the reaction. We also performed UV-pump/IR-probe experiments that indicated the electron transfer from the TEOA to the Re complex occurs on a timescale faster than diffusion, confirming the TEOA is preferentially solvating the photocatalyst. While this may not be the primary method of electron transfer, it is observed and should be considered in understanding all aspects of the catalytic mechanism.

We next explored preferential solvation from the perspective of the preferential solvating molecule[7]. Sodium thiocyanate was selected because it is known to preferentially solvate betaine-30[8], a molecule with a similar dipole moment to the rhenium photocatalyst and it also has a CN stretching frequency in close proximity to the totally symmetric A'(1) stretch of the rhenium photocatalyst. Different concentrations of sodium thiocyanate were added to 1.5 mM solutions of $Re(bpy)(CO)_3Cl$ in THF and we found that there was no effect on the spectral dynamics of either the molecule, though they were in close proximity to each other. We did observe an energy transfer, primarily from the lower frequency A'(1) band of the Re complex to both bands present in the Na^+SCN^- (one from the contact ion pair and one from a dimer of two contact ion pairs). This energy transfer appears as cross peaks in the 2DIR spectra. These cross peaks shifted as a function of time, on a timescale independent of the spectral diffusion of either of the separate bands involved in the energy transfer, allowing us to observe directly, non-Gaussian dynamics.

The next work discussed the dynamics of a polymer, (PfPp; 8-mer) whose vibrational probes are embedded within the polymer units[9]. The end unit of the polymer composed of an iron-dicarbonyl unit (end-chain) and the repeating unit contains iron-monocarbonyls (inner-chain). These distinct environments are spectrally resolved, which allowed us to monitor their independent, site-specific dynamics in solution, both dilute and concentrated, as well as in a solvent-free film. The FFCF decay times increased with concentration going from dilute to concentrated film for both probe environments, which makes sense due to the more constrained environment as the sample gets more concentrated. The inner-chain possessed faster dynamics than the end chain in all concentrations, as would be expected because of the smaller range of conformations the inner-chains have compared with the end-chain unit. The experiments were complemented by Langevin simulations using a coarse grained model.

The final work described in this thesis focused on the two close-lying bands of the CN stretches in the DSSC, N719 in DMF. For the first time, we were successful at spectroscopically resolving the two bands, both inhomogeneously broadened and only $7cm^{-1}$ away from each other. Only through the nonrephasing spectrum, in which the peaks elongate along the anti-diagonal, were we able to do this, as they were not resolved completely in the absorptive spectrum. Their independent spectral dynamics were found to be quite similar (FFCF decay times: both 2.9 ± 0.3

ps), while there inhomogeneities were found to be different. This difference also seems to be reflected in the Gaussian fits of the FTIR spectrum, with the lower frequency exhibiting more inhomogeneous broadening than the higher frequency band, fwhm = 30.3 cm^{-1} and fwhm = 14.3 cm^{-1}, respectively. Their anharmonicities were also determined to be different, with the higher frequency having a larger anharmonicity (~25 cm^{-1}) than the lower frequency (~17 cm^{-1}). The dye molecules were studied both free in solution and bound to TiO_2 nanoparticles in solution in the solvent DMF. The spectral diffusion of the dye bound to TiO2 was similar to that of the free N719 (2.7 ± 0.4 ps). The vibrational lifetime of the bound version, however, was 20% faster the free form (bound: 41 ± 2 ps, free: 52 ± 2 ps). The N719 was also studied in DMSO, and the previously mentioned trend was observed: the bands in DMSO had a longer spectral diffusion time (3.8 ± 0.3 ps) than in DMF (2.9 ± 0.3 ps), consistent with the donicity picture (DN_{DMSO} = 29.8 > DN_{DMF} = 26.6). The solvent choice seemed to affect the anharmonicity of the higher frequency mode, but more experiments are needed to confirm such an affect.

8.2 FUTURE OUTLOOK

These techniques have proven to be a powerful tool in understanding reaction mechanisms from the perspective of the reactants, intermediates and the solvent. Understanding what roles each participant is playing in the reaction at each step, will no doubt lead to optimization of reactions on a grander scale. While this work primarily focused on the known steps of a photo-induced catalytic reaction, the principles can be expanded to all multi-step chemical reactions whose time scales are on the order of our ultrafast experiments or slower. Two observed trends overlap in the different systems that were focused on: 1. Altering a molecular compound distant from the probe region has little effect on the observed spectral diffusion decay time constant, and 2. The spectral diffusion trends of multiple systems follow an increase in the decay time constant with an increase in the donicity of the solvent.

While this work has provided valuable insight to understanding the optimized reaction conditions for heterogeneous catalysts, this specific reaction could not be used on a large scale for the reducing CO_2. More realistic reactions photocatalytic systems could also be studied using the techniques described in this work by incorporating electrodes into the reaction sample cell as

the source of the electrons, instead of a sacrificial electron donor. With this modification, one could watch the reaction in real time as it occurs.

The transient-2DIR technique can also be used on a wide variety of complexes with a long-lived electronic state to gain better insight of the spectral dynamics, such as spectral diffusion and vibrational lifetimes, of these excited states.

Finally, polarization-dependent XAS can be used to observe possible anisotropic structural changes and dynamics resulting from the photo-initiated metal-to-ligand, ligand-to-ligand, and ligand-to-metal CT states of the Re family pf photocatalysts.

REFERENCES

1. Vanderzwan, G.; Hynes, J. T., Time-Dependent Fluorescence Solvent Shifts, Dielectric Friction, and Nonequilibrium Solvation in Polar-Solvents. *Journal of Physical Chemistry* 1985, *89* (20), 4181-4188.

2. Kiefer, L. M.; King, J. T.; Kubarych, K. J., Dynamics of Rhenium Photocatalysts Revealed Through Ultrafast Multidimensional Spectroscopy. *Accounts of Chemical Research* 2015, *48* (4), 1123-1130.

3. Kiefer, L. M.; Kubarych, K. J., Solvent-Dependent Dynamics of a Series of Rhenium Photoactivated Catalysts Measured with Ultrafast 2DIR. *Journal of Physical Chemistry A* 2015, *119* (6), 959-965.

4. Agarwal, J.; Fujita, E.; Schaefer, H. F.; Muckerman, J. T., Mechanisms for CO Production from CO_2 Using Reduced Rhenium Tricarbonyl Catalysts. *Journal of the American Chemical Society* 2012, *134* (11), 5180-5186.

5. Rodriguez, L.; Ferrer, M.; Rossell, O.; Duarte, F. J. S.; Santos, A. G.; Lima, J. C., Solvent Effects on the Absorption and Emission of $Re(R_2bpy)(CO)_3X$ Complexes and Their Sensitivity to CO_2 in Solution. *Journal of Photochemistry and Photobiology a-Chemistry* 2009, *204* (2-3), 174-182.

6. Morimoto, T.; Nakajima, T.; Sawa, S.; Nakanishi, R.; Imori, D.; Ishitani, O., CO_2 Capture by a Rhenium(I) Complex with the Aid of Triethanolamine. *Journal of the American Chemical Society* 2013, *135* (45), 16825-16828.

7. Kiefer, L. M.; Kubarych, K. J., NOESY-Like 2D-IR Spectroscopy Reveals Non-Gaussian Dynamics. *Journal of Physical Chemistry Letters* 2016, *7* (19), 3819-3824.

8. Baiz, C. R.; Kubarych, K. J., Ultrafast Vibrational Stark-Effect Spectroscopy: Exploring Charge-Transfer Reactions by Directly Monitoring the Solvation Shell Response. *Journal of the American Chemical Society* 2010, *132* (37), 12784-12785.

9. Wang, X. S.; Cao, K.; Liu, Y. B.; Tsang, B.; Liew, S., Migration Insertion Polymerization (MIP) of Cyclopentadienyldicarbonyldiphenylphosphinopropyliron (FpP): A New Concept for Main Chain Metal-Containing Polymers (MCPs). *Journal of the American Chemical Society* 2013, *135* (9), 3399-3402.

Appendix

A1. DENSITY FUNCTIONAL THEORY GEOMETRY AND FREQUENCIES FOR TRUNCATED DIMER

To confirm the assignment of the FTIR spectrum deduced from the coupling pattern revealed by 2D-IR spectroscopy, we performed density functional theory quantum chemistry calculations on a truncated dimer starting. We used Gaussian09[1] to compute DFT structures and harmonic frequencies with the B3LYP functional using a Gaussian 6-31+G(d) basis on the C, P, H and O atoms, and the LANL2DZ pseudopotential on the iron atoms. The unscaled CO stretching vibrations were calculated to have frequencies of 2087.19 cm^{-1} (dicarbonyl symmetric stretch), 2045.16 cm^{-1} (dicarbonyl anti-symmetric stretch), and 2007.82 cm^{-1} (monocarbonyl stretch). These agree, within the usual scaling, with the experimental values and assignment.

The coordinates of the dimer are the following:

Fe	4.765909	-0.478940	-0.315216
C	2.820273	-0.404999	-0.982960
C	1.692376	0.025154	-0.041796
C	0.331346	0.012614	-0.769700
P	-1.176729	0.614494	0.146968
C	-0.901302	-0.008830	1.872233
C	-0.973958	2.450006	0.298538
C	-0.913635	-1.398567	2.095146
C	-0.694191	-1.916232	3.373122
C	-0.466589	-1.058900	4.453929
C	-0.451169	0.320722	4.243128
C	-0.662084	0.842209	2.962193
C	-1.984390	3.186871	0.944664
C	-1.914164	4.577902	1.034197
C	-0.838985	5.266365	0.461921
C	0.162766	4.550164	-0.195228
C	0.097239	3.154089	-0.273566
Fe	-3.138721	0.111484	-0.877468
C	-2.877798	-1.815595	-0.658535
O	-1.846815	-2.381978	-1.013817
C	-4.040319	-2.673150	-0.129923

C	-3.898045	-4.185863	-0.334312
C	-5.084750	-4.970065	0.239712
C	-4.059561	0.280947	0.586623
O	-4.708484	0.439673	1.539633
C	4.228096	-1.338780	1.121572
O	3.908890	-1.928782	2.061390
C	4.568009	1.127542	0.363683
O	4.466914	2.197209	0.790029
H	2.621015	-1.416782	-1.356493
H	2.862841	0.269960	-1.848005
H	1.891047	1.020762	0.372692
H	1.630149	-0.649935	0.818794
H	0.065554	-1.007115	-1.071532
H	0.380059	0.599392	-1.697037
H	-1.080148	-2.081459	1.268529
H	-0.700111	-2.993210	3.521775
H	-0.299283	-1.463734	5.448810
H	-0.270022	0.999325	5.073139
H	-0.632093	1.917521	2.822656
H	-2.835935	2.671936	1.380272
H	-2.703978	5.123650	1.544437
H	-0.786372	6.350220	0.525101
H	1.002521	5.072703	-0.646529
H	0.891542	2.625975	-0.789775
H	-4.970460	-2.300317	-0.581549
H	-4.134475	-2.441242	0.942851
H	-2.963628	-4.526602	0.127728
H	-3.793478	-4.399523	-1.406395
H	-6.029795	-4.670145	-0.232409
H	-5.189440	-4.801839	1.319770
C	5.287621	-1.173188	-2.307592
C	5.678200	-2.144699	-1.348064
H	5.323592	-3.165385	-1.290921
C	6.657543	-1.537704	-0.485608
C	5.975275	0.038346	-2.028677
H	4.540962	-1.312400	-3.077762
C	6.839946	-0.199517	-0.903154
H	5.888466	0.964943	-2.580733
H	7.495358	0.527406	-0.440971
H	7.148316	-2.015166	0.352697
H	-2.114603	2.422605	-2.394877
H	-1.647197	-0.057903	-3.391093
C	-2.834429	1.617348	-2.464441
C	-2.580339	0.303802	-2.980935
C	-4.177623	1.676531	-2.030407
C	-3.790017	-0.438076	-2.880244
H	-3.928046	-1.466550	-3.187106
H	-4.665210	2.529690	-1.576586
C	-4.771784	0.389835	-2.267657
H	-5.795352	0.112121	-2.051129
H	-4.963140	-6.049137	0.081872

A2. DESCRIPTION OF LAMMPS INPUT FILES

The parameters used in the LAMMPS [2] force field and Langevin simulation runs are explained in the main text. The URL to obtain the LAMMPS distribution is: http://lammps.sandia.gov/index.html

REFERENCES

[1] M. J. Frisch *et al.*, Gaussian 09, Gaussian, Inc., 2009.

[2] S. Plimpton, J. Comput. Phys. **117**, 1 (1995).